2003-03

Ship shock trial simulation of USS Winston S. Churchill (DDG-81) surrounding fluid effect

Hart, David T.

Monterey, California. Naval Postgraduate School

NAVAL POSTGRADUATE SCHOOL
Monterey, California

THESIS

SHIP SHOCK TRIAL SIMULATION OF
USS WINSTON S. CHURCHILL (DDG81):
SURROUNDING FLUID EFFECT

by

David T. Hart

March 2003

Thesis Advisor: Young S. Shin

Approved for public release; distribution is unlimited.

THIS PAGE INTENTIONALLY LEFT BLANK

REPORT DOCUMENTATION PAGE			Form Approved OMB No. 0704-0188
Public reporting burden for this collection of information is estimated to average 1 hour per response, including the time for reviewing instruction, searching existing data sources, gathering and maintaining the data needed, and completing and reviewing the collection of information. Send comments regarding this burden estimate or any other aspect of this collection of information, including suggestions for reducing this burden, to Washington headquarters Services, Directorate for Information Operations and Reports, 1215 Jefferson Davis Highway, Suite 1204, Arlington, VA 22202-4302, and to the Office of Management and Budget, Paperwork Reduction Project (0704-0188) Washington DC 20503.			
1. AGENCY USE ONLY ***(Leave blank)***	**2. REPORT DATE** March 2003	**3. REPORT TYPE AND DATES COVERED** Master's Thesis	
4. TITLE AND SUBTITLE: Ship Shock Trial Simulation of USS Winston S. Churchill (DDG-81): Surrounding Fluid Effect			**5. FUNDING NUMBERS**
6. AUTHOR(S) David T. Hart			
7. PERFORMING ORGANIZATION NAME(S) AND ADDRESS(ES) Naval Postgraduate School Monterey, CA 93943-5000			**8. PERFORMING ORGANIZATION REPORT NUMBER**
9. SPONSORING / MONITORING AGENCY NAME(S) AND ADDRESS(ES)			**10. SPONSORING / MONITORING AGENCY REPORT NUMBER**
11. SUPPLEMENTARY NOTES The views expressed in this thesis are those of the author and do not reflect the official policy or position of the Department of Defense or the U.S. Government.			
12a. DISTRIBUTION / AVAILABILITY STATEMENT Approved for public release; distribution is unlimited.			**12b. DISTRIBUTION CODE**

ABSTRACT

The USS Winston S. Churchill (DDG-81) shock trial was conducted in May and June of 2001 off the coast of Naval Station Mayport, Florida. Because the USS Winston S. Churchill best represented the new line of Flight II-A Arleigh Burkes, it was chosen to undergo ship shock trials for its class. These trials are necessary in order to evaluate the vulnerability and survivability of the hull and the mission essential equipment in a "combat shock environment". However, shock trials are very expensive, require extensive planning and coordination, and represent a potential hazard to the marine environment and its mammals. Computer modeling and simulation are showing themselves to be a plausible alternative in investigating the dynamic response of a ship under these shock trials conditions.

This thesis investigates the use of computer ship and fluid modeling, coupled with underwater explosion simulation and compares it to actual shock trial data from the USS Winston S. Churchill. Of particular concern in this study is the amount of fluid that must be modeled to accurately capture the structural response of a full ship finite element model. Four fluid meshes were constructed and used to study the ship's response to an underwater explosion. Each simulation data was analyzed to determine which mesh best represented the actual ship shock trial results

14. SUBJECT TERMS USS Winston S. Churchill (DDG81), Ship Shock Modeling and Simulation, Fluid Mesh, Truegrid, LS-DYNA, USA, Underwater Shock Analysis, Underwater Explosion			**15. NUMBER OF PAGES** 111
			16. PRICE CODE
17. SECURITY CLASSIFICATION OF REPORT Unclassified	**18. SECURITY CLASSIFICATION OF THIS PAGE** Unclassified	**19. SECURITY CLASSIFICATION OF ABSTRACT** Unclassified	**20. LIMITATION OF ABSTRACT** UL

NSN 7540-01-280-5500 Standard Form 298 (Rev. 2-89)
Prescribed by ANSI Std. 239-18

THIS PAGE INTENTIONALLY LEFT BLANK

Approved for public release; distribution is unlimited.

SHIP SHOCK TRIAL SIMULATION OF USS WINSTON S. CHURCHILL (DDG81): SURROUNDING FLUID EFFECT

David T. Hart
Lieutenant, United States Navy
B.S.N.E., North Carolina State University, 1996

Submitted in partial fulfillment of the
requirements for the degree of

MASTER OF SCIENCE IN MECHANICAL ENGINEERING

from the

NAVAL POSTGRADUATE SCHOOL
March 2003

Author: David T. Hart

Approved by: Young S. Shin
Thesis Advisor

Young W. Kwon
Chairman, Department of Mechanical Engineering

THIS PAGE INTENTIONALLY LEFT BLANK

ABSTRACT

The USS Winston S. Churchill (DDG-81) shock trial was conducted in May and June of 2001 off the coast of Naval Station Mayport, Florida. Because the USS Winston S. Churchill best represented the new line of Flight II-A Arleigh Burkes, it was chosen to undergo ship shock trials for its class. These trials are necessary in order to evaluate the vulnerability and survivability of the hull and the mission essential equipment in a "combat shock environment". However, shock trials are very expensive, require extensive planning and coordination, and represent a potential hazard to the marine environment and its mammals. Computer modeling and simulation are showing themselves to be a plausible alternative in investigating the dynamic response of a ship under these shock trials conditions.

This thesis investigates the use of computer ship and fluid modeling, coupled with underwater explosion simulation and compares it to actual shock trial data from the USS Winston S. Churchill. Of particular concern in this study is the amount of fluid that must be modeled to accurately capture the structural response of a full ship finite element model. Four fluid meshes were constructed and used to study the ship's response to an underwater explosion. Each simulation data was analyzed to determine which mesh best represented the actual ship shock trial results.

THIS PAGE INTENTIONALLY LEFT BLANK

TABLE OF CONTENTS

LIST OF FIGURES

LIST OF TABLES

THIS PAGE INTENTIONALLY LEFT BLANK

ACKNOWLEDGMENTS

I would like to thank all of the people who have supported me through this great learning and growth opportunity. This thesis is the culmination of all of the engineering education I have had the opportunity to receive and has cemented my desire to continue to work in exciting and technically challenging areas the Navy has to offer.

I would like especially like to thank the following people for making this thesis possible:

I would like to thank Professor Young S. Shin for his incredible vision and technical mastery in the field of ship shock modeling and simulation. It is only with his invaluable guidance and mentoring that this project was made possible.

CAPT David Lewis and CDR Jeff Riedel for their continued support and funding of the Naval Postgraduate School's ship shock simulation and modeling program.

Ilbae Ham for his tireless effort in converting the DDG-81 NASTRAN model into the LS-DYNA keyword format. Lieutenant Nathan Schneider for his help and assistance throughout the course of this study.

My wife Erin, for her love and support through the challenging times and for her shared happiness during the exciting times.

THIS PAGE INTENTIONALLY LEFT BLANK

I. INTRODUCTION

A. BACKGROUND

The USS Winston S. Churchill (DDG-81) shock trial was conducted in May and June of 2001 approximately 100 nautical miles off the coast of Naval Station Mayport, Florida. It is the third ship in a new line of 23 Arleigh Burke (DDG-51) class guided missile destroyers, referred to as Flight IIA ships. Compared to the baseline DDG-51 class, Flight IIA ships are five feet longer and feature dual helo hangers. In addition, the USS Winston S. Churchill was fitted with a 5"/62 caliber gun and a Q-70 combat information center (CIC) console. Under OPNAV Instruction 9072.2, the lead ship of a new class, or a ship subjected to major upgrades, must undergo ship shock trials. These trials are necessary in order to evaluate the survivability of the hull and the mission essential equipment in the "combat shock environment" [Ref. 1]. Because of all of its upgrades, the USS Winston S. Churchill was chosen to represent the new Flight IIA ships, and therefore undergo ship shock trials.

Section 2366 of title 10, United States Code (10 USC 2366) requires realistic testing of ship hulls and weapons systems to analyze their strengths and weaknesses under actual combat conditions [Ref. 2]. During such testing, ships are subjected to live fire munitions that they may encounter in actual combat conditions. The Navy uses these results to determine how well the ships personnel; hull and equipment would survive in a shock environment. This information is then used to improve the shock hardening of the ship and any follow-on ships of the same class. However, shock trials are very expensive, require extensive planning and coordination, and represent a potential hazard to the marine environment and its animals.

Computer modeling and simulation are now showing themselves to be a plausible alternative to live fire testing in the investigation of the dynamic response of a ship under shock trials conditions. Historically, all of a ship's components required individual physical testing due to the insufficiencies of computer analysis methods available. However, in the last decade many of these deficiencies were addressed and computer modeling and simulation are now in the forefront of defense acquisition and testing [Ref. 3]. With more detailed finite element (FEM) ship models, ship shock simulation can

hopefully play a significant role in ship design and live fire testing and evaluation. This could greatly reduce the costs and the potential physical and environmental hazards associated with live fire testing.

B. SCOPE OF THIS WORK

The background for this research stems from work completed at the Naval Postgraduate School (NPS) on the computer modeling and simulation of the ship shock trial of the USS John Paul Jones (DDG-53) [Ref. 4]. The results from the USS John Paul Jones fluid/structure model, when compared to the results of the actual ship shock trials, were promising enough to warrant further investigation into the surrounding fluid mesh and its effects on simulation response [Ref. 5]. This thesis investigates the use of computer ship and fluid modeling, coupled with underwater explosion simulation and compares it to actual shock trial data from the USS Winston S. Churchill. Of particular concern in this study is the amount of fluid that must be modeled to accurately capture the structural response of a full ship finite element model. Four different fluid meshes were constructed and used to study the ship's response to an underwater explosion. Each simulation data was analyzed to determine which mesh best represented the actual ship shock trial results.

The finite element mesh generation program Truegrid [Ref. 6] was used to model the fluid mesh. Gibbs & Cox, Incorporated developed the three-dimensional finite element model of USS Winston S. Churchill used in the simulation. Analysis of the coupled ship model and fluid mesh was conducted using the Nonlinear Dynamic Analysis Code, LS-DYNA [Ref. 7], coupled with the Underwater Shock Analysis Code, USA [Ref. 8].

II. UNDERWATER EXPLOSION PHENOMENA

A. SEQUENCE OF EVENTS

The underwater explosion (UNDEX) phenomena first begins with the detonation of a high explosive, such as TNT or HBX-1. A chemical reaction occurs from the original explosive material that produces very high temperatures and intense pressure gas. The temperature and pressure that are produced are on the order of 3000 C and 50,000 atm pressure [Ref. 9]. This reaction occurs so rapidly that the chemical transformation of the original material cannot keep up with its own physical disturbance. A high explosive such as TNT or HBX-1 occurs on the order of nanoseconds and contains all the energy of the explosion a small volume, which prevents it from having time to escape [Ref. 10]. This confinement produces a destructive effect characterized by a "large and rapid evolution of energy" [Ref. 9].

Following the release of energy from the initial explosion is the formation of an underwater shock wave. For the UNDEX analysis, water is assumed to be homogenous and unable to support shear stress. Although water is generally assumed to be incompressible under normal conditions, this is not the case for the fluid surrounding the explosive. Under these circumstances, the water in this area is compressible and obtains a high radial velocity [Ref. 10]. As a result, an UNDEX produces a hot mass of gas at such intense pressure that a high velocity compression wave is created. This compression wave, or "shock wave", propagates radially outward from the detonation point at velocities on the order of 5000 ft/sec, approximately the speed of sound in water. Due to the discontinuous rise in pressure, the shock wave is characterized by a steep frontal wave, followed by an exponentially decaying and broadening wave. The rapidity of the shock wave is dependent on the pressure magnitude, temperature and density of the surrounding median. Figure 1 shows this type of pressure distribution for a 300lb TNT underwater explosion [Ref. 9].

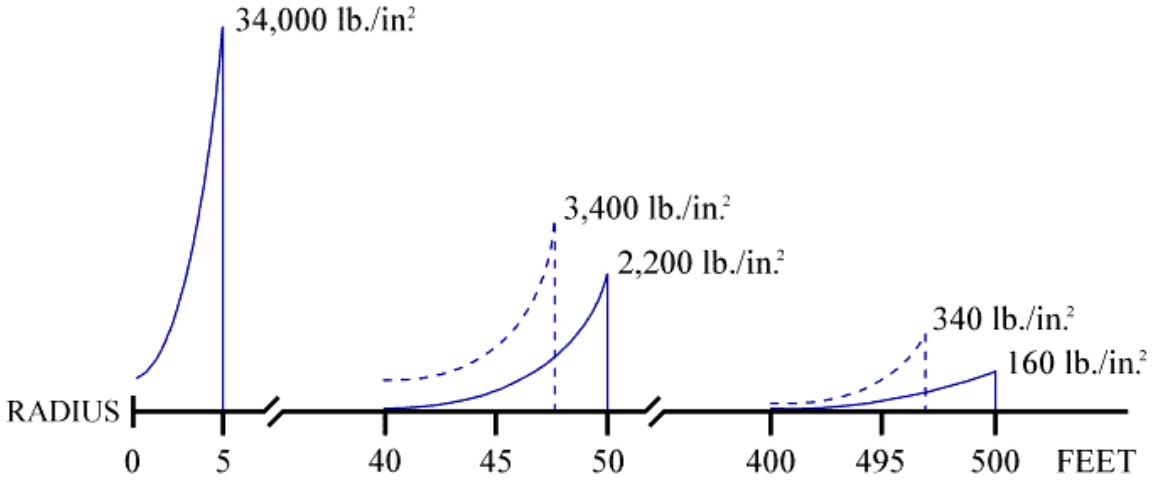

Figure 1. Shock Wave Pressure Profile for a Radially Expanding Wave From a 300lb. TNT Charge [from Ref. 9]

The resulting shock wave pressure profile is proportional to the inverse of the distance from the charge, 1/d. Empirical equations derived for the pressure profile of the expanding shock wave are accurate for distances from 10 to 100 charge radii and for durations of roughly one decay constant [Ref. 10]. The following relations were used to determine the pressure profile P(t), the peak pressure in the shock front (P_{max}), the decay constant for the shock front (θ), the maximum bubble radius (A_{max}), and the first bubble time (T).

$$P(t)=P_{max}e^{-\frac{t-t_1}{\theta}} \quad \text{(psi)} \quad (1)$$

$$P_{max}=K_1\left(\frac{W^{\frac{1}{3}}}{R}\right)^{A_1} \quad \text{(psi)} \quad (2)$$

$$\theta=K_2W^{\frac{1}{3}}\left(\frac{W^{\frac{1}{3}}}{R}\right)^{A_2} \quad \text{(msec)} \quad (3)$$

$$A_{max}=K_6\frac{W^{\frac{1}{3}}}{(D+33)^{\frac{1}{3}}} \quad \text{(ft)} \quad (4)$$

$$T=K_5\frac{W^{\frac{1}{3}}}{(D+33)^{\frac{5}{6}}} \quad \text{(sec)} \quad (5)$$

where:

W = weight of the explosive (lb)
R = distance from the explosive to the target (ft)
D = depth of the explosive (ft)
t_1 = arrival time of the shock front (msec)
t = time of interest (msec)
K_1, K_2, K_5, K_6, A_1, A_2 = constants dependent on explosive type

As stated before, the chemical reaction that occurs from a high explosive produces gases at very high temperatures and intense pressure. The high pressure of the gases acts on the surrounding fluid median and imparts a radially expanding compression wave on the water. This wave carries approximately one-half of the energy generated by the explosion. At the formation of this shock wave, the pressure of the gas is much higher than hydrostatic pressure of the surrounding fluid, but as it expands, it eventually reaches that of the surrounding fluid. When this occurs, the gas bubble continues to grow radially outward until it reaches its maximum radius given by Equation 4 above. Once the bubble's maximum radius is reached, the hydrostatic pressure exerted on its equilibrium causes the radial flow to reverse and collapse the bubble. This oscillation of the gas bubble continues until all energy is dissipated or until the bubble is vented to the free surface, Figure 2. The resulting phenomenon produces pressure pulses that generate radially expanding pressure waves [Ref. 10]. These occurrences and their migration are of particular concern in UNDEX explosions because they can cause severe damage if they collapse on the ship's hull [Ref. 11].

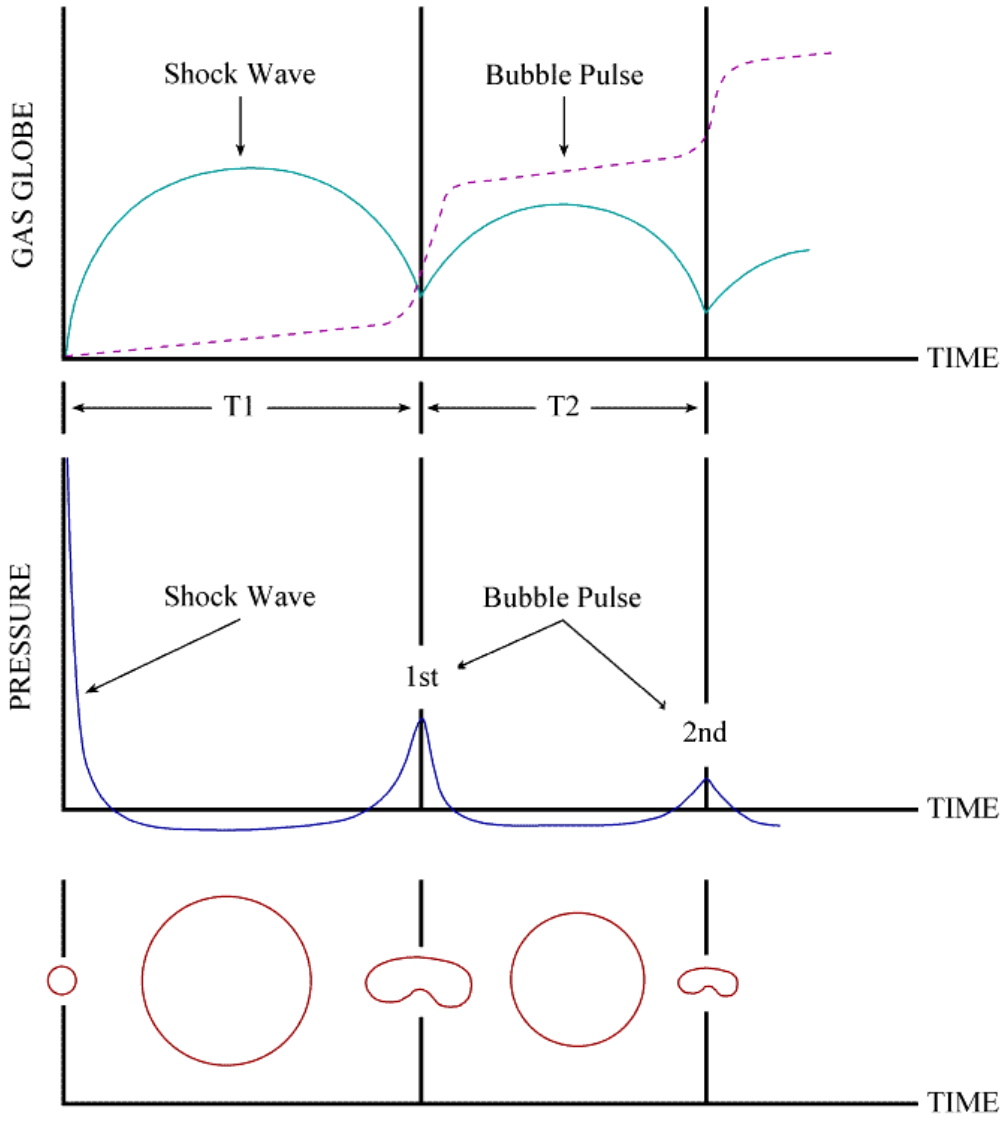

Figure 2. Migration, Pressure Pulse, and Pulsation of the Gas Products Produced by an Underwater Explosion [from Ref. 10]

B. FLUID-STRUCTURE INTERACTION

Fluid-structure interaction is important because the impinging shock wave, or pressure pulse, carried in the bulk fluid surrounding the ship can excite dynamic responses on the ship's structure. This section lists the generalized differential equations for handling the fluid-structure interaction. The following discretized differential equation represents the dynamic response of the structure:

$$[M]\{\ddot{x}\}+[C]\{\dot{x}\}+[K]\{x\}=\{f\} \qquad (6)$$

where:

$[M]$ = structural mass matrix

$[C]$ = structural damping matrix

$[K]$ = structural stiffness matrix

$\{f\}$ = applied force vector

$\{x\}$ = structural displacement vector

dots denote temporal derivative

Equation 6 represents the balance of all forces acting upon the ship's structure. These include acceleration dependent inertial forces, velocity dependent damping forces, displacement dependent internal forces and acoustic fluid pressure forces [Ref. 17].

The Doubly Asymptotic Approximation (DAA) [Ref. 12] is used to solve the fluid-structure interaction problem. DAA is aptly named because it allows for the approximation of both early and late times in the interaction process between the scattered-wave pressures and the normal fluid-particle velocity components. This method also allows for the solution of the fluid-structure interaction in terms of wet-surface response only. The DAA is as follows:

$$[M_f]\{\dot{p}_S\}+\rho c[A_f]\{p_S\}=\rho c[M_f]\{\dot{u}_S\} \qquad (7)$$

where:

$[M_f]$ = fluid mass matrix

$[A_f]$ = diagonal area matrix for the fluid mesh

$\{u_s\}$ = scattered wave fluid particle velocities

$\{p_s\}$ = scattered wave pressure vectors

ρ = density of the fluid

c = fluid sound velocity

Dot denotes a temporal derivative

For short acoustic wavelengths and high frequency motion (early time response), $p_S=\rho c u_S$. For long acoustic wavelengths and low frequency motion (late time response), $[A_f]\{p_S\}=[M_f]\{\dot{u}_S\}$ [Ref. 12].

The excitation of the wet surface hull structure by an incident shock wave, "f" in Equation 6, is given by:

$$f=-GA_f(p_I+p_S) \tag{8}$$

where p_I and p_S are pressure vectors of the incident and scattered shock waves, respectively. Equation 8 shows that the fluid pressure field acting on the structural wet surface can be broken down into an incident wave and a scattered wave [Ref. 18]. In order to relate the scattered wave fluid particle velocities to the structure response, the following kinematic relation is applied:

$$\left[G^T\right]\{\dot{x}\}=\{u_I\}+\{u_S\} \tag{9}$$

where "T" represents matrix transpose.

Equation 9 expresses that the normal fluid velocities must match the normal structural velocities on the wetted surface. Substituting Equation 8 into Equation 6, and Equation 9 into Equation 7, results in the following two interaction equations.

$$[M]\{\ddot{x}\}+[C]\{\dot{x}\}+[K]\{x\}=-[G][A_f](p_I+p_S) \tag{10}$$

$$[M_f]\{\dot{p}_S\}+\rho c[A_f]\{p_S\}=\rho c[M_f]\left([G]^T\{\ddot{x}\}-\{\dot{u}_I\}\right) \tag{11}$$

The only unknowns in Equations 10 and 11 are "x" and "p_S" which can be solved using a staggered solution scheme.

C. CAVITATION

During a UNDEX event, there are two types of cavitation that can occur, "local" and "bulk" cavitation. Local cavitation occurs near the interface of the surrounding fluid and the ship structure, also known as the fluid-structure interface. Bulk cavitation occurs near the interface of the air and the fluid, also know as the free surface.

1. Local Cavitation

The phenomenon of local cavitation occurs along the fluid-structure interface of a ship due to the interaction of the impinging shock wave and the flexible surface of the structure. In its most basic form, Taylor Flat Plate Theory describes this interaction. This states that when an air-backed plate of mass is subjected to an incident plane shock wave,

a reflective shock wave is generated off the plate. Consider the following shock wave, illustrated in Figure 3, impinging on an air backed infinite flat plate.

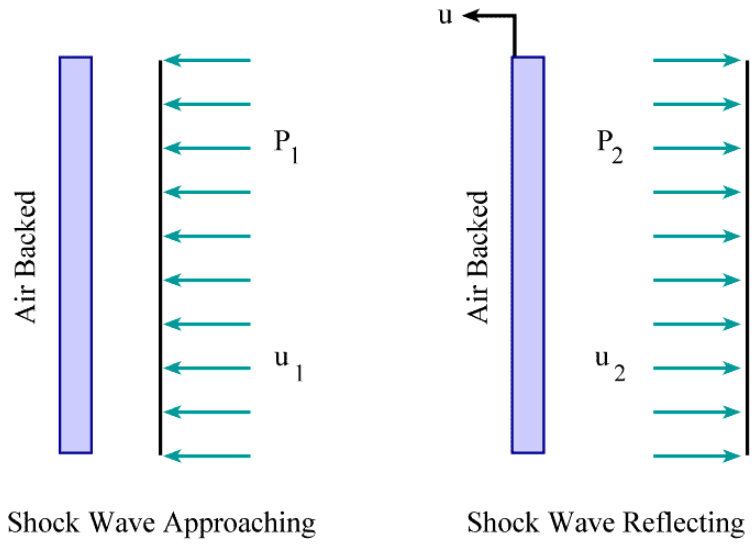

Figure 3. Taylor Plate Subjected to a Plane Wave [from Ref. 11]

The equation of motion, from Newton's second law of motion, for the flat plate is:

$$m\frac{du}{dt}=P_1+P_2 \qquad (12)$$

The velocities (u) and pressures (P) of the fluid particles behind the incident and reflected shock waves are u_1, P_1 and u_2, P_2 respectfully. Velocity of the interface between the surface of the plate and the fluid is given by:

$$u=u_1-u_2 \qquad (13)$$

The pressure of the fluid particles behind the incident and reflected shock wave is:

$$P_1=\rho C u_1 \text{ and } P_2=\rho C u_2 \qquad (14) \text{ and } (15)$$

where ρ and C are the density and velocity of the acoustic median.

Substituting Equation 14 and 15 into Equation 13 results in the following equation for the velocity of the fluid particle along the fluid-structure interface:

$$u=\frac{P_1-P_2}{\rho C} \qquad (16)$$

Solving for the reflected shock wave pressure by substituting in Equation 1 yields:

$$P_2=P_1-\rho C u=P_{max}e^{-\frac{t}{\theta}}-\rho C u \qquad (17)$$

From these expressions, the resulting equation of motion, given by Newton's second law of motion, now becomes:

$$m\frac{du}{dt}+\rho Cu=2P_{max}e^{-\frac{t}{\theta}} \tag{18}$$

Solving this first order linear differential equation results in the following relationships for velocity and pressure.

$$u=\frac{2P_{max}\theta}{m(1-\beta)}\left[e^{\left(-\frac{\beta t}{\theta}\right)}-e^{\left(-\frac{t}{\theta}\right)}\right] \tag{19}$$

$$P_2=\frac{P_{max}}{(1-\beta)}\left[-(2\beta)e^{\left(-\frac{\beta t}{\theta}\right)}+(1+\beta)e^{\left(-\frac{t}{\theta}\right)}\right] \tag{20}$$

$$P_1+P_2=P_{max}\left[\frac{2}{1-\beta}e^{\left(-\frac{t}{\theta}\right)}-\frac{2\beta}{1-\beta}e^{\left(-\frac{\beta t}{\theta}\right)}\right] \tag{21}$$

where $\beta=\frac{\rho C\theta}{m}$.

The above equations show that as β becomes larger, the total pressure along the fluid-structure interface becomes negative. Since the fluid cannot support this negative pressure, a region of local cavitation is created along the ship's hull [Ref. 10].

2. Bulk Cavitation

Bulk cavitation is created by the compressive shock wave reflecting from the free surface. As the incident pressure shock wave reflects off the free surface, it creates a reflected tension, or rarefaction, wave. Tension is created from the pressure wave as it travels away from the free surface, producing a negative pressure. Water is unable to support the negative pressure in this area and it collapses, creating a large area of cavitation. This bulk cavitation area is characterized by an upper and a lower boundary, the extent of which is dependent upon the size, type and depth of the charge [Ref. 10]. Figure 4 shows a typical cross sectional view of the bulk cavitation region.

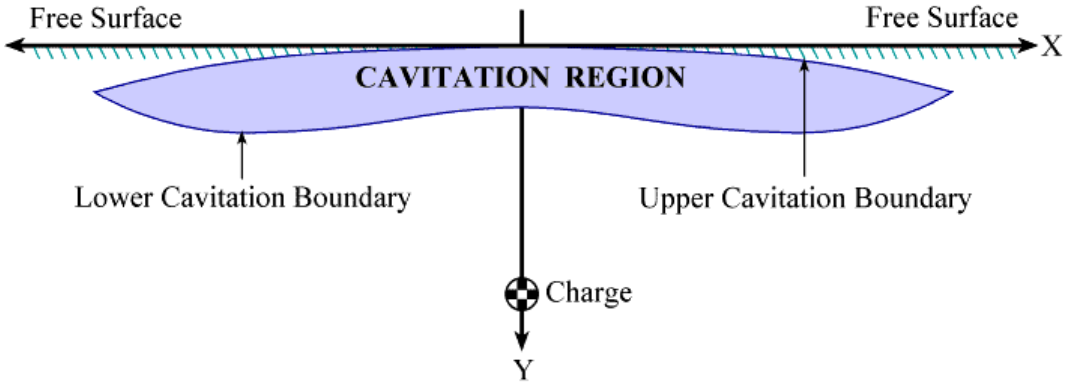

Figure 4. Illustration of the Bulk Cavitation Region Produced by an Underwater Explosion [from Ref. 10]

The underwater explosion geometry and shock wave pressure profile are shown in Figures 5 and 6.

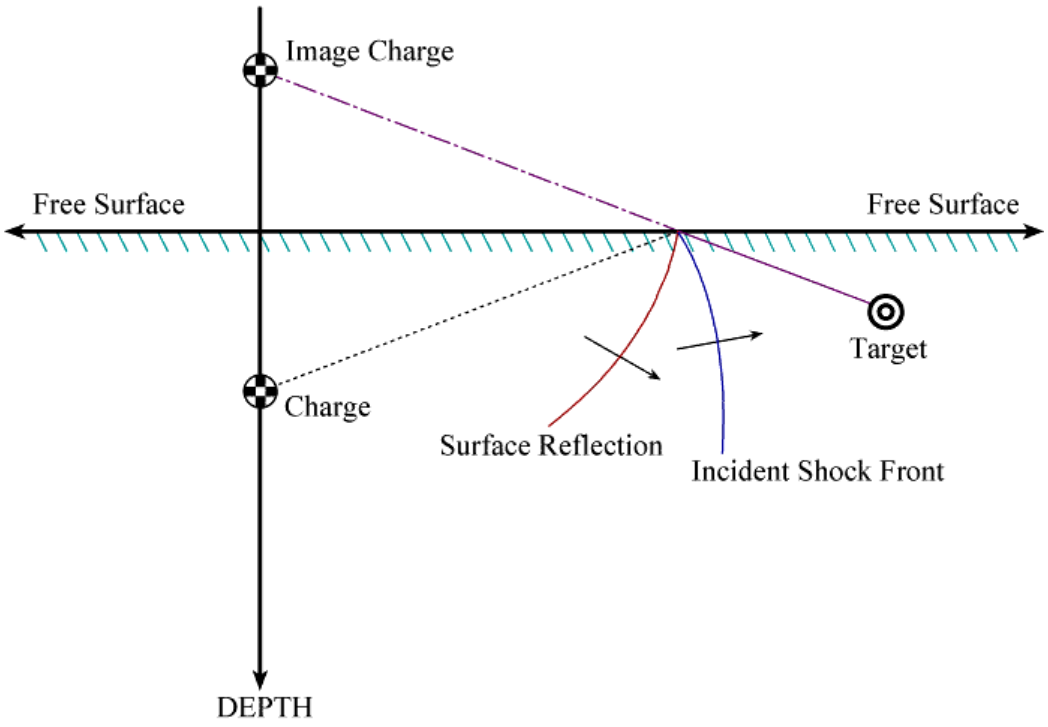

Figure 5. Underwater Explosion Geometry for Calculation of the Bulk Cavitation Equations [from Ref. 10]

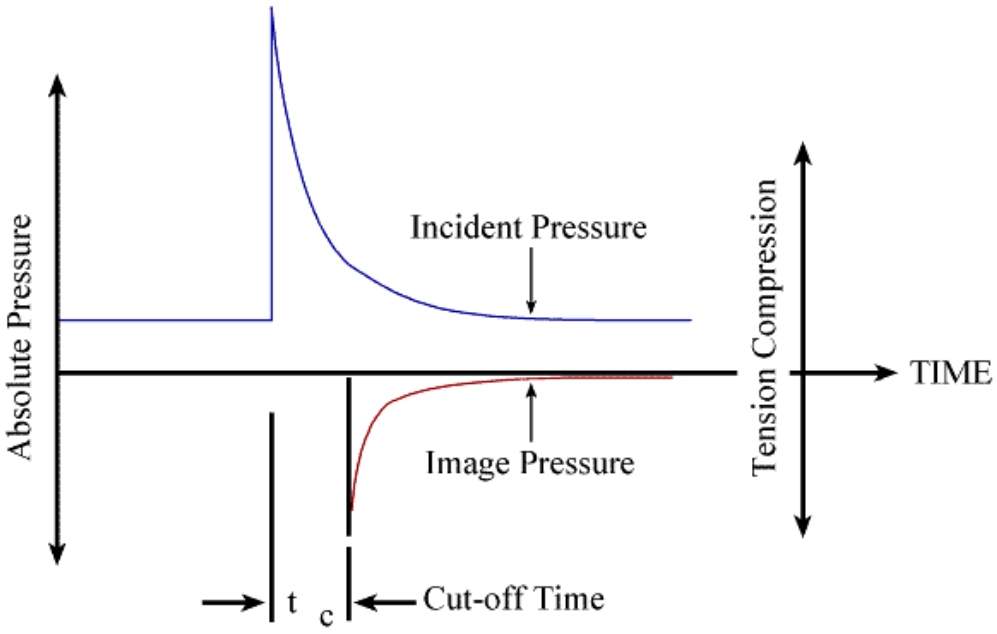

Figure 6. Shock Wave Pressure Profile with Cut-Off Time [from Ref. 11]

The upper cavitation boundary is defined as the area where the net pressure equals zero, due to the incident and reflected shock waves. Below the surface this is not the case. Pressures do not add up to zero and may even be negative. Since water is unable to support this type of negative pressure, cavitation occurs. The extent of this upper cavitation region is determined from the following expression:

$$F(x,y)=K_1\left(\frac{W^{\frac{1}{3}}}{r_1}\right)^{A_1} e^{-\frac{(r_2-r_1)}{C\theta}}+P_A+\gamma y-K_1\left(\frac{W^{\frac{1}{3}}}{r_2}\right)^{A_1}=0 \qquad (22)$$

and

$$r_1=\sqrt{(D-y)^2+x^2} \text{ and } r_2=\sqrt{(D+y)^2+x^2} \qquad (23) \text{ and } (24)$$

where:

x, y = horizontal and vertical range
r_1 = distance from charge
r_2 = distance from image charge
C = acoustic velocity
D = depth of charge
θ = shock wave decay constant
P_A = atmospheric pressure
γ = weight density of water
W = charge weight
K_1, K_2 = shock wave parameters

The lower cavitation boundary region is determined by equating the decay rate of the reflected/rarefraction wave's breaking pressure to that of the absolute pressure of the surrounding fluid. Breaking pressure is determined from the rarefraction wave, which reduces a particular fluid location to the point of cavitation, or zero psi. The lower cavitation boundary is determined from the following expression:

$$G(x,y)=-\frac{P_i}{C\theta}\left\{1+\left[\frac{r_2-2D\left(\frac{D+y}{r_2}\right)}{r_1}\right]\left[\frac{A_2 r_2}{r_1}-A_{2\text{-}1}\right]\right\}- \frac{A_1 P_i}{r_1^2}\left[r_2-2D\left(\frac{D+y}{r_2}\right)\right]+\gamma\left(\frac{D+y}{r_2}\right)+\frac{A_1}{r_2}\left(P_i+P_A+\gamma y\right)=0 \quad (25)$$

where all variables are defined in Equation 22 above and

$$P_i=K_1\left(\frac{W^{\frac{1}{3}}}{R}\right)^{A_1} e^{-\frac{(r_2-r_1)}{C\theta}} \quad (26)$$

This region will remain in the cavitated state until its absolute pressure rises above zero psi [Ref. 10].

THIS PAGE INTENTIONALLY LEFT BLANK

III. FEM MODEL AND SIMULATION CODE

A. 3-DIMENSIONAL FINITE ELEMENT SHIP MODEL

The USS Winston S. Churchill (DDG-81) three-dimensional finite element model used in this thesis was obtained from Gibbs & Cox, Inc. in the form of a MSC/NASTRAN input deck [Ref. 13]. This model represents the largest and most complex finite element ship model constructed to date [Ref. 14]. Model construction was based on the USS John Paul Jones (DDG-53) model used in previous studies at NPS [Ref. 5]. Figure 7 shows the comparison of the DDG-81 and DDG-53 finite element models.

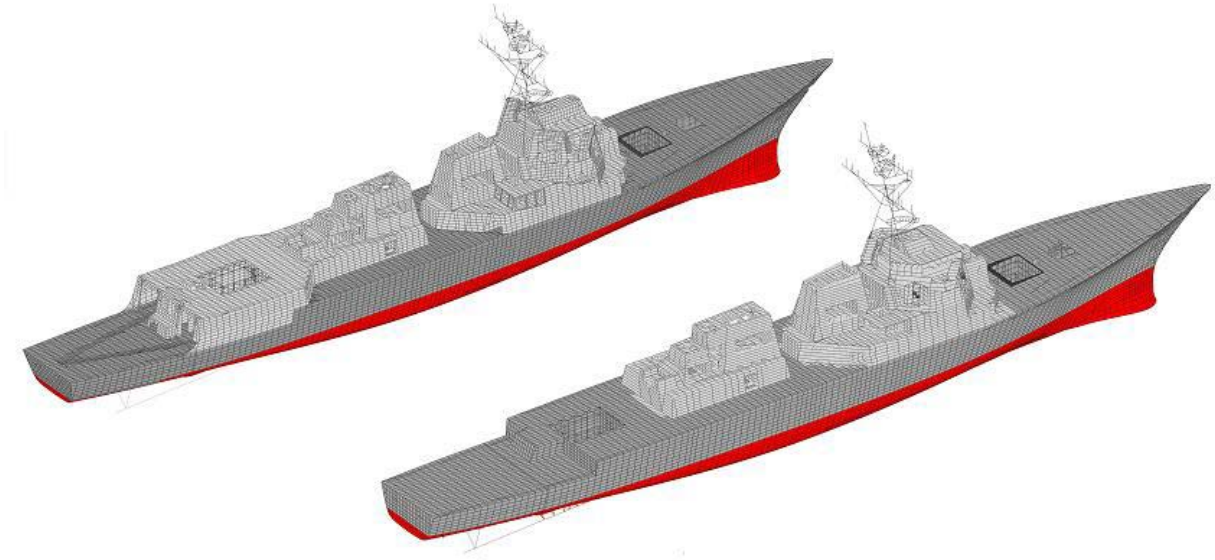

Figure 7. DDG-81 and DDG-53 Finite Element Model Comparison Showing Structural Changes [from Ref. 14]

The DDG-81 FEM model incorporates all of the features of the new Flight IIA class of Arleigh Burke (DDG-53) guided missile destroyers. These additions include, but are not limited to, dual helo hangers, six additional vertical launch cells (VLS), and installation of a 5"/62 caliber gun. A full list of the Flight IIA class ship modifications is outlined on Figure 8.

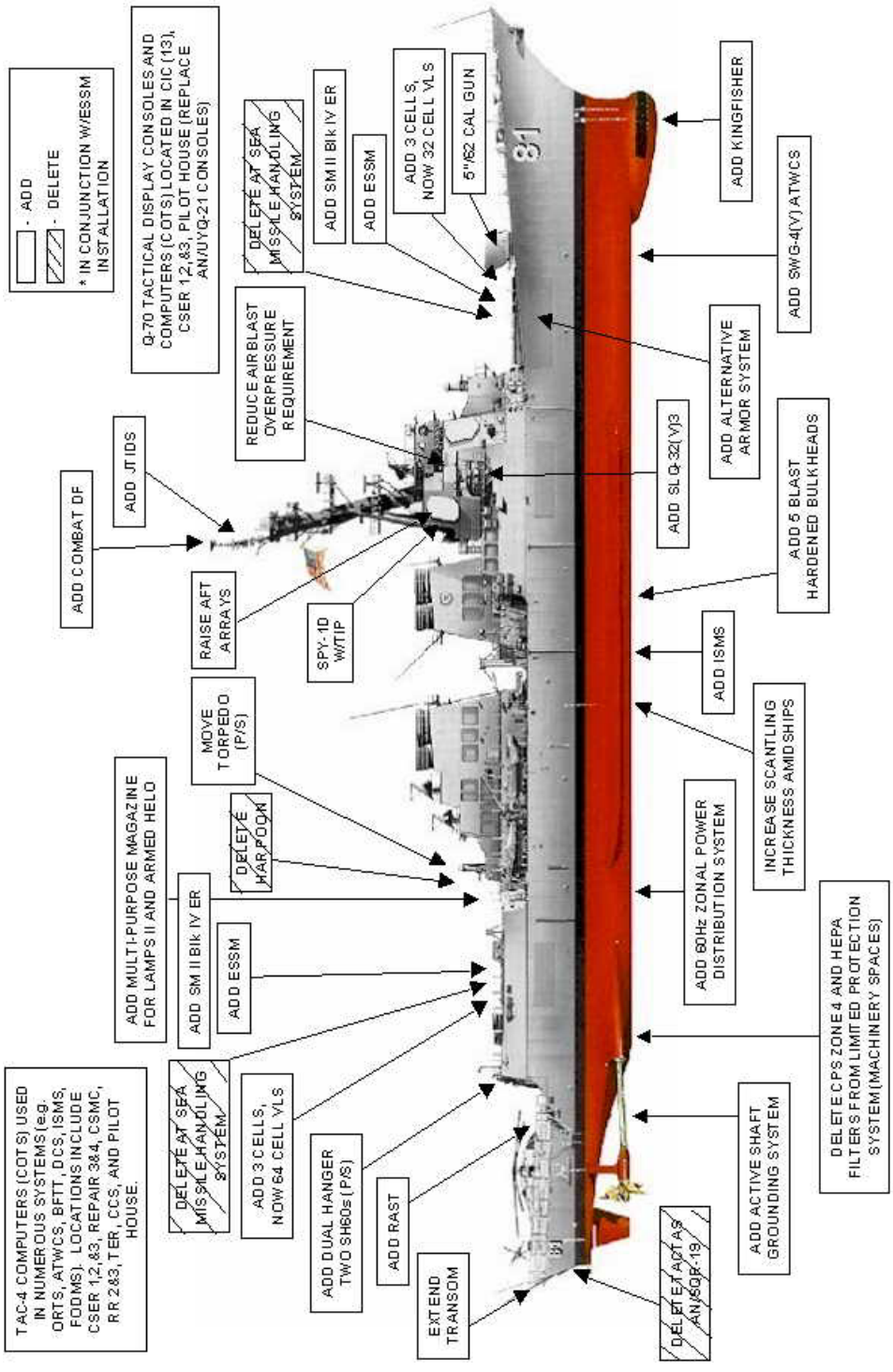

Figure 8. Complete Illustration of the Flight IIA Modifications [from Ref. 15]

The Gibbs & Cox finite element model has a nominal size of 27"x 48" and is based on the ship's structural fabrication drawings. The ship model was subdivided into various levels and then reconstructed piece by piece (Figure 9). All of these parts were then reassembled into the full finite element model. The accuracy of the model was further increased by the addition of all major equipment that could influence the dynamic response of the keel, major bulkheads, and shock sensor areas. These included propulsion gas turbines, reduction gears, VLS modules, 5" gun, SPY 1D array faces, ship service gas turbine generators, and propulsion shafting, Figure 10 [Ref. 14].

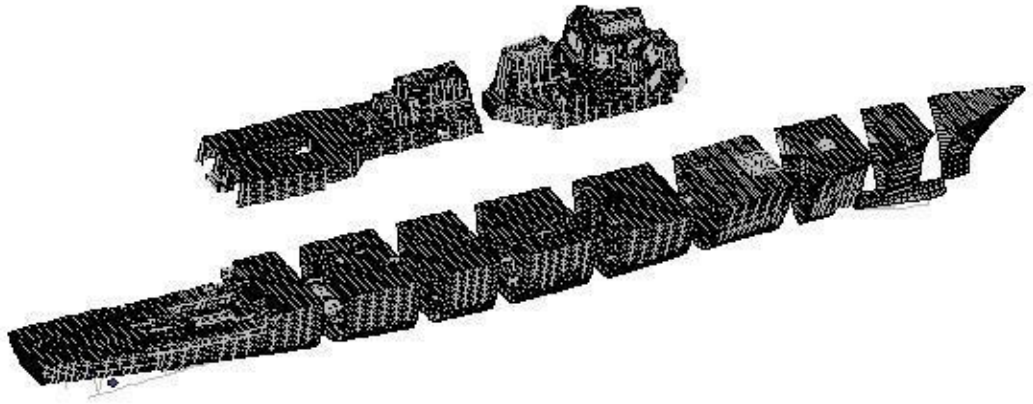

Figure 9. DDG-81 Full Ship FEM Subassembly [from Ref. 14]

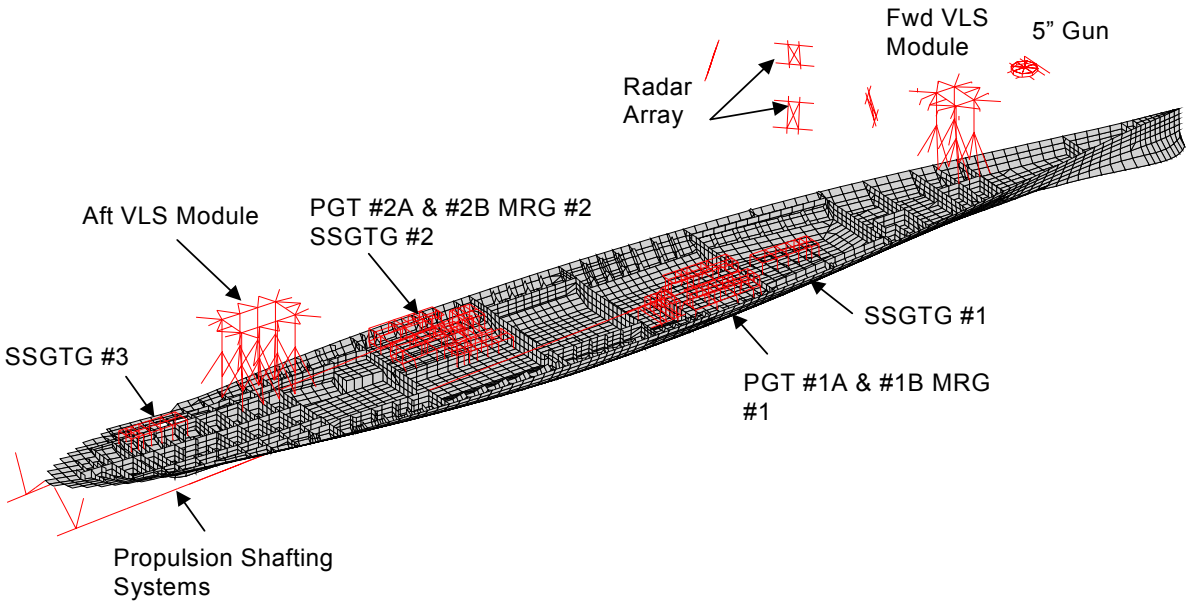

Figure 10. DDG-81 Full Ship FEM Equipment/Foundation Model [from Ref. 14]

In order to match the actual weight distribution of the DDG-81 during the May and June 2001 shock trials, several modifications were added to the finite element model. These included ordnance load-out, liquid loading, and personnel. The model specifications are listed in Table 1, and Figures 11 -13 show cut away views of the model.

Table 1 DDG-81 Finite Element Model Summary [from Ref. 14]

Number of Nodes	40,514
Number of Degrees of Freedom	243,084
Number of Beam Elements	49,397
Number of Lumped Masses	92,541
Number of Thin Shell Elements	48,662
Number of Spring Elements	416
Number of Rigid Body Constraint Sets	107

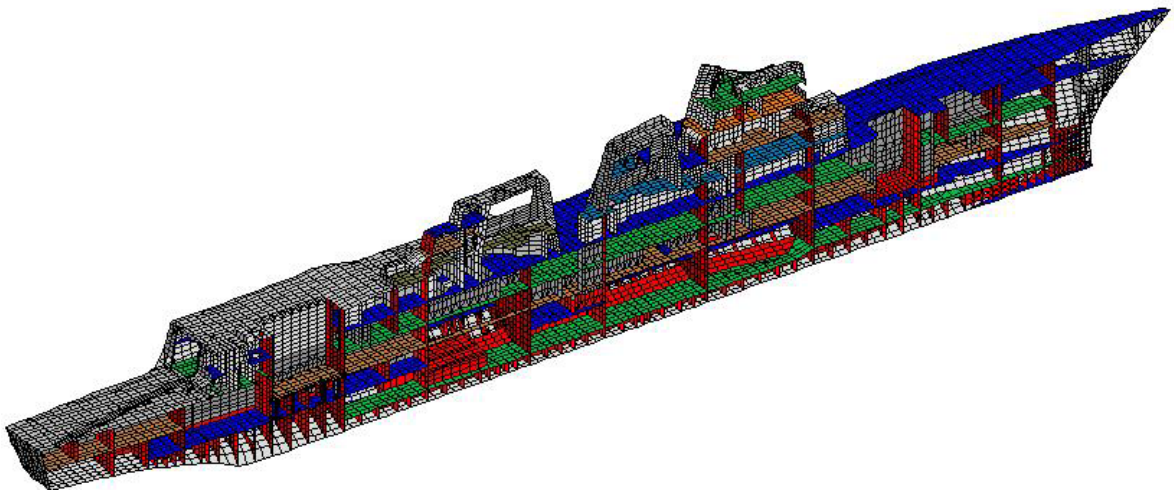

Figure 11. DDG-81 Full Ship FEM Centerline Cutaway [from Ref. 14]

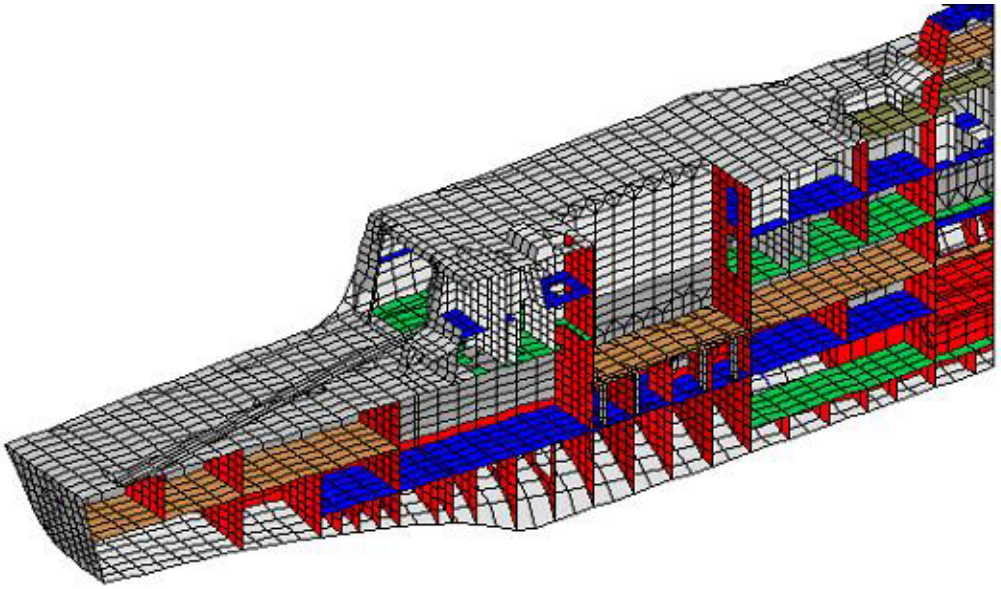

Figure 12. DDG-81 Full Ship FEM Stern Cutaway [from Ref. 14]

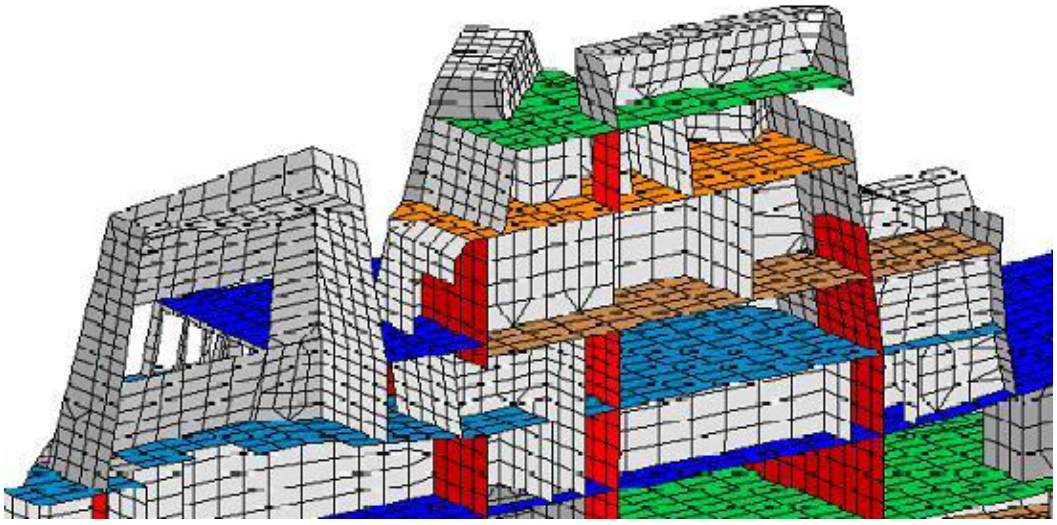

Figure 13. DDG-81 Full Ship FEM Superstructure Cutaway [from Ref. 14]

B. SIMULATION CODE

Several analysis programs were used in running the ship shock trial simulations of the USS Winston S. Churchill. The initial finite element ship model from Gibbs & Cox was converted from a MSC/NASTRAN input deck into nonlinear dynamic analysis code (LS-DYNA) keyword file. LS-DYNA was coupled with the underwater shock analysis code (USA) to conduct the shock simulation.

1. Pre-Processing and LS-DYNA

LS-DYNA is a general finite element program for analyzing the dynamic response of large structures, including structures coupled to fluids. It is a non-linear three-dimensional analysis code that performs the time integration for the structure.

2. Underwater Shock Analysis Code

The underwater shock analysis code (USA) [Ref. 8] was used to calculate the transient response of the ship's wet-surface structure to an incident shock wave. USA is a boundary element code that solves the ship's structure interaction equations using the doubly asymptotic approximation (DAA) used in Equation 7. As stated in the fluid-structure interaction section, the DAA method models the response in terms of the wet-surface variables only, eliminating the need for a fluid volume. This technique has been shown to work well for a submerged structure, such as a submarine, but does not accurately depict the ship shock phenomena near the free surface. With addition of bulk and local cavitation associated with a ship, the problem becomes more complex. Now it changes from a simple acoustic-reflection problem into a complex reflection-refraction problem. For the surface shock, a finite element (FEM) volume of fluid elements must be modeled in order to recreate the effects of both bulk and local cavitation. Therefore, a fluid mesh is created that surrounds the ships hull and extended outwards in order to capture the cavitation phenomenon. The DAA boundary is truncated to the outer surface of the fluid mesh [Ref. 4].

The USA code is comprised of three processors: Fluid Mass Processor (FLUMAS), Augmented Matrix Processor (AUGMAT), and Time Integration Processor (TIMIT) [Ref. 16].

a. FLUMAS

The FLUMAS processor generates the fluid mass matrix for the ship's wet surface structure in an infinite, inviscid, and incompressible fluid. It also calculates the number of independent coordinates necessary to define the hull's structural and fluid degrees of freedom (DOF) on the wet surface. The user-defined inputs include [Ref. 16,17,18]:

1. Fluid mesh and element definitions.
2. Location of the free surface.
3. Fluid properties: mass density and acoustic speed of sound.
4. Atmospheric properties: pressure and acceleration due to gravity.

Finally, the FLUMAS processor generates the directional cosines for the normal pressure force and the nodal weights for the fluid element pressure forces. The area matrix for the fluid is diagonal and mass matrix for the fluid is symmetric [Ref. 12].

b. AUGMAT

The AUGMAT processor uses the output of the FLUMAS processor fluid mass matrix and the LS/DYNA's structural mass matrix to generate input matrices for the TIMIT processor [Ref. 16,17]. By combining the FLUMAS and the LS/DYNA matrices into one file, AUGMAT creates a more efficient way for TIMIT to access the data.

c. TIMIT

The TIMIT processor gathers information from AUGMAT and uses this data to carry out the direct integration of the structural equation (Equation 10) and the fluid equation (Equation 11). This the most time consuming step of the USA code analysis. The LS-DYNA processor solves the structural equations and the TIMIT processor solves the fluid equations. By extrapolating the coupling terms for each, both equations can be solved at every time step using an unconditionally stable staggered

integration procedure. Output from the TIMIT processor is saved as a binary history file (D3THDT) and as an ASCII file (NODOUT) at each step. This is a time history of displacement, velocity and wet-surface pressure for all designated nodal numbers [Ref. 16,17]. Nodes that correlate to the sensor locations for the actual ship shock trials are designated in the LS-DYNA DATABASE_HISTORY_NODE command line.

3. Post Processing

Results from LS-DYNA and USA code are used to produce post-processing graphics. These graphics are visualizations of ship shock simulation in three-dimensional and time dependant UERD plots of velocity.

a. Glview

GLview is a powerful post processing 3D visualization and animation tool for viewing large-scale model response information [Ref. 20]. GLview has the ability to import binary and ASCII output data from the LS/DYNA and USA processors to produce visualization models and time-dependent plot data. Its animation package displays time-dependent results in both scalar and vector format for such things as stresses, strains, displacement, velocities and accelerations in the fluid-structure model. However, GLview is unable to directly import ship shock trial data. A second program, UERD, must therefore be used to compare the ship shock simulation data to the actual shock trial data. This was achieved by using GLview to extract the ASCII history file for each sensor node from the LS-DYNA NODOUT file, exporting them as separate ASCII files, and importing them into the UERD program.

b. Underwater Explosion Research Department (UERD)

The Underwater Explosions Research and Development Project office in Bethesda, MD designed the UERDtools computer program. This program was specifically designed for analyzing shock trial data. With a host of capabilities such as drift compensation, interpolation, filtering, and error analysis, the UERD program allows users to create high quality plots of shock data. It also allows direct import of shock trial data for initial manipulation, such as drift compensation and filtering. The LS-

DYNA/USA simulation data can then be brought in from the ASCII file generated by GLview. Once both sets of data have been imported, the program allows the time set of both plots to be interpolated to the same time step. This is a necessary requirement when conducting error analysis/correlation between the LS-DYNA/USA simulation data and the actual shock trial data.

THIS PAGE INTENTIONALLY LEFT BLANK

IV. FLUID MESH CONSTRUCTION

The purpose of this study is to investigate the optimum depth of fluid volume that must be modeled to accurately capture the dynamic response of the full FEM ship model. Using the Truegrid batch mesh generator, a finite element fluid mesh for the DDG81 full ship model was generated. The sonar dome, keel and bow areas represented the most extreme geometries of the ship structure, and were the most challenging aspect of the FEM modeling. Nodal placement along these areas on the ship's hull required careful consideration in order to ensure a good mesh generation.

Optimum depth of the fluid volume was determined by comparing the results of the LS-DYNA/USA code to the results of the DDG-81 ship shock trial data. Results were obtained by analyzing data from four FEM models: a fluid mesh liner, a one-half fluid mesh, a full fluid mesh and a 2X fluid mesh. Table 2 summarizes the specifics of each fluid model.

Table 2 Fluid Volume Model Specifics

Fluid Model	Nominal Size (feet)	Nodes	Fluid Volume Elements	DAA fluid boundary faces
Mesh Liner	15inches	9856	9666	4838
1/2 Mesh	495x70x35	70378	68503	5090
Full Mesh	573x140x70	135568	129582	5090
2X Mesh	632x280x140	158894	149942	5090

A. TRUEGRID MESH GENERATOR

The Truegrid batch mesh generator produces multi-block, structural meshes composed of solid hexahedral elements and /or quadrilateral shell and beam elements. If the program is unable to generate a six-sided solid element, it compensates by creating wedges, pyramids or tetrahedrons. This feature, coupled with a host of projection, mapping, and interpolation options, allows the user to generate high quality meshes on complex geometries [Ref. 6].

Truegrid's most powerful tool for constructing a fluid FEM model is its extrusion technique. The extrusion technique consists of pulling a set of user-defined polygons, one at a time, following the mesh lines generated by the construction of the block part.

User-defined polygons for the fluid FEM model are those extrapolated from the ship structure's wetted surface. This results in an extruded mesh that exactly matches the structural mesh, a prerequisite for any successful fluid modeling.

A detailed description of the Truegrid modeling commands and the fluid mesh generation is contained in Appendix B and C.

B. USA CODE STABILITY CRITERIA

The nodal spacing adjacent to the FEM ship structural model is critical to the stability of the USA code. The code requires that the nodal spacing cannot exceed a defined thickness, D, given by the following equation:

$$\frac{2D\rho}{\rho_S t_S} \leq 5 \qquad (27)$$

where ρ is the density of water, D is the thickness of the fluid elements normal to the ship structure, ρ_S is the density of the submerged structure, and t_S is the thickness of the submerged structure. For the DDG-81 ship model, the critical element thickness normal to the structure is nine inches.

C. FLUID MESH LINER

A thin fluid mesh liner was used as the "building block" for the remaining three fluid meshes used in this study. This layer ensures that the fluid mesh remains orthogonal to the ship around the majority of the structure. It further ensures that the critical element size of nine inches is achieved around its entire wetted surface. For this study, the first layer of fluid mesh for the liner was set at seven inches in order to achieve the densest mesh possible around the ship's hull without exceeding a time step calculation for the solid fluid elements of 4.0x10e-6 [Ref. 7].

The fluid mesh liner remains orthogonal around the entire wetted surface structure with the exception of two areas: the ship's liner seams and the waterline. Complex surface areas such as the keel, sonar, stern and bow were merged together, which created liner seams. Where the liner seams were fused together, several gaps occurred. To ensure that there were no abrupt changes in the mesh topology around these gaps, a wedge shaped element was inserted to smooth out the transition. The second compromise to the

orthogonality of the fluid liner was along the waterline. For the DDG-81 shock trial, the required waterline was 21.5 feet. The FEM model of the ship was 21.2 feet from the bow to structural frame 370. From Frame 370 to the stern it graduated up to 25.75 feet. In order to maintain the waterline at the required 21.5-foot waterline, a second fluid mesh liner was used. The second mesh liner, eight inches thick, was merged with the first 7-inch layer to step the waterline down to the required 21.5 feet.

Therefore, the new two-layer fluid mesh liner, was used to:

- Maintain orthogonal elements around the hull.
- Meet the stability requirements for the USA code.
- Ensure proper orientation of the ship with respect to the waterline.
- Serve as the smallest mesh compared in the simulation.

Figure 14 shows the completed inner fluid liner and Table 2 lists the liner fluid volume specifics.

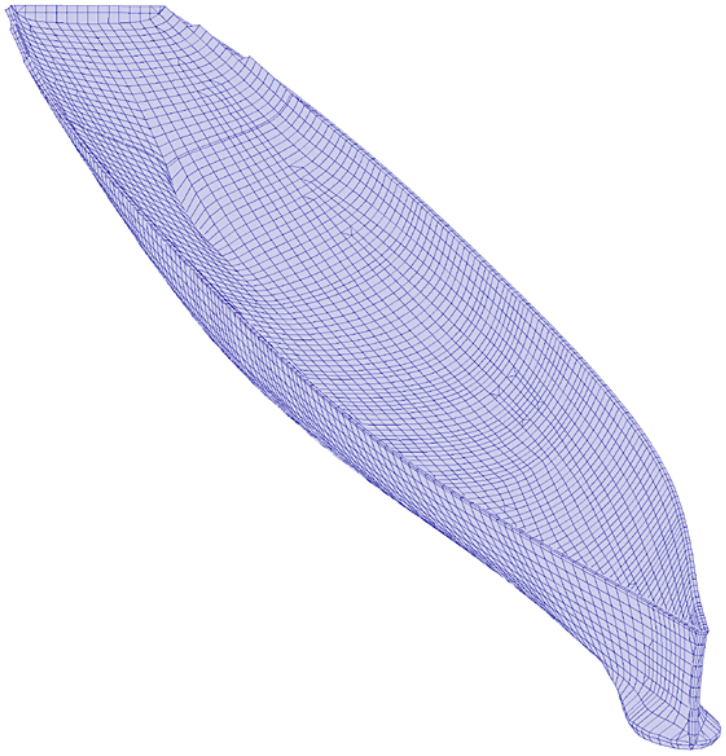

Figure 14. Completed Fluid Mesh Liner. Liner Nominal Size is 15 inches Around Entire Wetted Surface.

D. ONE-HALF FLUID MESH

The one-half fluid mesh was used as the second mesh for comparison in the simulation. Mesh size was determined by setting the depth of the fluid mesh to one-half the depth of the maximum lower cavitation boundary given in Equation 25. As a result, the mesh has a nominal size of 495 feet long, 70 feet wide, and 35 feet deep. Table 2 lists the specifics of the one-half fluid mesh.

To create the fluid mesh, a layer of fluid volume was generated around the ship's structure and merged with the fluid mesh liner. Next, the conical bow and the stern plugs were used to fill and perfectly merge this area in with the remaining fluid mesh. The wedge elements from the fluid mesh liner, and spline curves generated in Truegrid, were used to ensure that the transition of the mesh lines outward around the sonar dome and the bow curve were smooth. Finally, the nodal spacing of the fluid elements was increased radially outward from the mesh liner. This was accomplished by using the AS [Ref. 6] command to specify the nodal spacing of the first element along the edge of the one-half fluid mesh. The remainder of the nodes were then distributed by arc length, ensuring a smooth transition in size of each element as it radiated outward.

Figure 15 shows the completed one-half fluid mesh.

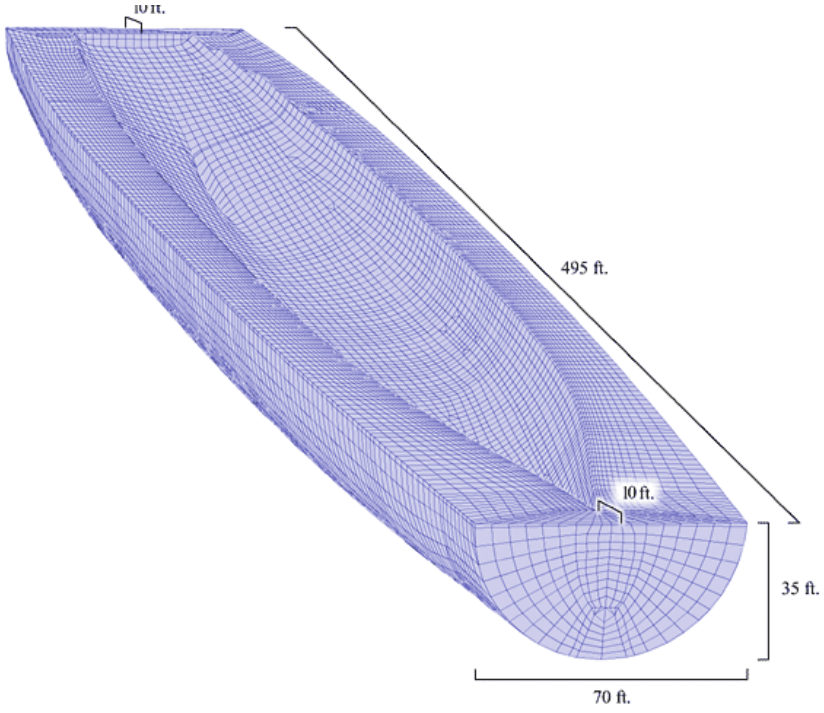

Figure 15. Completed 1/2 Fluid Mesh. 1/2 Mesh Nominal Size is 495'x70'x35'

E. FULL FLUID MESH

The third fluid mesh used in the simulation comparison was the full fluid mesh. Its size was determined by setting the depth of the fluid mesh to the maximum depth of the lower cavitation boundary (Equation 25). The resulting mesh has a nominal size of 573 feet long, 140 feet wide, and 70 feet deep. Figure 16 shows the completed full mesh model and Table 2 lists the full fluid mesh volume specifics.

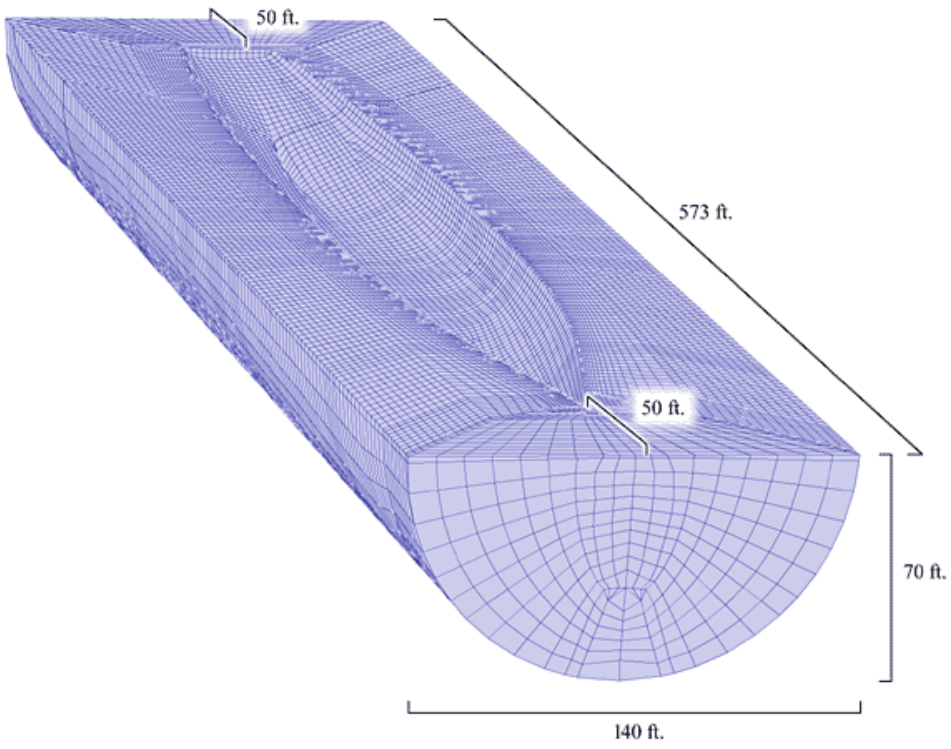

Figure 16. Completed Full Fluid Mesh. Full Mesh Nominal Size is 573'x140'x70'

F. 2X FLUID MESH

The final mesh used in the comparative study was the 2X fluid mesh. Its size was taken as two times the depth of the lower cavitation boundary. This resulted in a nominal mesh size of 632 feet long, 280 feet wide, and 140 feet deep. Table 2 lists the volume specifics for the 2X fluid mesh and Figure 16 presents the finished 2X mesh model.

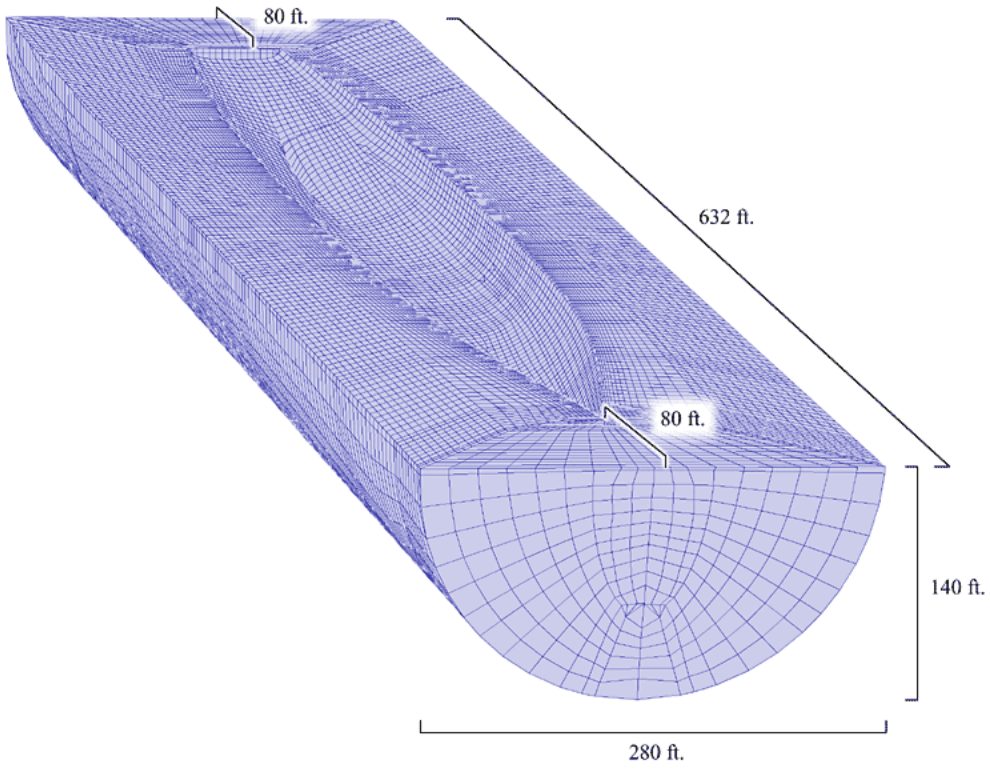

Figure 17. Completed 2X Fluid Mesh. 2X Mesh Nominal Size is 632'x280'x140'

G. FLUID MESH MATERIAL PROPERTIES

Fluid mesh elements are modeled as solid elements with Mat_Acoustic Type 90 material properties in LS-DYNA (weight density of 0.93452E-04 lbf/in^3 and acoustic speed of 60687.6 in/sec). The Mat_Acoustic model tracks pressure stress waves for small irrotational compressible motions with either linear or bilinear behavior. Using the bilinear fluid, the model is unable to transmit negative total pressure, making it possible to model the cavitation area around the hull structure [Ref. 4].

V. SIMULATION AND RESULTS

The actual shock trials consist of three different geometries for the charge location, titled SHOT-1, SHOT-2 and SHOT-3. Because it is the closest and most severe explosion experienced during the shock trials, the SHOT-3 charge geometry is the only investigation addressed in this paper. For this particular geometry, a 10,000-pound HBX-1 explosive charge was detonated off the port side. Table 3, lists the vertical response node locations that are compared in order to determine the minimum depth of fluid required to accurately capture the dynamic response of the full ship's FEM model. For the coupled LS-DYNA/USA simulation, the computational time step is 4.0E-6 seconds and the total computational time is 500ms after the shock wave impinges on the hull structure.

Table 3 Vertical Velocity Response Sensor Location

Sensor	Node	X(Node)	Y(Node)	Z(Node)	Compartment/Location	Compt#/Area
V2000V	120217	5328.0	0.0	82.0	PASSAGE	4-022-0-L
V2002V	142489	4656.0	27.0	82.0	SONAR COOLING EQ RM	4-042-0-L
V2007V	210430	4080.0	0.0	82.0	AMR #1	4-126-0-E
V2008VI	210894	4080.0	174.0	177.0	AMR #1	4-126-0-E
V2009VI	210808	4080.0	-174.0	177.0	AMR #1	4-126-0-E
V2010V	220589	3504.0	0.0	85.5	AMR #1	4-126-0-E
V2011VI	221188	3504.0	216.0	177.0	AMR #1	4-126-0-E
V2012VI	221102	3504.0	-216.0	177.0	AMR #1	4-126-0-E
V2013V	221601	3504.0	0.0	280.0	ENGINE RM #1	4-174-0-E
V2014V	230461	2952.0	0.0	85.5	AMR #2	4-220-0-E
V2016V	242399	2544.0	0.0	116.0	ENGINE RM #2	4-254-0-E
V2018VI	340992	672.0	0.0	364.8	PASSAGE	2-410-0-L
V2019V	340167	672.0	0.0	196.5	GENERATOR RM	3-370-0-E
V2020V	350052	288.0	0.0	211.0	STEERING GEAR RM	4-442-0-E
V2026V	312302	1992.0	0.0	55.0	ESCAPE TRUNK	4-296-1-T
V2032V	330764	1152.0	0.0	196.0	FAN ROOM	3-362-0-E
V2034V	330759	1152.0	-135.0	193.3	FAN ROOM	3-362-0-E
V2035V	330769	1152.0	135.0	193.3	FAN ROOM	3-362-0-E
V2108V	212196	4080.0	312.0	390.0	PASSAGE	1-078-1-L
V2124V	222060	3504.0	-375.4	390.0	PASSAGE	1-158-1-L
V2125V	222436	3504.0	375.4	390.0	PASSAGE	1-158-8-L

A. RAYLEIGH DAMPING

The FEM ship structural damping was implemented by using the LS-DYNA Damping_Global and Damping_Part_Stiffness keyword options. The global damping option applies the mass weighted nodal damping to the mass centers of the rigid bodies. The "damping part stiffness" option applies the Rayleigh stiffness damping coefficients to the specified parts. The Rayleigh damping matrix is represented by the following expression:

$$C = \alpha M + \beta K \tag{28}$$

where C, M, and K are the damping, mass and stiffness matrices. The mass and stiffness proportional damping constants are represented as α and β, respectively [Ref. 7]. Based on a comprehensive study of the two-second ship shock trial data for USS John Paul Jones (DDG-53), damping values used for this thesis were: $\alpha = 19.2$ and β=2.09x10^{-6} [Ref. 23].

B. RUSSELL ERROR FACTOR

The Russell error factor was developed in order to quantify the error, or correlation, between the two data sets of the simulation results and measured shock trial transient response. The Russell correlation and error factors are given by the following equations [Ref. 22]:

$$A=\sum_{i=1}^{N} f_1(i)^2 \tag{29}$$

$$B=\sum_{i=1}^{N} f_2(i)^2 \tag{30}$$

$$m=\frac{(A-B)}{\sqrt{AB}} \tag{31}$$

$$C=\sum_{i=1}^{N} f_1(i) f_2(i) \tag{32}$$

$$p=\frac{C}{\sqrt{AB}} \tag{33}$$

$$RM=\text{sign}(m)\log_{10}(1+|m|) \tag{34}$$

$$RP=\frac{\cos^{-1}(p)}{\pi} \tag{35}$$

$$RC=\sqrt{\frac{\pi}{4}\left(RM^2+RP^2\right)} \tag{36}$$

where f_1, and f_2 are the two vectors of transient data being considered. RM, RP and RC are the Russell magnitude, phase and comprehensive error factors, respectively.

Magnitude and phase error factors are used to compare both sets of data results. The magnitude of the error factor indicates which response is larger in magnitude, the simulation results or the shock trial results. The phase error factor is interpreted as a direct measure of the phase angle between the two responses. Phase error is bound between 0.0 and 1.0, while the magnitude error is unbound. Even though the magnitude error is unbound, it was developed in such a way that the worst magnitude difference is equal to 1.0. This scaling of the magnitude and phase error factors allows formulation of a comprehensive error factor, with 1.0 being the worst case [Ref. 22].

Reference 24, suggests that the Russell comprehensive error factor is the most suitable for the shock transient response comparison. It also recommends that the following criteria be used to rank the correlation between the simulation data and the actual shock trial data.

Table 4 Shock Simulation Transient Response Correlation Criteria

$RC \leq 0.15$	Excellent
$0.15 \leq RC \leq 0.28$	Acceptable
$RC \geq 0.28$	Poor

Due to the validity of this previously documented research, the acceptance criteria for the comprehensive error factors given in Table 4 were used for this study.

C. SIMULATION RESULTS

A vertical velocity time history of 200 millisecond (msec) was used as the primary comparison for determining the minimum depth of fluid required to accurately capture the actual ship response. This time history was the first critical point that was sufficient to capture the initial peak, or early time, response of the structure. The Russell error factor was then used to calculate the difference between the measured and

calculated data. The overall criteria of $RC \leq 0.28$ was used to determine which fluid mesh best captured the response of the actual shock trial data. Due to the extensive number of plots, only four of the 200msec vertical velocity response plots are presented in this study. Those chosen, the two keel and the two bulkhead sensors, best represent the overall data response of the fluid mesh model. This allows for maximum data interpretation within a minimum, but key, group of plots. All of the Russell's error factors for the vertical velocity meters are presented to show a better depiction of the comparison of the four fluid mesh models.

Next, a time history of 500msec was presented with the optimum, or full fluid, mesh (Section 2E). This was the first time history that was able to capture the early time peak response as well as later ringing of the low amplitude velocity. This data was compared to the actual shock trial data and Russell's error factors were used to calculate how well the two compared. Due to space limitations, only eight of the 500msec response plots are presented in this section, the remainder are in Appendix A. Finally, an initial investigation into the vertical acceleration comparison of the simulation results to the trial results was conducted. The results of the comparison are contained in Appendix A.

The shock trial data and LS-DYNA/USA simulation data was prepared in the following manner. First, the actual shock trial data was low pass filtered at 250Hz to remove any undesired high frequency noise. Due to the movement of the ship, the majority of the energy in the response is in the lower frequency. Therefore, filtering out the 250Hz high frequency noise allows a more accurate picture of the transient response of the actual shock trial data. Next, actual shock trial data was high pass filtered at 3Hz to remove the low frequency drift inherent in the velocity meters. The LS-DYNA/USA simulation data was prepared in a similar manner. The data was filtered at 1.8Hz and 250Hz to remove the high frequency noise and low frequency drift of the data. Since LS-DYNA does not compensate for the low frequency rigid body mode effects, the simulation data was required to be high pass filtered at 1.8Hz. All filtering for the LS-DYNA/USA simulation data and shock trial data was accomplished with a 2-pole Bessel high and low pass filter.

1. 200msec Vertical Velocity Response Comparison

Four 200msec plots were chosen that showed the optimum and the minimum results for the keel and bulkhead LS-DYNA/USA simulation data. Each plot was then compared against the four fluid mesh models. Figure 18 represents keel sensor number V2012V and the best keel response comparison obtained. The sensor was located in Auxiliary Machinery Room 1, starboard 18 feet of centerline, and 84 feet forward of the initial shock wave point of impact. By implementing the Russell's error factor, measures for sensor V2012V were determined for all four fluid mesh models and are presented in Table 5 below. Comparisons show that the full fluid mesh most accurately captures the 4.3 ft/sec initial vertical velocity response and the first period of the ship response. This is the best correlation between the four fluid meshes and the shock trial simulation for sensor V2012V. The Russell's error factor measures were well within the excellent correlation criteria for the full fluid mesh with: RM=-0.0100, RP=0.0848, and RC=0.0756.

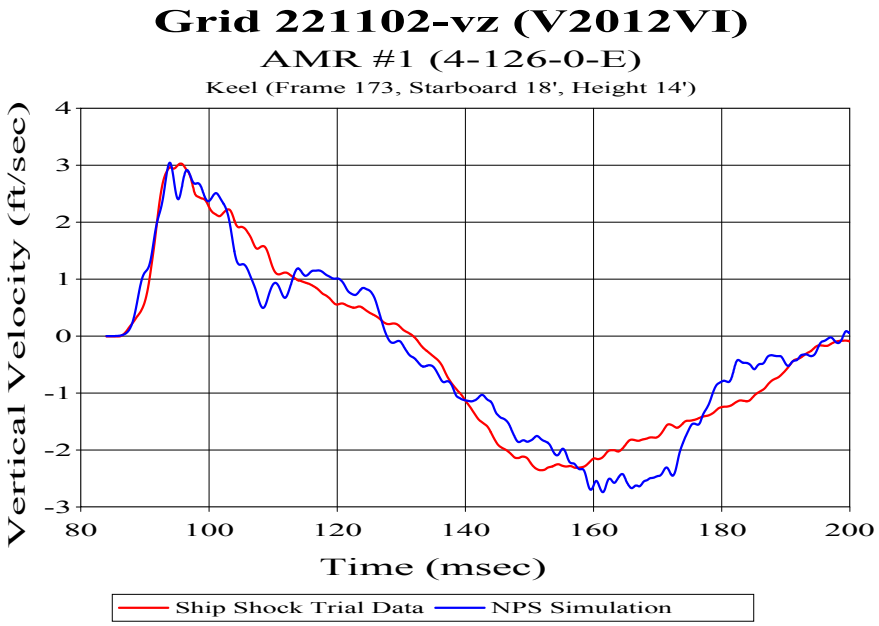

Figure 18. Keel Sensor V2012VI 200msec Comparison

Table 5 Keel Sensor V2012VI Russell's Error Comparison

MESH	RM	RP	RC
FLUID LINER	-0.2193	0.3052	0.3331
1/2 MESH	-0.3243	0.1026	0.3015
FULL MESH	-0.0100	0.0848	0.0756
2X MESH	-0.3097	0.1485	0.3044

The least accurate keel correlation between the four fluid meshes and the shock trial data was with sensor V2000V (Figure 19). This sensor was located centerline in Passageway 235 feet forward of the point of shock wave impact. Plots show that although the best results for sensor V2000V were obtained with the full fluid mesh, it showed a poor comparison between the 4.6-ft/sec initial velocity experience of the ship and that predicted by the LS-DYNA/USA simulation. This dissimilarity was due to the instability and oscillation of the ship shock trial data, which resulted in a large comprehensive error for this sensor. The Russell's error factor measure for the Full Fluid Mesh was RM=-0.2445, RP=0.2909, and RC=0.3368. Table 6 lists the error factor measures for sensor V2000V for the four fluid meshes.

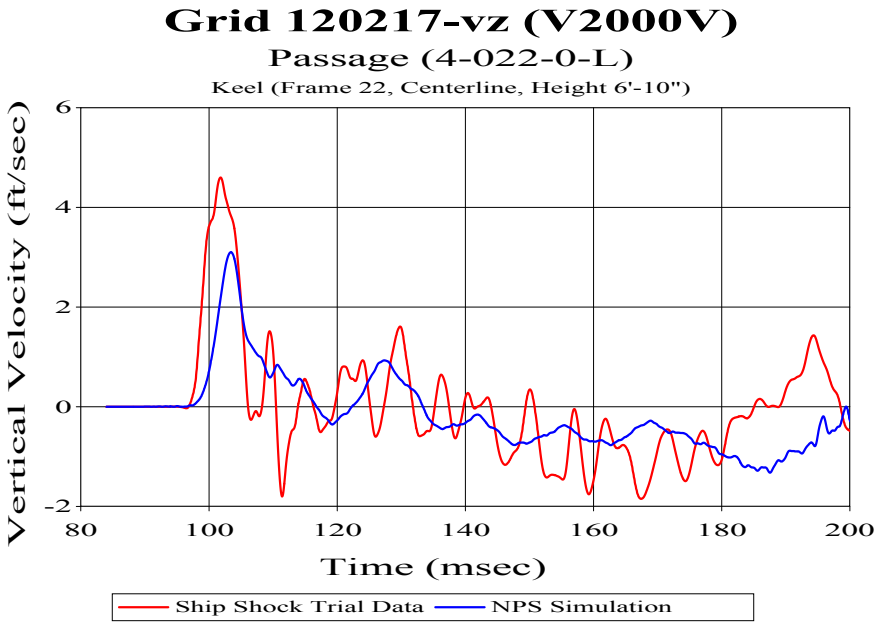

Figure 19. Keel Sensor V2000V 200msec Comparison

Table 6 Keel Sensor V2012VI Russell's Error Comparison

MESH	RM	RP	RC
FLUID LINER	-0.3284	0.2920	0.3894
1/2 MESH	-0.3978	0.2966	0.4397
FULL MESH	-0.2445	0.2909	0.3368
2X MESH	-0.6022	0.3148	0.6022

Figure 20 shows that the best bulkhead vertical velocity response comparison was at sensor V2013V. This sensor was located in Engine Room Number 1, at Frame 174, 83 feet forward of the point of initial shock wave impact. The keel sensor was located centerline and experienced an initial vertical velocity of 2.66 ft/sec. Correlation between the four fluid meshes and the actual shock trail data was best represented by the full fluid mesh. The full mesh accurately captured the initial vertical velocity and first period of the ship response. Error factor measures between the full mesh response and the shock trial data show excellent results, where: RM=-0.0303, RP=0.0854, and RC=0.0803. Table 7 lists the Russell's error factors for the four fluid meshes.

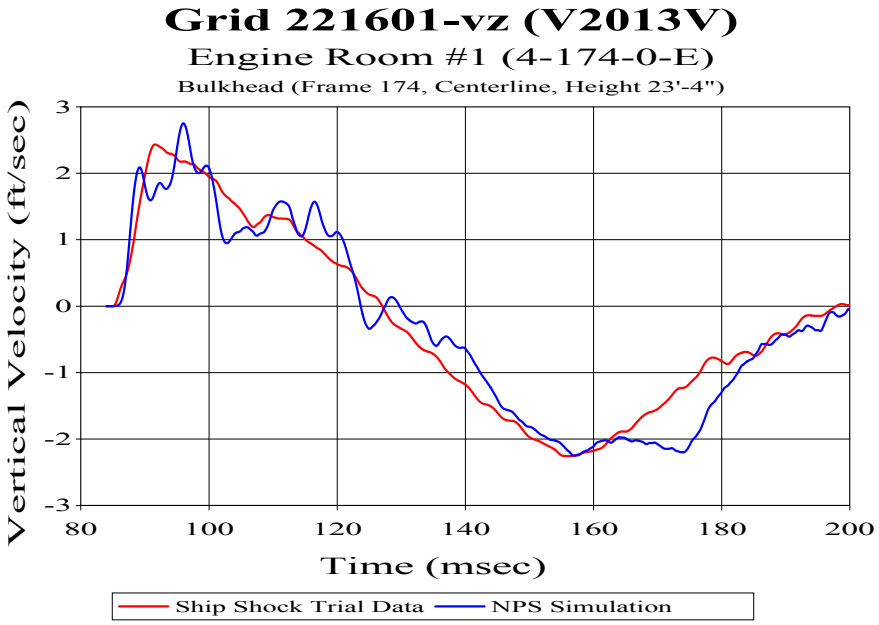

Figure 20. Bulkhead Sensor V2013V 200msec Comparison

Table 7 Bulkhead Sensor V2013VI Russell's Error Comparison

MESH	RM	RP	RC
FLUID LINER	-0.2517	0.2790	0.3330
1/2 MESH	-0.2881	0.1473	0.2868
FULL MESH	-0.0303	0.0854	0.0803
2X MESH	-0.3048	0.1543	0.3027

The last bulkhead sensor comparison was sensor V2018VI. This sensor was located in Passageway 2-410-0-L, 153 aft of the initial point of impact. The initial vertical velocity of the sensor was approximately 4.6 ft/sec. Again, the best results were obtained with the full fluid mesh simulation. The Russell's error factor measures for the 200msec comparison were: RM=-0.1336, RP=0.1525, and RC=0.1796. Although these results represented the worst bulkhead sensor response comparison for the 200msec run, they are still well within the acceptable criteria range. Table 8 lists sensor V2018VI's 200msec comparison for the four fluid meshes.

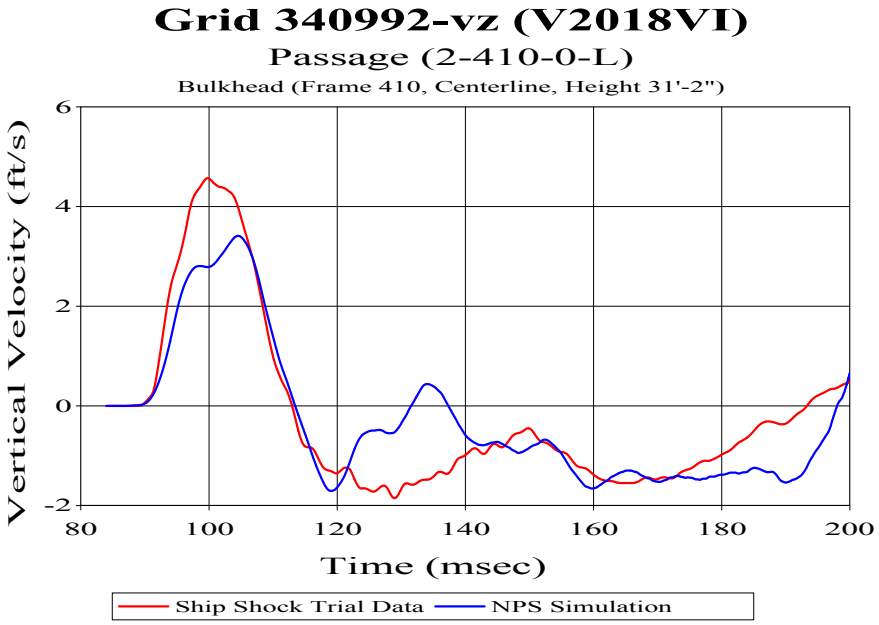

Figure 21. Bulkhead Sensor V2018V 200msec Comparison

Table 8 Bulkhead Sensor V2018VI Russell's Error Comparison

MESH	RM	RP	RC
FLUID LINER	-0.2055	0.2405	0.2803
1/2 MESH	-0.0807	0.2748	0.2538
FULL MESH	-0.1336	0.1525	0.1796
2X MESH	-0.3806	0.2692	0.4132

From the study of all twenty-one vertical velocity sensors, the full fluid mesh was the most accurate mesh used to capture the actual ship's response. Its model predicted the best initial vertical response and first period of the ship dynamic response. Table 9 contains a detailed listing of the Russell error factors for all vertical velocity sensors for the full fluid mesh model in the 200msec comparisons. The results show that twenty of the twenty-one comprehensive error comparisons are below 0.28. Of the twenty that are below 0.28, fourteen are below 0.15, and of these, four are below 0.10. This clearly shows that the full fluid mesh model accurately captures the early time response and is an excellent comparison to the actual shock trial results.

The 200msec Russell error comparisons for the remaining three fluid mesh models investigated are contained in Appendix A. For these models, the comprehensive error factors decreased as the mesh size increased out to the cavitation boundary, and increased as the mesh was truncated further out. Dr. John DeRuntz, author of the USA code, presented a possible explanation for this disparity. He suggested that as the fluid region and mesh size increased past a certain point, the shock wave front could possibly be lost to dispervisve effects in an extremely large mesh. This explanation can be correlated to the results seen in the decrease in initial peak velocity as the fluid mesh size was increased from the full fluid mesh to the 2X Mesh.

Table 9 Full Fluid Mesh 200msec Russell's Error Comparison

Sensor	RM	RP	RC
V2012VI	0.0100	0.0848	0.0756
V2013V	0.0303	0.0854	0.0803
V2124V	-0.0233	0.0992	0.0903
V2009VI	0.0060	0.1084	0.0962
V2016V	-0.0077	0.1152	0.1023
V2011VI	-0.0310	0.1204	0.1102
V2108V	0.0109	0.1262	0.1123
V2010V	-0.0447	0.1199	0.1134
V2125V	-0.0596	0.1222	0.1205
V2002V	0.0565	0.1370	0.1314
V2026V	-0.0789	0.1255	0.1314
V2034V	-0.1006	0.1092	0.1316
V2008VI	-0.0134	0.1580	0.1405
V2014V	0.0656	0.1526	0.1472
V2035V	-0.1153	0.1272	0.1521
V2020V	-0.1024	0.1437	0.1564
V2007V	-0.0988	0.1478	0.1576
V2032V	-0.1261	0.1562	0.1779
V2018VI	-0.1336	0.1525	0.1796
V2019V	-0.1872	0.1532	0.2144
V2000V	-0.2445	0.2909	0.3368

2. 500msec Vertical Velocity Response Comparison

From the comparison of the four fluid mesh models presented, the full mesh was determined to be the optimum and the minimum amount of mesh required to accurately capture the response of the FEM model. The full fluid mesh was then used to compare the simulation data and the shock trial data out to 500msec. The following eight plots present four bulkhead and four keel sensors to quantify how well the simulation data compared to the actual shock trial data. These plots also present the most and the least accurate bulkhead and keel vertical response comparisons obtained with the LS-DYNA/USA simulation data. The remaining 13 vertical velocity plots are contained in Appendix A.

Figures 22 and 23, show the vertical velocity response at the bulkhead, Frame 127 of Auxiliary Machinery Room Number 1 (AMR1). This compartment was just forward of amidships and approximately 130 feet forward of the initial shock wave impact point, Frame 257. The two sensors, V2008VI and V2009VI, were located 14ft 8in port and starboard of centerline, respectively. Maximum vertical velocity in this compartment

was approximately 4 ft/sec. These plots show that the simulation predicted velocity responses compared extremely well with the actual shock trial data. The results for sensors V2008VI and V2009VI fell in the acceptable and excellent Russell's error criteria range, respectively. The magnitude, phase, and comprehensive error factors for sensor V2008VI were: RM=-0.0488, RP=0.2334, and RC=0.2113; and for sensor V2009VI they were: RM=-0.0386, RP=0.1562, RC=0.1425.

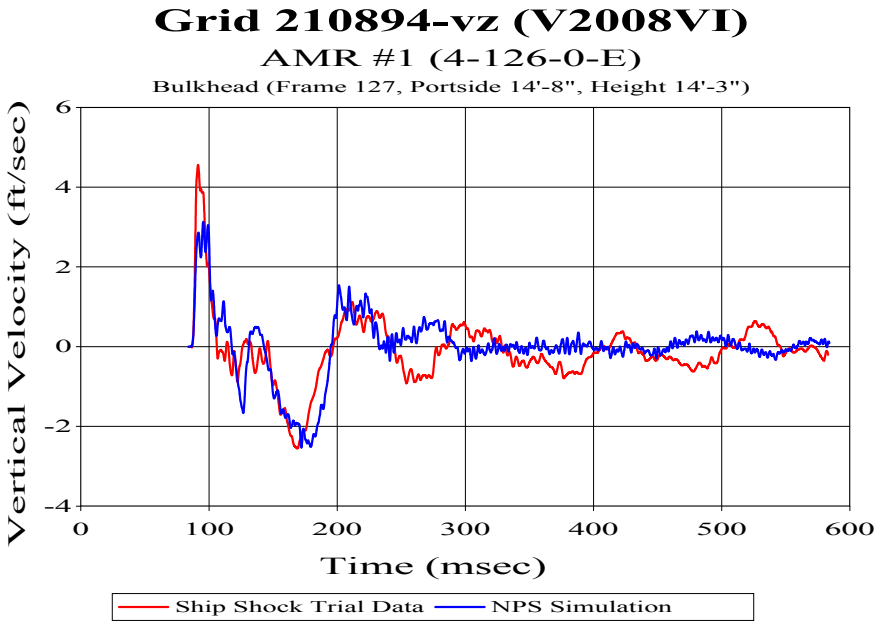

Figure 22. Bulkhead Sensor V2008VI: (RM=-0.0488, RP=0.2334, RC=0.2113)

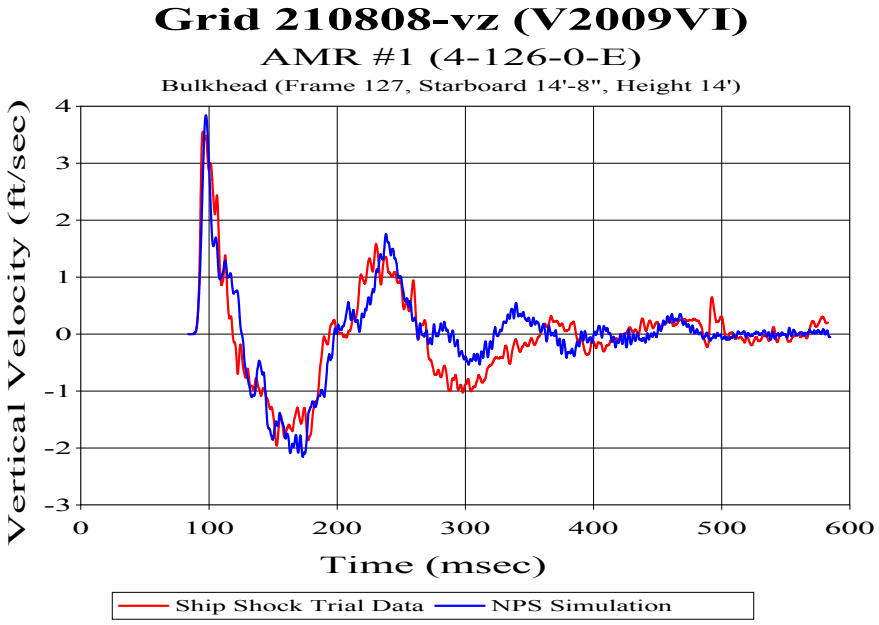

Figure 23. Bulkhead Sensor V2009VI: (RM=-0.0386, RP=0.1562, RC=0.1425)

The bulkhead vertical velocity plot of sensor V2124V, Frame 173 and 31 feet to starboard is shown in Figure 24. The sensor was located 84 feet forward of the initial shock wave impact point. Initial vertical velocity of the bulkhead was 3.4 ft/sec and compared extremely well to the simulation predicted vertical velocity. The Russell's error measure for the sensor were: RM=-0.0583, RP=0.1424, and RC=0.1363. The RC of 0.1363 classifies the correlation as excellent and represented the best correlation obtained for the bulkhead vertical velocity comparisons. A Russell's error factor magnitude of RM=-0.0583, indicated that the level of the simulation result compared almost exactly with the shock trial data response. This was due to how well the magnitude of the simulation response compared to that of the shock trial response up to 200ms (Figure 25). For this time frame, the RM=-0.0233, RP=0.0992, and RC=0.0903. These numbers are an excellent correlation between the simulated and the actual shock trial data.

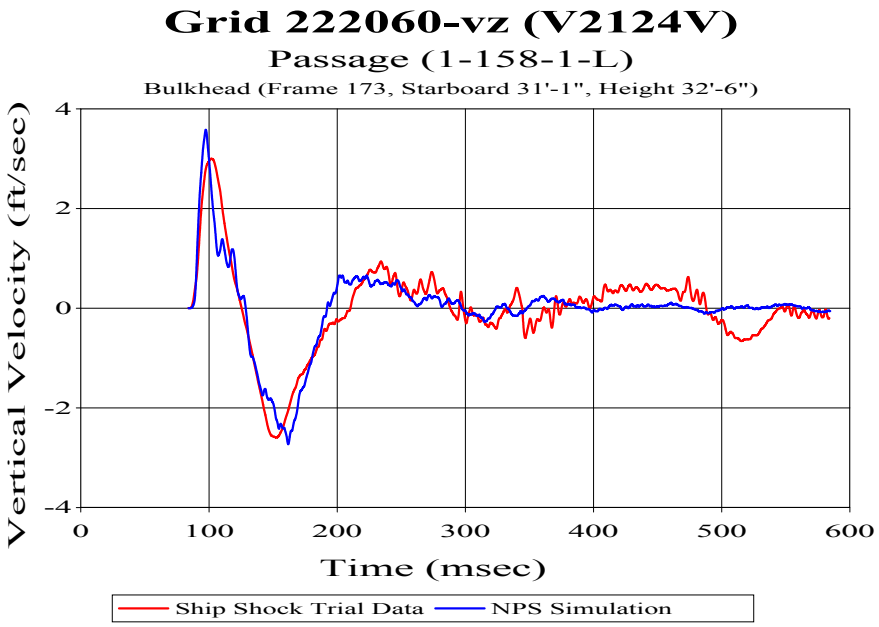

Figure 24. Bulkhead Sensor V2124V: (RM=-0.0583, RP=0.1424, RC=0.1363)

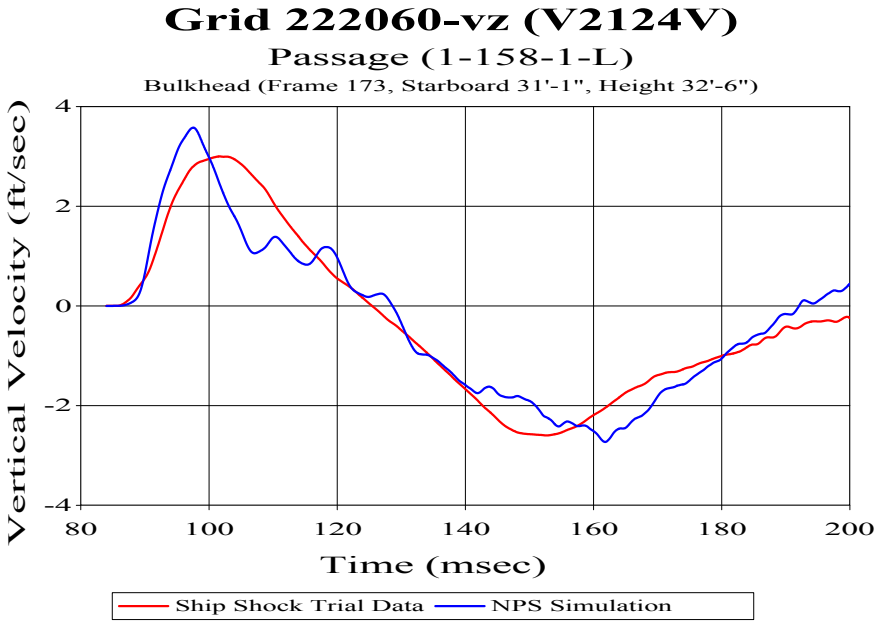

Figure 25. Bulkhead Sensor V2124V to 200ms: (RM=-0.0233, RP=0.0903, RC=0.0903)

The final bulkhead vertical velocity comparison was for sensor V2019V, located 153 feet after of the point of initial impact, Figure 26. The sensor was located on the centerline in the generator room at Frame 410. This comparison showed the most disparity between the LS-DYNA simulation results and the actual shock trial results. The Russell's error factor measures for this comparison were: RM=-0.1059, RP=0.2331, and RC=0.2269. Although higher than the other comprehensive RC's, the 0.2269 result was still well within the 0.28 acceptability correlation criteria.

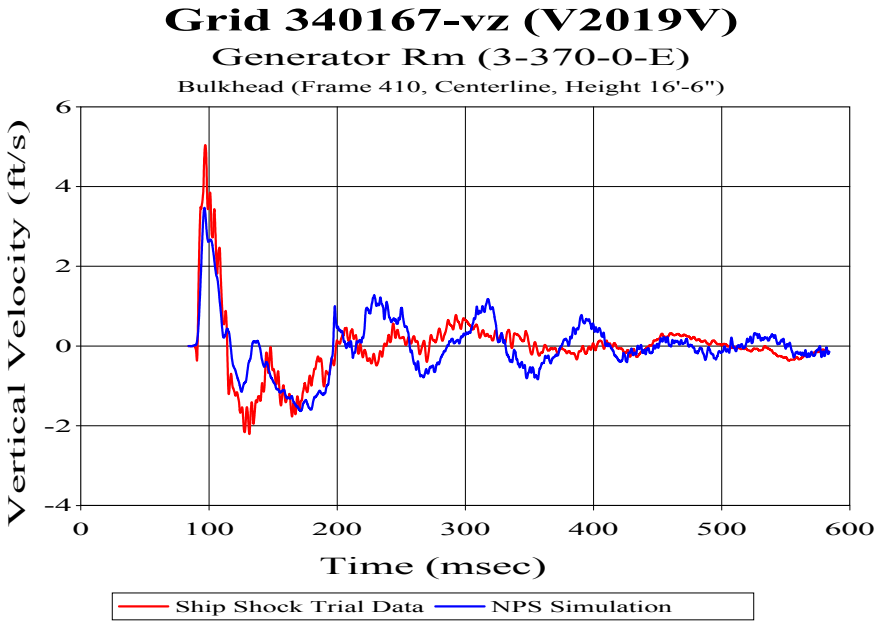

Figure 26. Bulkhead Sensor V2019V: (RM=-0.1059, RP=0.2331, RC=0.2269)

The next four vertical velocity response comparisons were for the four keel response sensors. The first two that were compared were the two keel sensors for AMR1, V2011V and V2012V. These two sensors were in the same compartment as the two bulkhead sensors V2008VI (Figure 22) and V2009VI (Figure 23). The two keel sensors were located at Frame 172, located 85 feet forward of the initial shock wave impact

point, and 18 feet port and starboard, respectively. Sensor V2011VI was located on the portside and showed an acceptable parallel between the LS-DYNA/USA simulation data and the shock trial data (Figure 27). The Russell's error factor measure for the comparison was: RM=-0.0906, RP=0.1972, and RC=0.1923. Although the results were well within the acceptable criteria, Figure 27 shows that the simulation results compared almost exactly with the actual trial results up to 200ms. The RC of 0.1923 for the 500ms comparison was due to the larger phase error in the simulation results after 200ms. Up to 200ms, the Russell's error factor measures were: RM=-0.0310, RP=0.1204 and RC=0.1102, which showed an excellent correlation between the data for the initial loading response.

Sensor 2012V, 18 feet starboard of centerline showed an excellent parallel between the simulation and actual response results (Figure 28). The Russell's error factor measure for the comparison was: RM=-0.0263, RP=0.1326, and RC=0.1200. This correlation was the best keel comparison obtained between the LS-DYNA/USA simulation results and the actual shock trial results.

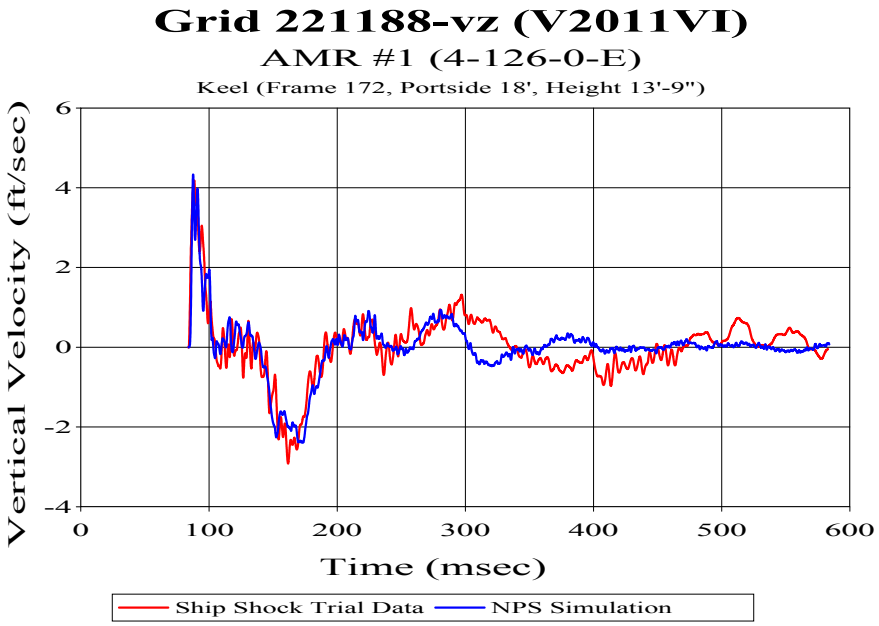

Figure 27. Keel Sensor V2011VI: (RM=-0.0906, RP=0.1972, RC=0.1923)

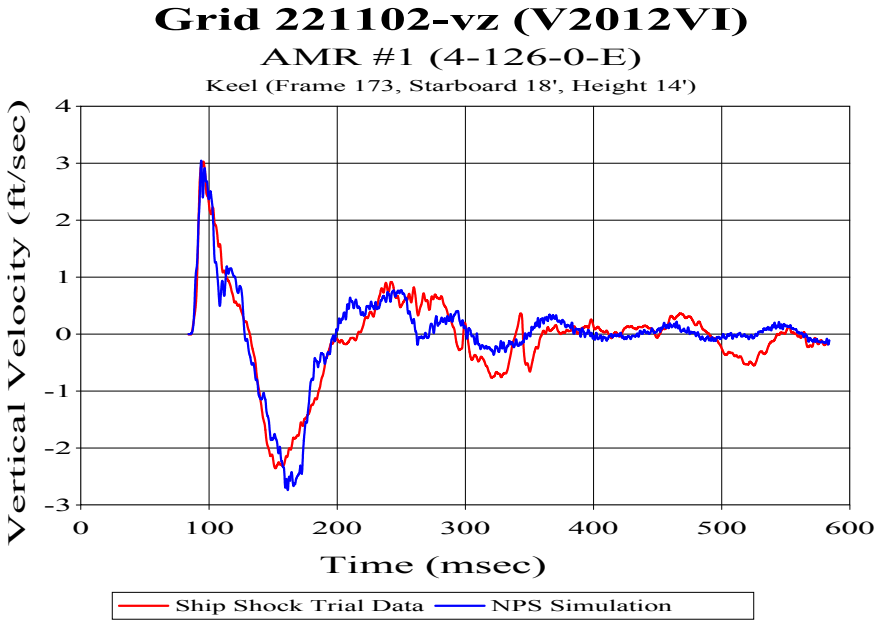

Figure 28. Keel Sensor V2012VI: (RM=-0.0263, RP=0.1329, RC=0.1200)

Figure 29 shows the vertical velocity response at keel sensor V2016V. This sensor was located in Engine Room Number 2, at Frame 254, 3 feet forward of the point of initial shock wave impact. This keel sensor was located three inches to starboard of centerline and captured the 4.4 ft/sec vertical velocity initially experienced by the amidships section of the hull. The LS-DYNA simulation results compared extremely well to the actual shock trial response with the error factor measures of: RM=-0.0291, RP=0.1592, and. RC=0.1434. These results were within the excellent correlation criteria and showed that the simulation data accurately captured the initial vertical velocity response at the point of shock wave impact.

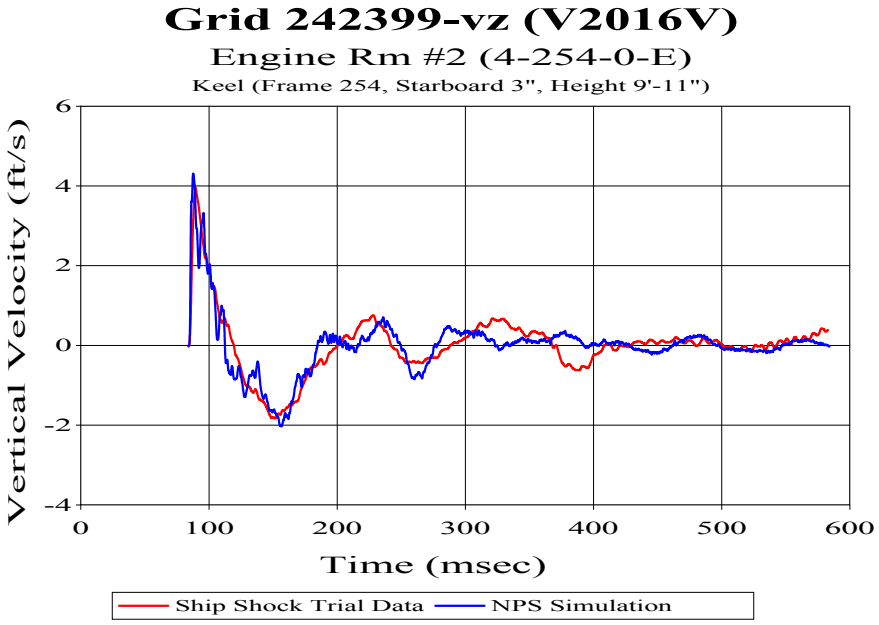

Figure 29. Keel Sensor V2016V: (RM=-0.0291, RP=0.1562, RC=0.1434)

The fourth and final keel sensor comparison presented is for sensor V2000V, located in a passageway 235 feet forward of the point of shock wave impact. Its response represented the least accurate keel sensor correlation between the simulation data and the shock trial data (Figure 30). LS-DYNA/USA simulation data was unable to capture the ship's initial vertical response of 4.6 ft/sec. Deviation was due to the fluctuation of the ship shock trial data, which resulted in a large comprehensive error for this sensor. This lead to a weak association between the two data sets. Russell's error factor measures for the comparison were: RM=-0.2419, RP=0.3164, and RC=0.3529.

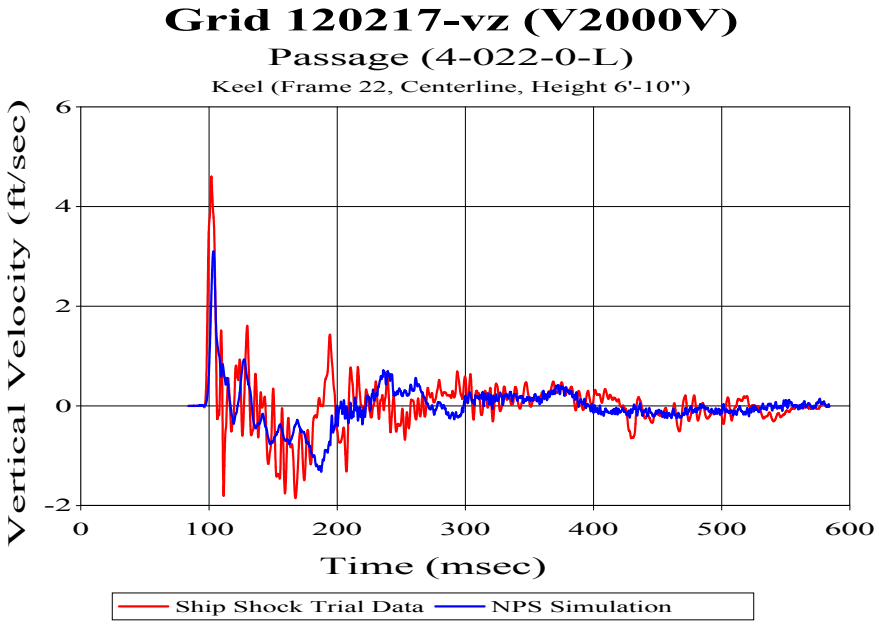

Figure 30. Keel Sensor V2000V: (RM=-0.2419, RP=0.3164, RC=0.3529)

Table 10 lists the entire Russell error factor measures for the twenty-one keel and bulkhead sensors that were compared in this study. These values are presented from the best to the least accurate parallels in comprehensive Russell's error factor measures. The table shows that twenty of the twenty-one keel and bulkhead sensors were within the acceptable correlation criteria of $RC \leq 0.28$. Five of the sensors, V2012VI, V2124V, V2013V, V2009VI, and V2016V, were in the excellent correlation criteria category. The remainder of the acceptable sensor RC's ranged from 0.1577 to 0.2285, with the mean value of the results equal to $RC_{mean}=0.2003$. Sensor V2000V, presented the most inferior correlation between the simulation data and actual shock trial data with a comprehensive error factors of 0.3529. The large comprehensive error factors were due to the poor relationship between the magnitude and phase of the simulation and the shock trial data.

Overall, the correlation between the LS-DYNA/USA results and the ship shock trial data compared extremely well and demonstrated the validity of the modeling and simulation techniques presented in this study. Appendix A presents the remaining thirteen plots of the comparisons between the LS-DYNA/USA simulation data and the shock trial data.

Table 10 Russell Error Factor's for all Twenty Vertical Velocity Sensor's

Sensor	RM	RP	RC
V2013V	-0.0263	0.1329	0.1200
V2012VI	-0.0583	0.1424	0.1363
V2108V	0.0038	0.1543	0.1368
V2124V	-0.0386	0.1562	0.1425
V2016V	-0.0291	0.1592	0.1434
V2009VI	-0.1113	0.1388	0.1577
V2034V	0.0173	0.1787	0.1591
V2026V	-0.0542	0.1849	0.1707
V2014V	0.0372	0.1949	0.1759
V2011VI	-0.0906	0.1972	0.1923
V2002V	-0.1240	0.1873	0.1991
V2035V	-0.0513	0.2243	0.2039
V2018VI	-0.1039	0.2055	0.2041
V2008VI	-0.1290	0.1937	0.2063
V2125V	-0.0488	0.2334	0.2113
V2010V	-0.0449	0.2456	0.2213
V2032V	0.1399	0.2083	0.2224
V2020V	0.1334	0.2165	0.2254
V2019V	-0.1059	0.2331	0.2269
V2007V	-0.1464	0.2122	0.2285
V2000V	-0.2419	0.3164	0.3529

THIS PAGE INTENTIONALLY LEFT BLANK

VI. CONCLUSION AND RECOMMENDATIONS

This thesis investigates the use of computer ship and fluid modeling, coupled with underwater explosion simulation and compares it to actual shock trial data from the USS Winston S. Churchill (DDG-81). The three-dimensional simulation of the DDG-81 shock trials was performed using the coupled LS-DYNA/USA computational codes. Of particular concern in this study was the amount of fluid that must be modeled to accurately capture the structural response of a full ship finite element model. Four fluid meshes were constructed and presented to study the ship's response to an underwater explosion. Each simulation data was analyzed to determine which mesh best represented the actual ship shock trial results.

The study presented and compared twenty-one vertical velocity sensors located throughout the ship and compared the simulated data to the shock trial data. A clock time of 200msec was used to determine which fluid mesh model presented was the best comparison to the actual shock trial data. The Russell error measure was used to quantify and determine which mesh had the best correlation between the simulated and actual data. From this analysis, it was determined that the full fluid mesh, with a minimum fluid depth extending out to the maximum cavitation depth, was required to accurately capture the dynamic response of the shock trial. With this mesh, twenty of the twenty-one comprehensive error comparisons were below 0.28. Of the twenty that were below 0.28, fourteen were below 0.15, and of these four were below 0.10. This clearly shows that the full fluid mesh model most accurately captured the early time response and compared well to the actual shock trial results.

Finally, this study presented the comparison of the LS-DYNA/USA simulation using the full fluid mesh to the shock trial data for a clock time of 500ms. This was done to quantify how well the simulated data compared to shock trial data for the transient, or late time response. This study showed that twenty of the twenty-one keel and bulkhead sensors were within the acceptable correlation criteria of $RC \leq 0.28$. Sensors V2012VI, V2124V, V2013V, V2009VI and V2016V, were in the excellent correlation criteria category with comprehensive error factors of 0.1200, 0.1363, 0.1368, 0.1425, and 0.1434, respectively. Sensor V2000V presented the poorest correlation between the two sets of data with a comprehensive error factor of 0.3529.

The data that was presented in this study clearly demonstrates the validity of the computer modeling and simulation techniques in the analysis of actual ship shock trials data. It shows that these state of the art methods could possibly be used to:

- Identify potential high-risk areas during future shock trials.
- Provide an assessment tool for future design changes.
- Analyze different charge geometries for addressing live fire testing and evaluation issues for current real world threats.

Recommendations for areas of additional study:

1. In order to evaluate the ship's hull and system integrity, ship shock trials have traditionally been conducted with large charges in far-field explosions. However, attacks such as the strike on the USS Cole, have shown that severe damage by a near-field explosion can incapacitate a Naval vessel. It is suggested that current ship shock modeling and simulation technology be used to investigate near-field explosions and how they affect the survivability and vulnerability of a ship's hull.

2. The USS Winston S. Churchill shock trial simulations produced excellent calculations for the overall response of the ship. This investigation could be taken a step further by looking at the effects of shock trials on the ship's individual parts. Potential problem areas with specific shipboard equipment could be determined and analyzed under a replicated shock environment.

APPENDIX A. DDG81 RESPONSE PLOTS

A. 200MS VERTICAL VELOCITY COMPARISONS

Table 11 Fluid Mesh Liner 200msec Russell's Error Comparison

Sensor	RM	RP	RC
V2000V	-0.3284	0.2920	0.3894
V2002V	-0.0953	0.3096	0.2871
V2007V	-0.2074	0.2989	0.3224
V2008VI	-0.1413	0.3070	0.2995
V2009VI	-0.2038	0.2996	0.3211
V2010V	-0.1796	0.2776	0.2930
V2011VI	-0.2351	0.2723	0.3188
V2012VI	-0.2193	0.3052	0.3331
V2013V	-0.2517	0.2790	0.3330
V2014V	0.0409	0.2803	0.2510
V2016V	-0.0838	0.2462	0.2306
V2018VI	-0.2055	0.2405	0.2803
V2019V	-0.2193	0.2787	0.3143
V2020V	-0.2213	0.2682	0.3081
V2026V	-0.0328	0.2810	0.2508
V2032V	-0.1792	0.2799	0.2945
V2034V	-0.1850	0.2599	0.2828
V2035V	-0.1208	0.3076	0.2929
V2108V	-0.2230	0.3371	0.3582
V2124V	-0.1629	0.3625	0.3523
V2125V	-0.2443	0.3068	0.3476

Table 12 1/2 Fluid Mesh 200msec Russell's Error Comparison

Sensor	RM	RP	RC
V2000V	-0.3978	0.2966	0.4397
V2002V	-0.8131	0.3959	0.8015
V2007V	-0.5015	0.1983	0.4779
V2008VI	-0.5190	0.4017	0.5816
V2009VI	-0.4634	0.1357	0.4279
V2010V	-0.2777	0.1873	0..2969
V2011VI	-0.2966	0.1386	0.2901
V2012VI	-0.3243	0.1026	0.3015
V2013V	-0.2881	0.1473	0.2868
V2014V	0.0663	0.1722	0.1635
V2016V	-0.0858	0.1228	0.1328
V2018VI	-0.0807	0.2748	0.2538
V2019V	0.0459	0.1796	0.1643
V2020V	0.1331	0.1877	0.2039
V2026V	-0.0380	0.1802	0.1632
V2032V	0.0228	0.1198	0.1081
V2034V	0.0922	0.0881	0.1130
V2035V	0.0382	0.1219	0.1132
V2108V	-0.5072	0.3714	0.5571
V2124V	-0.3295	0.0879	0.3023
V2125V	-0.3143	0.1457	0.3070

Table 13 2X Mesh 200msec Russell's Error Comparison

Sensor	RM	RP	RC
V2000V	-0.6022	0.3148	0.6022
V2002V	-0.3407	0.1664	0.3360
V2007V	-0.4032	0.2202	0.4071
V2008VI	-0.3683	0.2736	0.4066
V2009VI	-0.3466	0.1847	0.3481
V2010V	-0.3472	0.1959	0.3533
V2011VI	-0.3287	0.1901	0.3365
V2012VI	-0.3097	0.1485	0.3044
V2013V	-0.3048	0.1543	0.3027
V2014V	-0.2080	0.1621	0.2337
V2016V	-0.2350	0.1687	0.2564
V2018VI	-0.3806	0.2692	0.4132
V2019V	-0.3924	0.2887	0.4317
V2020V	-0.4265	0.2606	0.4430
V2026V	-0.2738	0.2147	0.3084
V2032V	-0.4255	0.1587	0.4024
V2034V	-0.3917	0.1392	0.3684
V2035V	-0.4147	0.1442	0.3891
V2108V	-0.3856	0.1992	0.3846
V2124V	-0.3149	0.1734	0.3186
V2125V	-0.3355	0.2027	0.3474

B. 500MS VERTICAL VELOCITY PLOTS

The following plots are the remaining 13 vertical velocity comparisons.

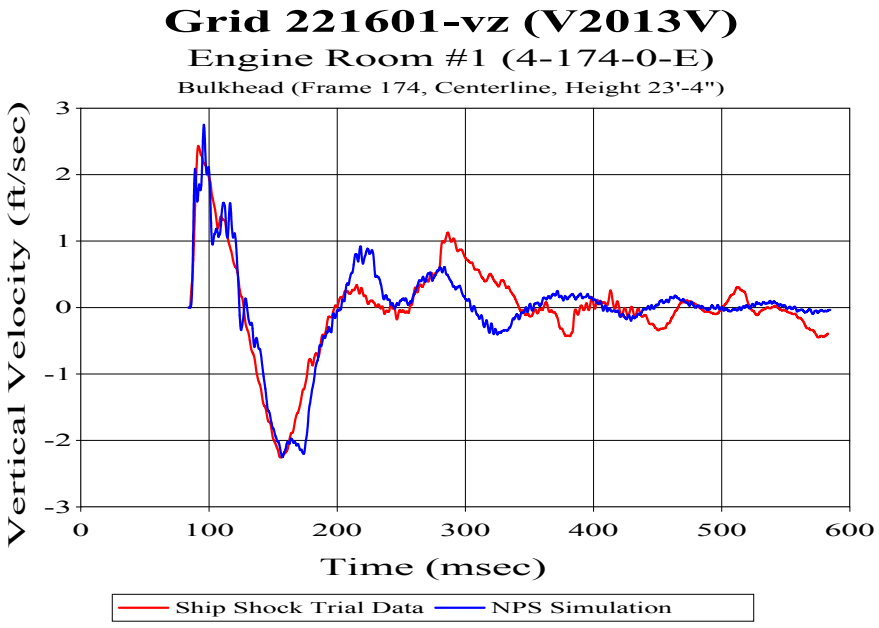

Figure 31. Bulkhead Sensor V2013V: (RM=0.0038, RP=0.1543, RC=0.1368)

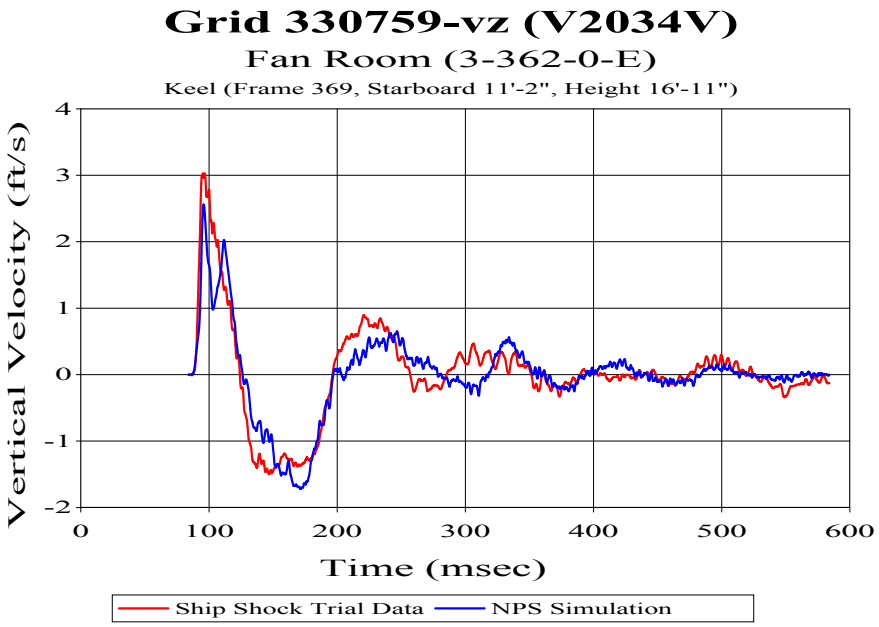

Figure 32. Keel Sensor V2034V: (RM=-0.1113, RP=0.1388, RC=0.1577)

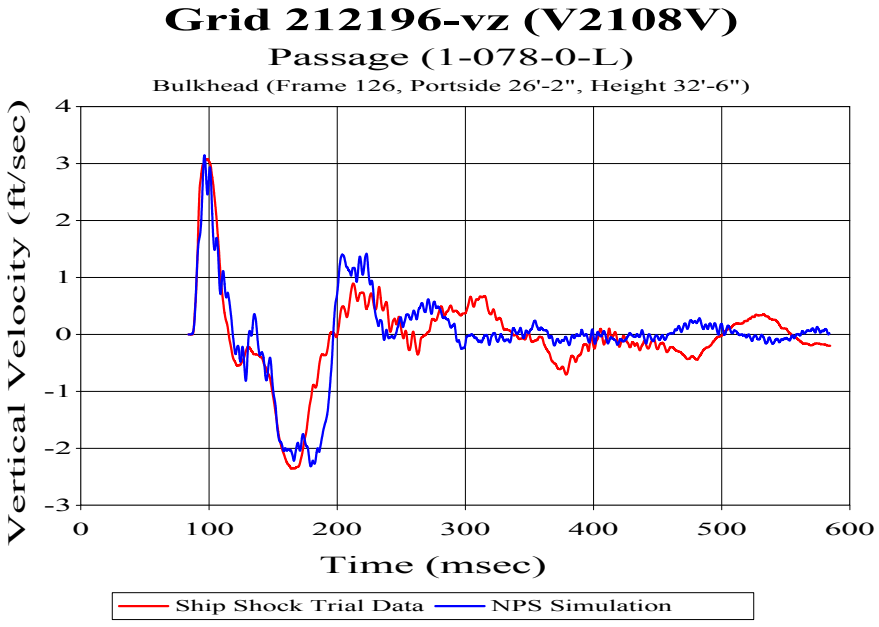

Figure 33. Bulkhead Sensor V2108V: (RM=-0.0173, RP=0.1787, RC=0.1591)

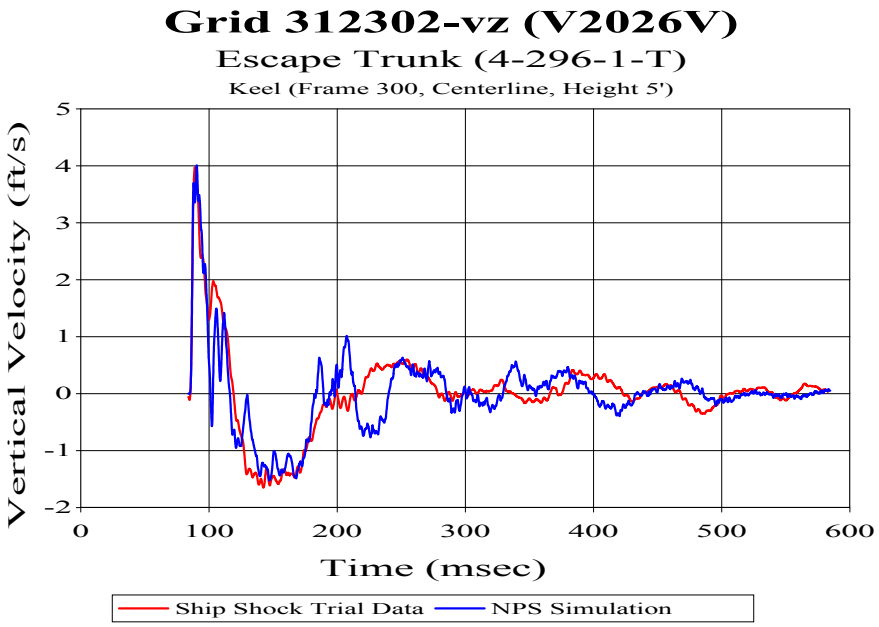

Figure 34. Keel Sensor V2026V: (RM=-0.0542, RP=0.1849, RC=0.1707)

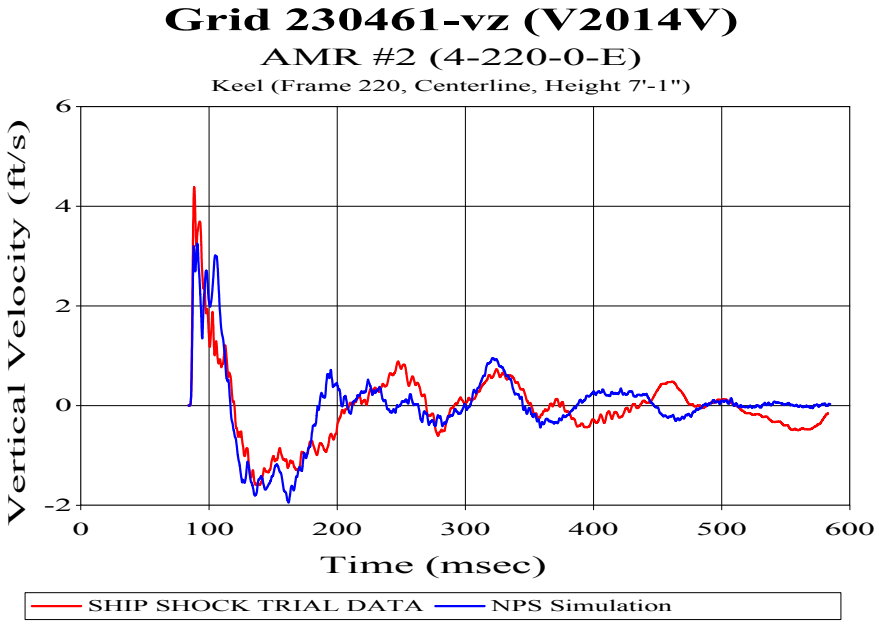

Figure 35. Keel Sensor V2014V: (RM=0.0372, RP=0.1949, RC=0.1759)

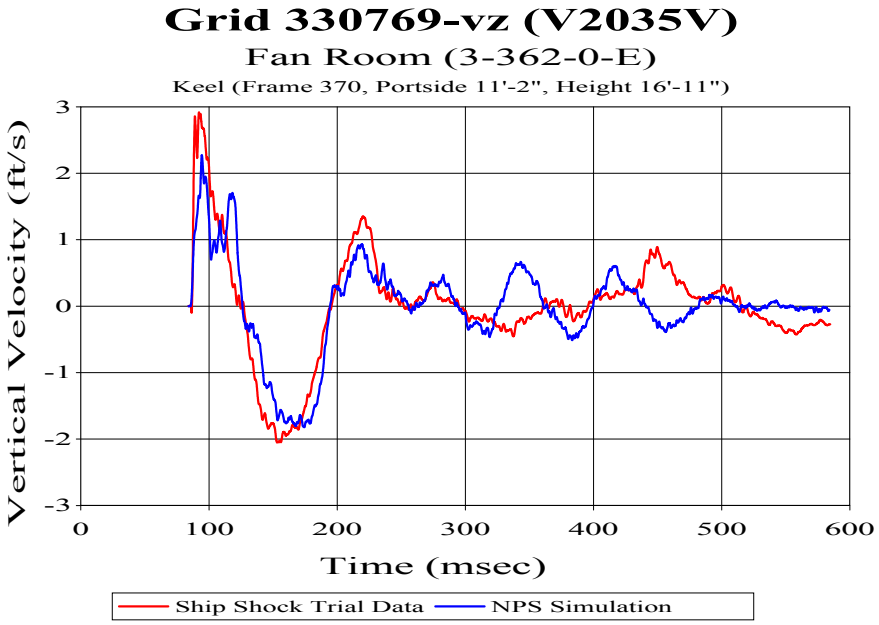

Figure 36. Keel Sensor V2035V: (RM=-0.1240, RP=0.1873, RC=0.1991)

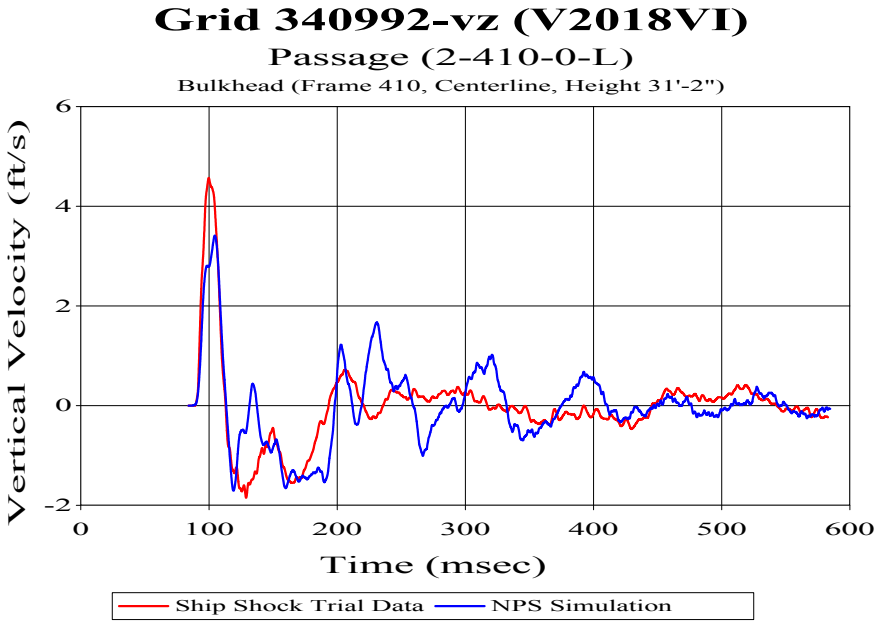

Figure 37. Bulkhead Sensor V2018VI: (RM=-0.0513, RP=0.2243, RC=0.2039)

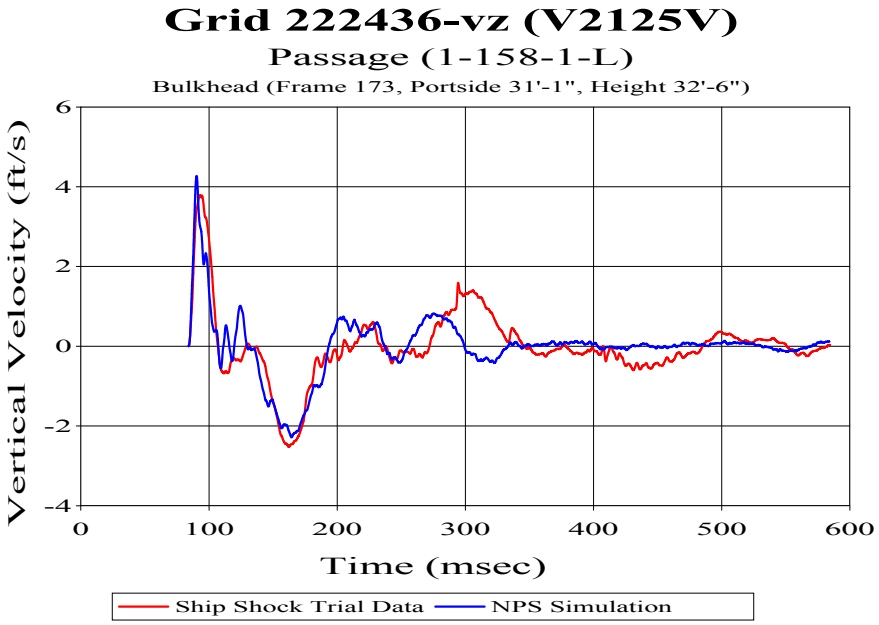

Figure 38. Bulkhead Sensor V2125V: (RM=-0.1039, RP=0.2055, RC=0.2041)

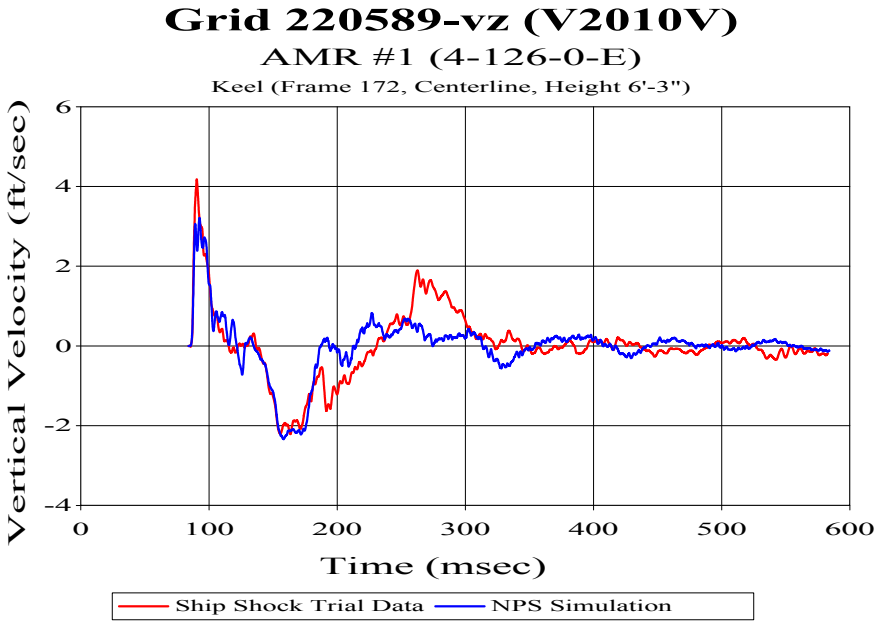

Figure 39. Keel Sensor V2010V: (RM=-0.1290, RP=0.1937, RC=0.2063)

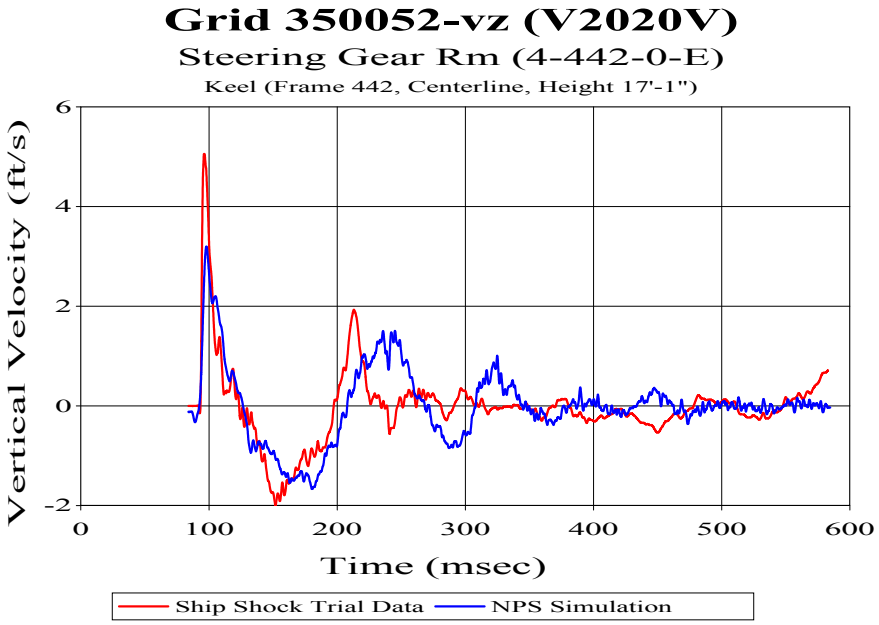

Figure 40. Keel Sensor V2020V: (RM=-0.0449, RP=0.2456, RC=0.2213)

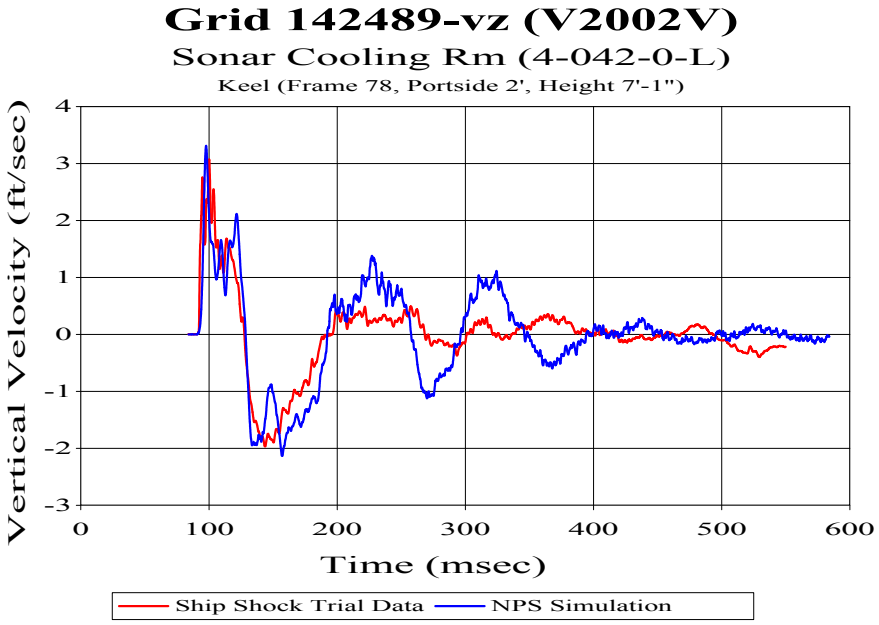

Figure 41. Keel Sensor V2002V: (RM=0.1399, RP=0.2083, RC=0.2224)

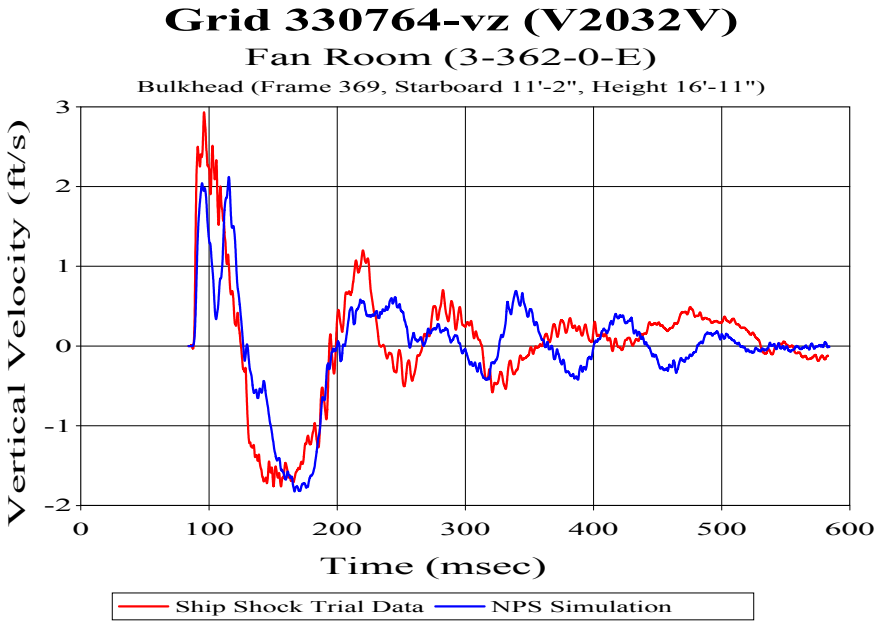

Figure 42. Bulkhead Sensor V2032V: (RM=-0.1334, RP=0.2165, RC=0.2254)

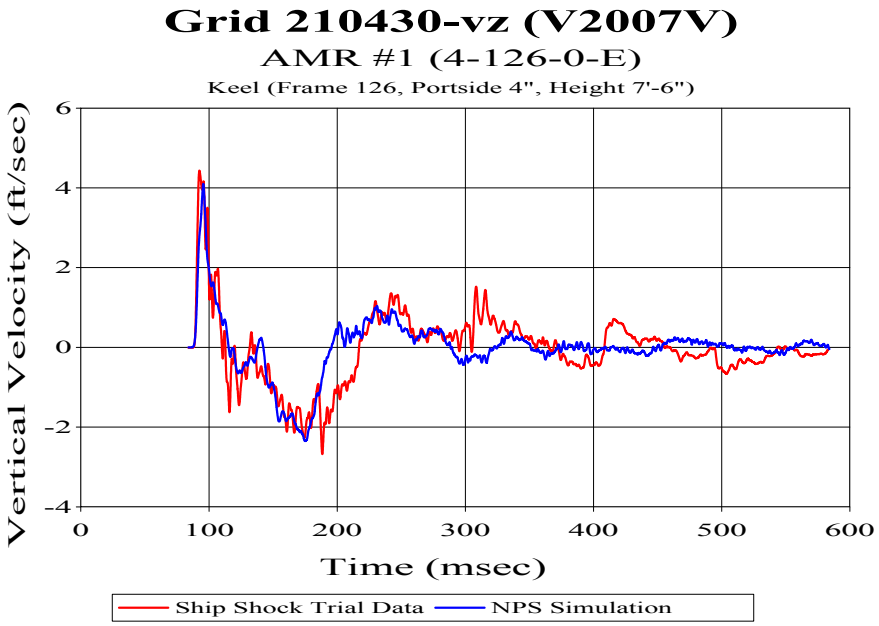

Figure 43. Keel Sensor V2007V: (RM=-0.1464, RP=0.2122, RC=0.2285)

C. VERTICAL ACCELERATION PLOTS

The following list of vertical acceleration sensors were compared to the LS-DYNA/USA simulation results (Table 14). Previous studies (Ref 5 and 25) only looked at vertical velocity data comparison as the acceptance criteria for simulation data. This investigation also provides an initial comparison and correlation of the vertical acceleration data from the ship shock trials.

To determine how well the vertical acceleration simulation data compares to the shock trial data, the study was completed in three parts. First, the simulation data was compared with a clock time of 100msec. This small time allowed for the comparison of the initial peak vertical acceleration. Next, the data was evaluated with a clock time of 200msec. This permitted the isolation and comparison of the initial peak vertical acceleration and the first period of the acceleration response. Lastly, a comparison with a clock time of 500msec was completed. This investigated how well the vertical acceleration simulation data matched up to the shock trial data in the transient response region. The same correlation acceptance criteria given in Table 4 of this study was used to quantify the correlation between the vertical acceleration simulation data and the shock trial data. Sensor V2310V is used to illustrate the correlation trend as the time of comparison is increased from 100 to 500msec.

Table 14 Vertical Acceleration Response Sensor Locations

Sensor	Node	X(Node)	Y(Node)	Z(Node)	Compartment/Location	Compt#/Area
A8516V	210993	4080.0	238.5	202.0	CREW LVG SPACE #2	3-097-2-L
A4701V	211371	4080.0	0.0	280.0	CREW LVG SPACE #2	3-097-2-L
A2101V	212058	4080.0	0.0	390.0	CIC PROJECTION ROOM	1-126-0-C
A2104V	222240	3504.0	0.0	390.0	CIC ANNEX	1-126-0-C
A3565V	231696	2952.0	-81.0	316.7	ACCESS TRUNK	3-220-0-T
A2310V	320746	1536.0	0.0	177.0	A/C MCHY & PUMP RM	5-300-01-E
A2413V	350220	288.0	0.0	273.4	RAST MACHINERY RM	2-442-0-E
A2116V	414367	3504.0	0.0	702.0	RR #2	03-142-0-C
A2109V	414953	4059.1	0.0	722.8	RR #1	03-128-0-C
A2240V	416269	3504.0	-135.0	848.0	STBD MAST LEG	MAST
A2237V	416419	3504.0	135.0	848.0	PORT MAST LEG	MAST

The following Russell error factors were obtained for the 100msec comparison of the simulation data and the shock trial data (Table 15). Results show that of the eleven vertical acceleration sensors compared, nine were in the acceptable correlation criteria range.

Table 15 100msec Vertical Acceleration Russell Error Factor Comparison

Sensor	RM	RP	RC
A2101V	-0.0335	0.1574	0.1426
A2104V	0.2642	0.3029	0.3562
A2109V	0.0744	0.0765	0.0946
A2116V	0.1601	0.1231	0.1789
A2237V	0.0625	0.2293	0.2106
A2240V	0.0173	0.1367	0.1221
A2310V	-0.0669	0.1485	0.1443
A2413V	-0.2842	0.1051	0.2686
A3565V	0.0736	0.2630	0.2420
A4701V	-0.2530	0.1477	0.2596
A8516V	-0.0201	0.3643	0.3224

Figure 44 shows bulkhead vertical acceleration sensor A2310V in the A/C Machinery and Pump Room. The sensor was located 80 feet aft of the shock waves initial point of impact, centerline, and experienced an initial vertical acceleration of 45.7 G's. The plot shows that the LS-DYNA simulation data measures up to the shock trial data of 100msec. The Russell's error factors for the correlation were: RM=-0.0669, RP=0.1485, and RC=0.1443. These values are well within the correlation acceptance criteria and show that the simulation data accurately captures the initial peak acceleration experienced by the ship.

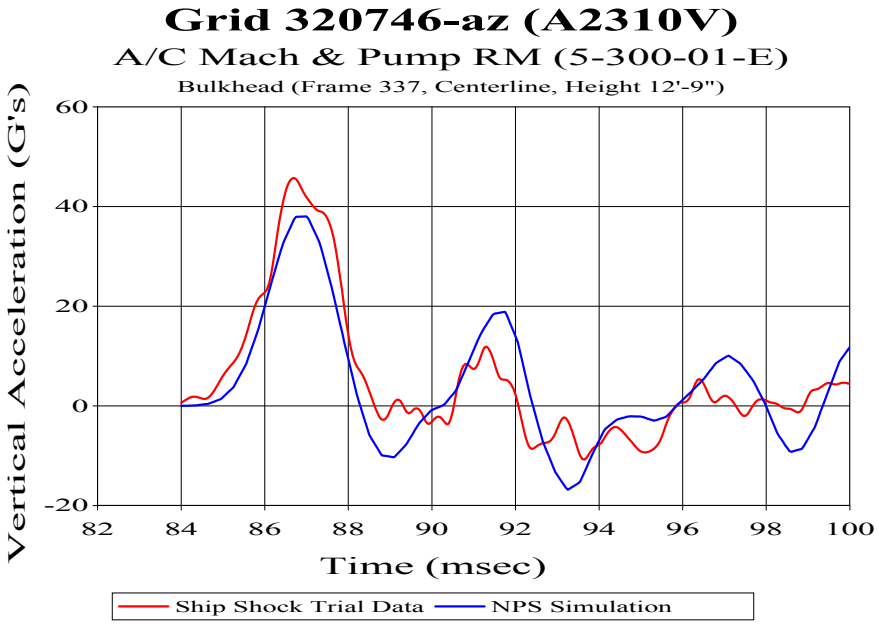

Figure 44. Bulkhead Vertical Acceleration Sensor A2310V

Table 16 shows the Russell error factors obtained for the 200msec comparison of the simulation and the shock trial data. The 200msec comparison shows that of the eleven sensors evaluated, seven of the sensors were in the acceptable correlation criteria range.

Table 16 200msec Vertical Acceleration Russell Error Factor Comparison

Sensor	RM	RP	RC
A2101V	0.1351	0.2686	0.2665
A2104V	0.2647	0.3139	0.3639
A2109V	0.1632	0.1765	0.2130
A2116V	0.0572	0.1750	0.1632
A2237V	0.1601	0.2524	0.2649
A2240V	-0.0197	0.1761	0.1570
A2310V	0.1096	0.2624	0.2520
A2413V	-0.2690	0.2318	0.3147
A3565V	0.2096	0.3241	0.3421
A4701V	-0.0526	0.2778	0.2506
A8516V	0.1182	0.3672	0.3419

Figure 45 shows sensor A2310V as a representative plot of the vertical acceleration comparison. This plot shows that the initial 45.7 G acceleration peak damps out quickly in the actual shock trial data. The LS-DYNA/USA simulation data continues

to ring down between the 100 and the 200msec time frame. Russell's error factors for the 200msec correlation were: RM=0.1096, RP=0.2624, and RC=0.2520. The values slightly increased over the 100msec correlation results, but were still within the acceptable norm.

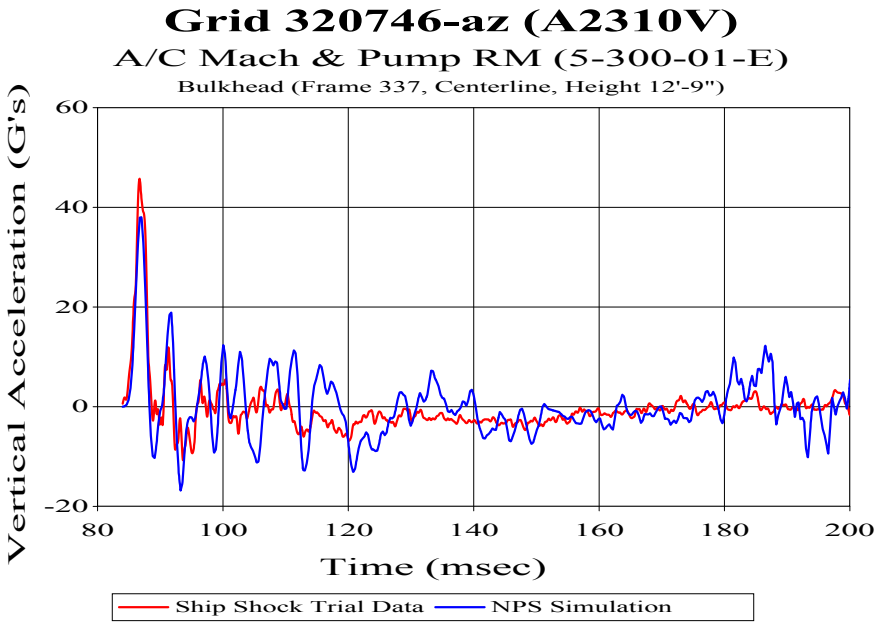

Figure 45. Bulkhead Vertical Acceleration Sensor A2310V

Table 17 shows the Russell error factors obtained for the 500msec comparison of the simulation data and the shock trial data. This shows that of the eleven sensors compared, only four of the sensors were in the acceptable correlation criteria range for the 500msec comparison.

Table 17 500msec Vertical Acceleration Russell Error Factor Comparison

Sensor	RM	RP	RC
A2101V	0.1626	0.2970	0.3001
A2104V	0.2836	0.3270	0.3836
A2109V	0.1743	0.2138	0.2444
A2116V	0.1049	0.2024	0.2020
A2237V	0.1817	0.2802	0.2960
A2240V	0.0265	0.2071	0.1850
A2310V	0.1585	0.5898	0.2928
A2413V	-0.1229	0.3120	0.2972
A3565V	0.2336	0.3371	0.3635
A4701V	0.0154	0.3111	0.2761
A8516V	0.1966	0.3959	0.3918

Figure 46 illustrates the decreasing correlation between the LS-DYNA/USA simulation data and the actual shock trial figures for sensor V2310V as the time compared increased to 500msec. Russell error factors for sensor V2310V at 500msec were: RM=0.1585, RP=0.5898, and RC=0.2928. It is important to note that even though the magnitude only increased slightly between the 200 and 500msec comparisons, the comprehensive error increased substantially because of phase differences between the two sets of data.

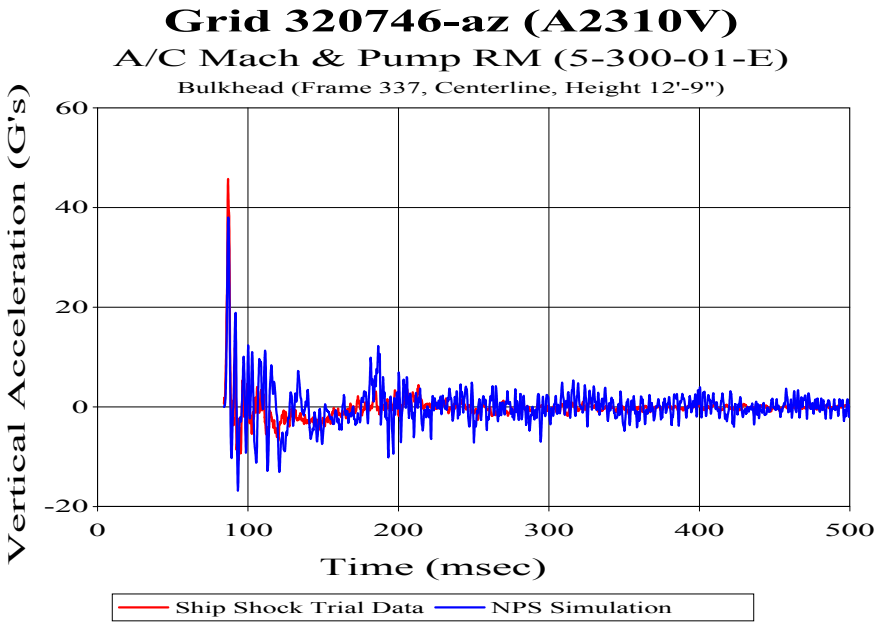

Figure 46. Bulkhead Vertical Acceleration Sensor A2116V

THIS PAGE INTENTIONALLY LEFT BLANK

APPENDIX B: USEFUL TRUEGRID MODELING COMMANDS

This appendix covers the basic commands that are required to generate a FEM fluid mesh using Truegrid batch mesh generator. A simple explanation is given here to help familiarize the reader with the commands used in Appendix C to construct the FEM fluid mesh model. These commands are not all inclusive. Additional commands, information, and examples can be found in the Truegrid users manual [Ref. 6]. Commands are listed in the order in which they were used to generate the DDG-81 full fluid mesh. A brief description of the commands is included to help in the understanding of the fluid mesh construction in Appendix C.

1. READMESH: The **readmesh** command is used to read in formatted files, such as Nastran or LS-DYNA. The data is stored to the Truegrid internal database as a Truegrid part. It is important to note that model's material cross-sectional properties for beams and shells, spring properties, and other specialized elements, do not convert directly into the Truegrid part. If needed, these features can be redefined within Truegrid.
2. DELMATS and DELSPDS: These two commands are used to delete material definitions, springs, and dampers from a model read in using the **readmesh** command. The NASTRAN models materials and springs do not directly translate into Truegrid format. The **delmats/delspds** command must be issued prior to writing the fluid mesh model out into LS-DYNA to avoid any complications.
3. CURD: The **curd** command defines a 3D curve. There are numerous types of curves that were used in the FEM fluid mesh generation. These included: **lp3**, **csp3**, **projcur** and **cpcd**. The **lp3** command is used to create a sequence of points, xyz, forming a 3D curve. The **csp3** curve generation command is used to create a 3D spline curve through a set of ordered points. This command allows the user to define the end derivatives. **Csp3** was extremely useful in generating the curve definitions for the mesh flow lines around the bow. The end derivative allowed the curve to remain normal at the node location on the hull and gently curve 90 degrees to the bottom of the fluid mesh. The **projcur** feature allows the user to project a curve onto a surface. Finally, the **cpcd**

command allows the user to create a curve that was previously defined using another command, such as **lp3**. **Cpcd** is useful for creating duplicate curves along the ship's hull.

4. BLOCK: The **block** command creates a part in a local 3D Cartesian coordinate system. Issuing the **block** command is the standard way to generate pieces in the Truegrid code. This is a multiple block structured mesh that can be molded into a desired mesh topology by using the numerous projection, interpolation, and relaxation algorithms available.
5. PB: The **pb** command assigns coordinate values to mesh vertices.
6. ENDPART: The **endpart** command is used to complete a part and save it to the internal database. Once this command is issued, the part is complete, and no further changes can be made.
7. FSET and FACESET: The **faceset** and **fset** commands are used to convert a defined **faceset** into a surface definition. Selecting the pick button in the environmental window, followed by sets and face button, activates the fset command. The left mouse button is then used to lasso the desired faces. Conversion of the defined **faceset** into a surface is accomplished by issuing the **faceset** command. This is useful when reading in the NASTRAN model because it allows the user to select the wetted surface of the hull and convert it into a surface. This is required when using the **blude** command.
8. BLUDE: The **blude** command is based upon the **block** command and is used to extrude a set of polygons through a user-defined faceset (**fset**). Extrusion begins by constructing a block part with no deleted regions, and pulling out the polygons in the defined faceset one at a time. This is accomplished by following the mesh lines formed by the block part. It is imperative that the extruded face of the block part completely covers the defined facesets to be selected. This command is extremely useful for the construction of the fluid mesh model described in Appendix C.
9. CURS and CUR: The **curs** and **cur** command distributes the edge nodes of a block part along a 3D curve. Each end point node of the edge of the block part is projected first, with the remainder of the vertices evenly distributed along the curve. Once the nodes have been distributed along the 3D curve, the

interior nodal distribution can be further controlled using the **res** and **as** commands.

10. SFI: The easiest way to conform a part to the desired topology is to use the **sfi** projection command. This command uses a complex algorithm to project each note of a specified region onto the closest point of the surface. The interior of the mesh is then interpolated and relaxed to maintain required spacing rules.
11. TFI and TMEI: The **tfi** and **tmei** commands are interpolation and relaxation algorithms used to produce a better quality mesh. Transfinite interpolation (**tfi**) interpolation is the most useful command when the edges of a face form a non-convex boundary and when their nodal geometric distribution is extreme. The **tfi** command also enforces the same relative spacing along the interior mesh contour lines of a face. The **tmei** command is a relaxation algorithm that improves the mesh quality by solving a Poisson equation. This command uses a weight factor to relax the linear iteration that solves the equation. **Tmei** should be experimented with to in order to obtain the desired mesh distribution.
12. BB: The **bb** command defines a block boundary interface for parts that should not move with respect to one another. A face, edge, or vertex of a part can be saved to form the geometry of another part at a later time. This command establishes the geometry to be saved and retrieves the geometry at a later time. The first time the command is initialized, the master side of the block boundary is defined, and the second time it is initialized, the slave side block boundary is defined. The **bb** transformation commands are extremely useful in the fluid mesh construction described in Appendix C. In particular, the normal offset transformation allows the user to specify nodal placement a certain distance away from the master side block boundary in the perpendicular direction.
13. DIAGNOSTICS: The diagnostics menu provides a way to measure the mesh quality of every element within a model. Examples of the measure options available are: the orthogonal test measures three angles at all eight corners of a brick element and plots how much they deviate from 90 degrees; the

Jacobian test measures the shape of each element; the smallest option determines the smallest dimension of an element.

14. LABELS CRACKS: The **labels cracks** is an extremely useful diagnostic tool for locating nodes along a mesh that have not been completely merged together. The command is issued by typing **labels cracks** followed by the minimum degree between the corresponding mesh lines. When used in conjunction with the **blude** command, **labels cracks** command ensures that a high quality hex mesh is generated.
15. STP: The **stp** command sets the tolerance by which surface nodes are merged. Only nodes that lie on the surfaces or exterior faces of parts are considered for merging. Exterior faces include sides of the mesh that are physically matching but are logically distinct faces of the mesh.
16. BPTOL: The **bptol** command is used to merge nodes between parts. The tolerance overrides the previously specified **stp** tolerance between the two parts.
17. POSTSCRIPT: The **postscript** command flags Truegrid to output the current physical screen as a .ps file. Clicking the draw button in the environment window draws postscript images of the model.

APPENDIX C: DDG-81 TRUEGRID FLUID MODEL

This appendix provides the majority of the Truegrid batch mesh file used to generate the full fluid mesh. The actual xyz coordinates for curve definitions are left out due to the extreme length of some of these commands. Enough of the command structure is included or described so that the work contained in this thesis can be reproduced.

To begin the fluid model mesh generation process, the DDG-81 FEM ship structural model was read into Truegrid. This is accomplished by using the **readmesh** command. **Readmesh** takes the formatted NASTRAN mesh, converts it into a Truegrid part and stores it to the internal database. Inserting the **exclude** command before the required **endpart** command, flags Truegrid to read it in the NASTRAN file and to only write out additions to the mesh, not the original complete FEM structural model. The **exclude** command also allows new nodes of the fluid mesh to be merged with excluded nodes. When these are written out they will have the original ship structural model node. This is a key requirement for the coupled structure/fluid model.

```
readmesh nastran DDG81.nas exclude endpart
```

The **delspds** and **delmats** commands delete all the numbered springs and materials from the read-in NATRAN model. This is done to ensure that materials and springs from the FEM model are not converted to LS-DYNA format when outputted.

```
delmats 1:346;
delspds 1:500;
```

The 3D curve definition command, **curd**, is used to define the areas along the bow, sonar and keel seams (Figure 47). As discussed in the mesh modeling section, these areas result in a gap when the mesh liner parts constructed are merged together. Wedge-shaped elements needed to fill in these gaps are constructed manually by using defined curves. The **lp3** command is used to generate these curves from a series of points for the sonar dome, keel, and bow areas, in order to form the line segments. Beginning at the stern, the curve should extend around the sonar dome and up to the waterline at the bow. This curve is then repeated for the port and starboard side. The **curd csp3** command is then used to generate spline curves through a series of ordered points around the stern and bow area. These are manual operations and must be checked and changed to ensure that proper spacing and distance from the hull is achieved.

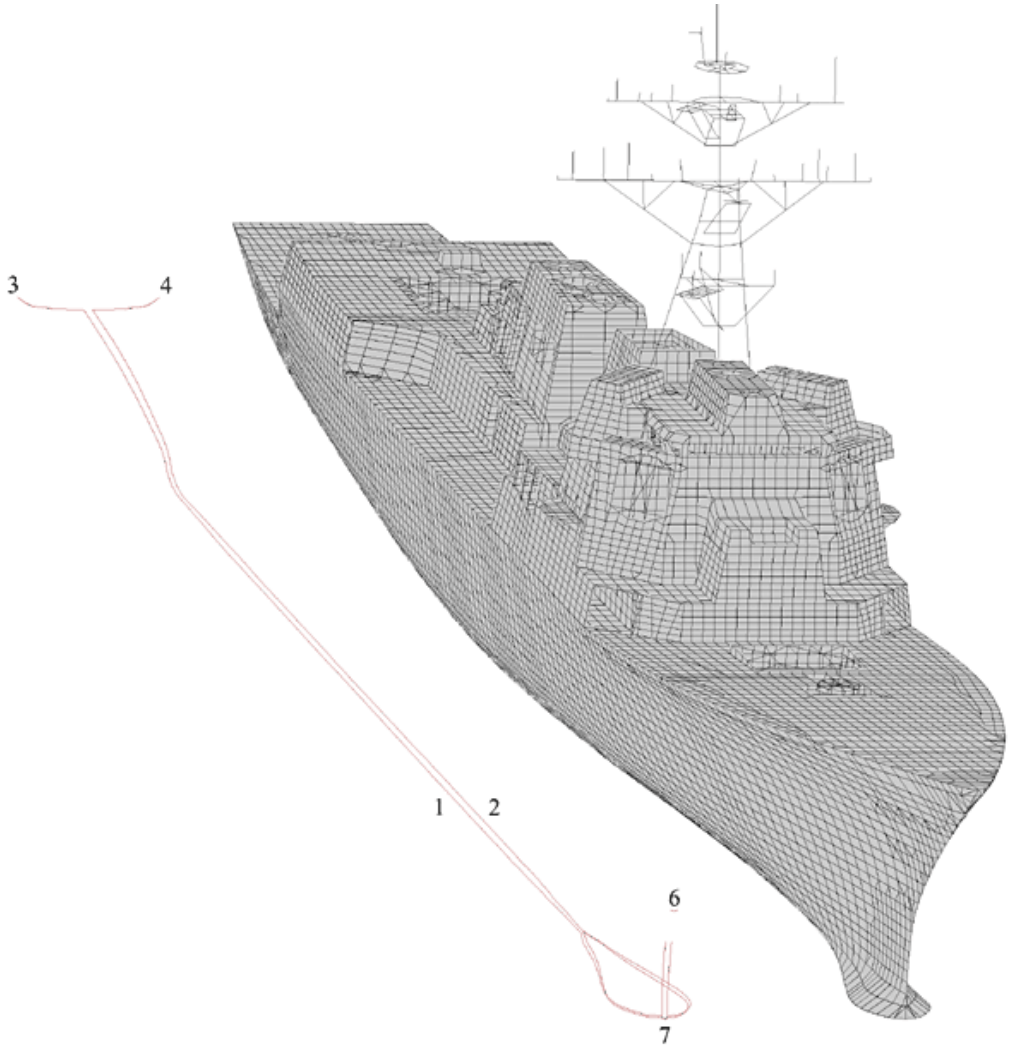

Figure 47. Bow, Sonar, Keel, and Stern curve definitions forming seams.

```
curd 1 lp3; curd 2 lp3; curd 3 csp3
curd 4 csp3; curd 6 csp3; curd 7 csp3
```

The **block** command is used to plug the holes in the NASTRAN FEM model that form the stern tube seals. The **pb** command is used to place the four edge vertices of the block. This command is repeated for the port plug.

```
c part - starboard sterntube plug
block 1 8;-1;1 4;1.1520000e+03 1.4880000e+03;
     -135;9.9440002e+01 1.2893800e+0;
```

Figure 48 shows the construction of the fluid mesh liner. This includes construction of the port and starboard inner mesh liner, port and starboard outer mesh

liner, sonar dome inner and outer mesh liner, stern inner and outer mesh liner, and bow inner and outer mesh liner.

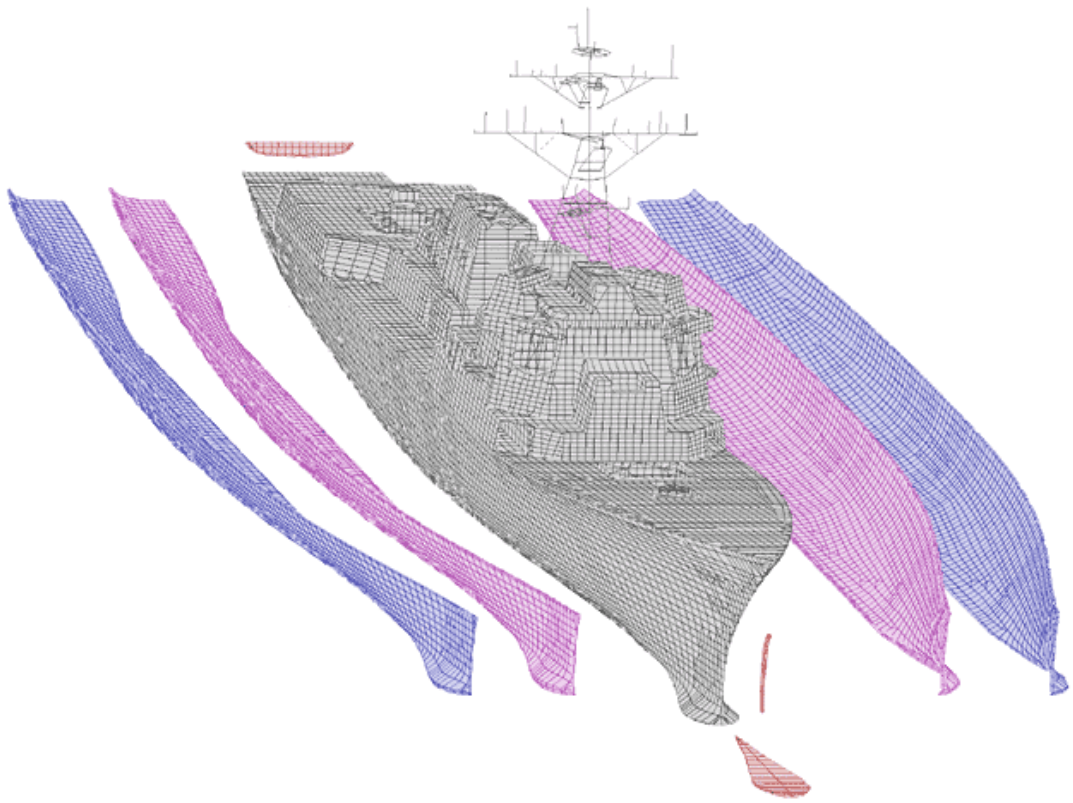

Figure 48. Fluid Mesh Liner Part Construction.

To begin the inner fluid mesh liner construction, use the **pick sets** option to define the face sets (**fset**) that form the wetted surface of the hull. This is a complex task due to the transition of the hull mesh line from 254 inches at the bow to 309 inches at the stern. Numerous surface definitions are required in order to maintain the transition of the hull mesh line to the required 258-inch waterline. By making the transition in two layers (Section 2C), the angle of transition from the hull mesh line to the waterline was minimized. The following facesets are defined to generate the transition of the mesh liner, Figure 49.

```
sd 1 faceset starboard (light blue)
sd 2 faceset port (pink)
sd 3 faceset sonar
sd 4 faceset stern (light green)
sd 7 faceset sterntop (orange)
sd 9 faceset stbdfwd (light blue)
sd 10 faceset stbdmid (gray)
sd 11 faceset stbdaft (tan)
```

```
sd 15 faceset portfwd (yellow)
sd 16 faceset portmid (gray)
sd 17 faceset portaft (tan)
```

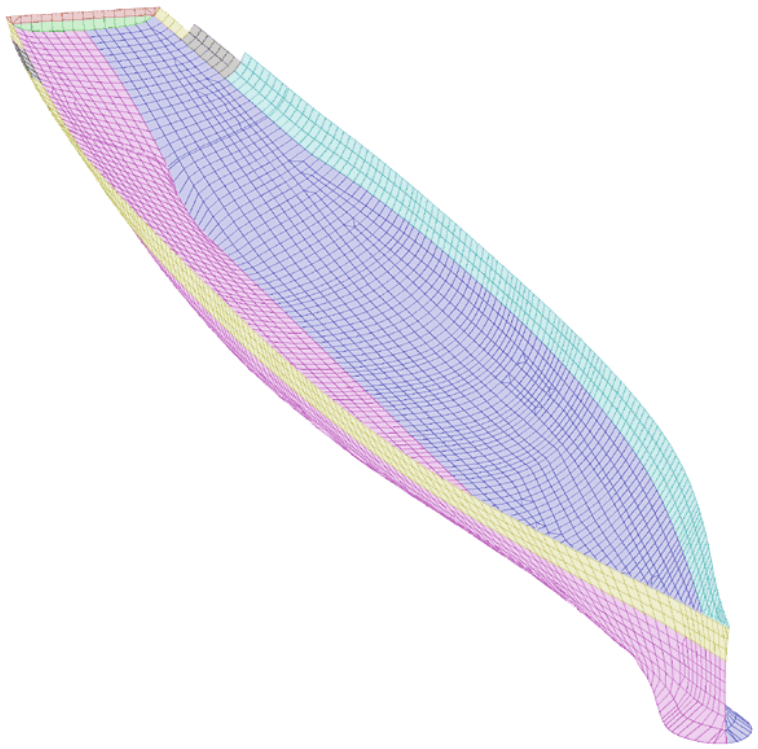

Figure 49. Mesh Defining Facesets

The **blude** command is used to extrude the port, starboard, and sonar inner mesh liner faceset polygons by one element orthogonally. All commands for the port side mesh are not included due to their repetitive nature. The block boundary (**bb**) command ensures that the liner is extruded orthogonal to the ship's wet-surface elements for the required seven inches. Port and starboard inner liners are only extruded up to the 175 inch mesh line on the ship model. The area from 175 inches to 258 inches needs to be constructed in separate parts in order to maintain the fluid waterline at 258 inches (Section 2C).

```
c part - starboard side liner
blude 4 starboard 1 203;1 2;1 40;
     -6.0459e+01 5.57134e+03 ;-7 0;0 250;
pb  1 2 2 1 2 2 x -6.0458e+01
pb 1 2 2 1 2 2 xyz -6.0458e+01 -1.919380e+02 2.508750e+02
pb 1 2 1 1 2 1 xyz -5.338200e+01 -4.300000e-12 2.247830e+02
pb 2 2 2 2 2 2 xyz 5.57134e+03 0.000000e+00 1.770000e+02
```

```
pb 2 2 1 2 2 1 xyz 5.581330e+03 0.000000e+00 0.000000e+00
insprt 1 5 2 2;insprt 1 6 1 2
pb 1 1 1 1 1 1 xyz -5.316302e+01 -1.182019e+01 2.180665e+02
pb 2 1 1 2 1 1 xyz 5.587133e+03 -7.000000e+00 5.574311e+00
pb 2 1 4 2 1 4 xyz 5.57275e+03 -7.00000e+00 1.7658592e+02
insprt 1 1 1 2;insprt 1 1 3 2
pb 3 1 1 3 1 1 xyz 5.557776e+03 -5.334840e+01 6.368494e+00
pb 2 2 1 2 2 1 xyz 7.122657e+00 0.000000e+00 2.207952e+02
pb 2 2 4 2 2 4 xyz -4.236153e+01 -2.230580e+02 2.52659e+02
pb 2 1 1 2 1 1 xyz 4.816480e+00 -1.407739e+01 2.103721e+02
pb 1 1 3 1 1 3 xyz -5.823256e+01 -1.800000e+02  2.4001e+02
pb 1 1 2 1 1 2 xyz -5.325460e+01 -1.845925e+01 2.182304e+02
pb 1 1 2 1 1 2 xyz -5.333850e+01 -2.656657e+01 2.183852e+02
pb 1 2 2 1 2 2 xyz -5.354422e+01 -1.852749e+01 2.254219e+02
pb 2 2 2 2 2 2 xyz 4.178131e+00 -2.516457e+01 2.201446e+02
pb 1 2 2 1 2 2 xyz -5.359683e+01 -2.453671e+01 2.256291e+02
pb 4 1 3 4 1 3 xyz 5570.2 -7.0000 167
pb 4 1 2 4 1 2 xyz 5585.8662 -7 5
mseq i 0 0 1
curs 4 1 1 4 1 4 1;curs 1 1 1 4 1 1 1;curs 1 1 1 1 1 4 3
edge 1 2 1 2 2 1 1.3;edge 1 2 2 2 2 2 1.1;edge 2 2 1 2 2 2 1.2
edge 1 2 1 1 2 2 1.4;edge 1 2 2 1 2 3 1.4;edge 1 2 3 1 2 4 1.4
sfi ; -2;;sd 1
tfi ; -2;;
bb 1 2 2 3 2 4 1; bb 1 1 2 3 1 4 1 normal 7;
relax 1 2 1 4 2 4 20 0 1
endpart
c part – sonar dome liner
blude 6 sonar 1 22;1 7 13;1 2;
 4.8977202e+03 5.5813301e+03;-2.5872097e+01 0 2.6026953e+01 ;-7 0;
pb 1 1 2 1 1 2 xyz 5.037687e+03 -2.014148e+01 -1.200000e-05
pb 1 3 2 1 3 2 xyz 5.038931e+03 2.024531e+01 -1.200000e-05
pb 2 1 2 2 1 2 xyz 5.520881e+03 -7.213502e+01 -1.200000e-05
pb 2 3 2 2 3 2 xyz 5.519453e+03 7.287714e+01 -1.200000e-05
curd 5 sdedge 3.1 sdedge 3.2
curs 2 1 2 2 3 2 5;curs 1 1 2 1 3 2 5;curs 1 1 2 2 1 2 5
curs 1 3 2 2 3 2 5
sfi ;; -2;sd 3
bb 1 1 2 2 3 2 5;bb 1 1 1 2 3 1 5 mz 7;
endpart
```

The port, starboard, and sonar dome inner liners generated above leave gaps between the liner parts. One is between the sonar dome and the port and starboard liners, another is between the port and starboard liners and one more is at the bow. As discussed in Section 2C, this area is smoothed out by filling in the gaps with wedge elements. The following **block** command generates the keel wedges that are manually placed in the liner seam. This is a difficult and lengthy task. A portion of the **pb** commands used along the liner is included to give the general feel of vertice placement.

```
c part - keel seam
block  1   2   3   4   5   6   7   8   9
  10  11  12  13  14  15  16  17  18  19
  20  21  22  23  24  25  26  27  28  29
  30  31  32  33  34  35  36  37  38  39
  40  41  42  43  44  45  46  47  48  49
  50  51  52  53  54  55  56  57  58  59
  60  61  62  63  64  65  66  67  68  69
  70  71  72  73  74  75  76  77  78  79
  80  81  82  83  84  85  86  87  88  89
  90  91  92  93  94  95  96  97  98  99
 100 101 102 103 104 105 106 107 108 109
 110 111;
 1 3 5;
 1 2;
 0 0 0 0 0 0 0 0 0 0 0 0 0 0 0 0 0 0 0 0 0 0 0 0 0 0 0 0 0 0 0
 0 0 0 0 0 0 0 0 0 0 0 0 0 0 0 0 0 0 0 0 0 0 0 0 0 0 0 0 0 0 0
 0 0 0 0 0 0 0 0 0 0 0 0 0 0 0 0 0 0 0 0 0 0 0 0 0 0 0 0 0 0 0
 0 0 0 0 0 0 0 0 0 0 0 0 0 0 0 0 0 0 0 0 0 0 0 0 0 0 0 0 0

pb 1 1 2 1 3 2 xyz  -5.3382000e+01 -4.3000000e-12 2.2478300e+02
pb 2 1 2 2 3 2 xyz  0.0000000e+00 0.0000000e+00 2.1950000e+02
pb 3 1 2 3 3 2 xyz  4.8000000e+01 0.0000000e+00 2.1475000e+02
pb 4 1 2 4 3 2 xyz  9.6000000e+01 0.0000000e+00 2.0993800e+02
pb 5 1 2 5 3 2 xyz  1.4400000e+02 0.0000000e+00 2.0493800e+02
pb 6 1 2 6 3 2 xyz  1.9200000e+02 0.0000000e+00 1.9956300e+02
pb 7 1 2 7 3 2 xyz  2.4000000e+02 0.0000000e+00 1.9375000e+02
pb 8 1 2 8 3 2 xyz  2.8800000e+02 0.0000000e+00 1.8737500e+02
pb 9 1 2 9 3 2 xyz  3.3600000e+02 -4.0000000e-12 1.831300e+02
pb 1 2 1 1 2 1 xyz  -5.316302e+01 -4.300e-12   [224.783-7]
pb 2 2 1 2 2 1 xyz  -1.663326e+00 0.0     [219.5-7]
pb 3 2 1 3 2 1 xyz   4.571579e+01 0.0     [214.75-7]
pb 4 2 1 4 2 1 xyz   9.374361e+01 0.0     [209.938-7]
pb 5 2 1 5 2 1 xyz   1.417535e+02 0.0     [204.938-7]
pb 6 2 1 6 2 1 xyz      190.3     0.0     [199.563-7]
pb 7 2 1 7 2 1 xyz      238.3     0.0     [193.75-7]
pb 8 2 1 8 2 1 xyz      286.4     0.0     [187.375-7]
pb 9 2 1 9 2 1 xyz      334.46 -4.000e-12 [180.313-7]
pb 1 3 1 1 3 1 xyz -5.316302e+01 1.182019e+01 2.180700e+02
pb 2 3 1 2 3 1 xyz -1.663326e+00 1.204896e+01 2.130087e+02
pb 3 3 1 3 3 1 xyz 4.6130913e+01 1.2188046e+01 2.0828041e+02
pb 4 3 1 4 3 1 xyz 9.4179070e+01 1.2313977e+01 2.0348006e+02
pb 5 3 1 5 3 1 xyz 1.4220929e+02 1.2415926e+01 1.9831958e+02
pb 6 3 1 6 3 1 xyz  1.9027414e+02 1.2511413e+01 1.9310388e+02
pb 7 3 1 7 3 1 xyz  2.3831377e+02 1.2388217e+01 1.8723999e+02
pb 8 3 1 8 3 1 xyz  2.8639667e+02 1.2205677e+01 1.8114807e+02
pb 9 3 1 9 3 1 xyz  3.3445029e+02 1.1947846e+01 1.7413083e+02
…etc
endpart
```

The above procedure is repeated to form the port and starboard sonar wedge, the stern wedge and the bow wedge elements (Figure 50).

```
c part - bow seam
block  1 2 3 4 5 6 7 8 9 10 11 12;1 3 5;1 2;
       0 0 0 0 0 0 0 0 0 0 0 0 0 0 0 0 0 0
c part - port sonar seam
block 1 2 3 4 5 6 7 8 9 10 11 12 13 14 15 16 17 18 19 20 21;
      1 3;1 2;
      0 0 0 0 0 0 0 0 0 0 0 0 0 0 0 0 0 0 0 0 0 0 0 0 0 0 0
c part - starboard sonar seam
block 1 2 3 4 5 6 7 8 9 10 11 12 13 14 15 16 17 18 19 20 21;
      1 3;1 2;
      0 0 0 0 0 0 0 0 0 0 0 0 0 0 0 0 0 0 0 0 0 0 0 0 0 0 0
c part - lower bow point
block 1 2;1 2 3 4 5;1 2 3;
 5.5813301e+03 5.5903301e+03
 -7.2183199e+00 -4.2583809e+00 0.0000000e+00 5.4507451e+00
6.8652916e+00
 -7.0000000e+00 -4.5 0
pb 1 1 1 1 5 3 xyz 5.581330e+03 0.000000e+00 0.000000e+00
pb 2 4 3 2 4 3 xyz 5.589370e+03 5.450745e+00 2.641622e+00
pb 2 1 3 2 1 3 xyz 5.587133e+03 -7.0e+00 5.574406e+00
pb 2 1 2 2 1 2 xyz 5.587133e+03 -7.0e+00 5.574406e+00
pb 2 3 2 2 3 2 xyz 5.590330e+03 0.000000e+00 0.000000e+00
pb 2 2 1 2 4 1 xyz 5.581330e+03 0.000000e+00 -7.000000e+00
pb 2 5 3 2 5 3 xyz 5.5871113e+03 7.0000000e+00 5.5744057e+00
pb 2 5 2 2 5 2 xyz 5.5871113e+03 7.0000000e+00 5.5744057e+00
pb 2 4 3 2 4 3 xyz 5.588941e+03 4.55474e+00 1.67601e+00
pb 2 2 3 2 2 3 xyz 5.58972754e+03 -4.13542e+00 2.37342e+00
pb 2 3 2 2 3 2 xyz 5.590302e+03 2.467076e-01 -2.566629e-02
pb 2 3 3 2 3 3 xyz 5.590302e+03 2.467076e-01 -2.566629e-02
pb 2 2 2 2 2 2 xyz 5.584231e+03 -3.5e+00 -7.127972e-01
pb 2 1 1 2 1 1 xyz 5.584231e+03 -3.5e+00 -7.127972e-01
pb 2 5 1 2 5 1 xyz 5.5842207e+03 3.5e+00 -7.128e-01
pb 2 4 2 2 4 2 xyz 5.5842207e+03 3.5e+00 -7.128e-01
insprt 1 4 2 1;
pb 2 3 2 2 3 2 xyz 5.584231e+03 -3.5e+00 -7.127972e-01
pb 2 3 3 2 3 3 xyz 5.590197e+03 -2.828914e+00 1.286794e+00
pb 2 2 3 2 2 3 xyz 5.589032e+03 -5.188249e+00 3.426201e+00
insprt 1 4 4 1;
pb 2 6 3 2 6 3 xyz 5.588267e+03 5.588913e+00 2.862391e+00
pb 2 5 3 2 5 3 xyz 5.589426e+03 3.337113e+00 7.968602e-01
pb 2 5 2 2 5 2 xyz 5.584221e+03 3.500000e+00 -7.127948e-01
mseq j 0 1 1 0
endpart

c part - stern keel point
block
1 2;1 2 3 4 5;1 2;
-54 -61;-12 -7 0 7 12;216 224;
pb 1 1 1 1 1 1 xyz -5.316302e+01 -1.182019e+01 2.180700e+02
pb 1 2 1 1 2 1 xyz -5.316302e+01 -5.91010e+00 2.179265e+02
pb 1 3 1 1 3 1 xyz -5.316302e+01 0.000 2.177830e+02
pb 1 4 1 1 4 1 xyz -5.316302e+01 5.91010e+00 2.179265e+02
pb 1 5 1 1 5 1 xyz -5.316302e+01 1.182019e+01 2.180700e+02
pb 1 1 2 1 5 2 xyz -5.338200e+01 -4.300000e-12 2.247830e+02
pb 2 1 1 2 5 1 xyz -6.10000e+01 0.000000e+00 2.180000e+02
```

```
pb 2 1 2 2 5 2 xyz -6.100e+01 0 2.1800e+02
endpart
```

The completed seam wedges are shown in Figure 50.

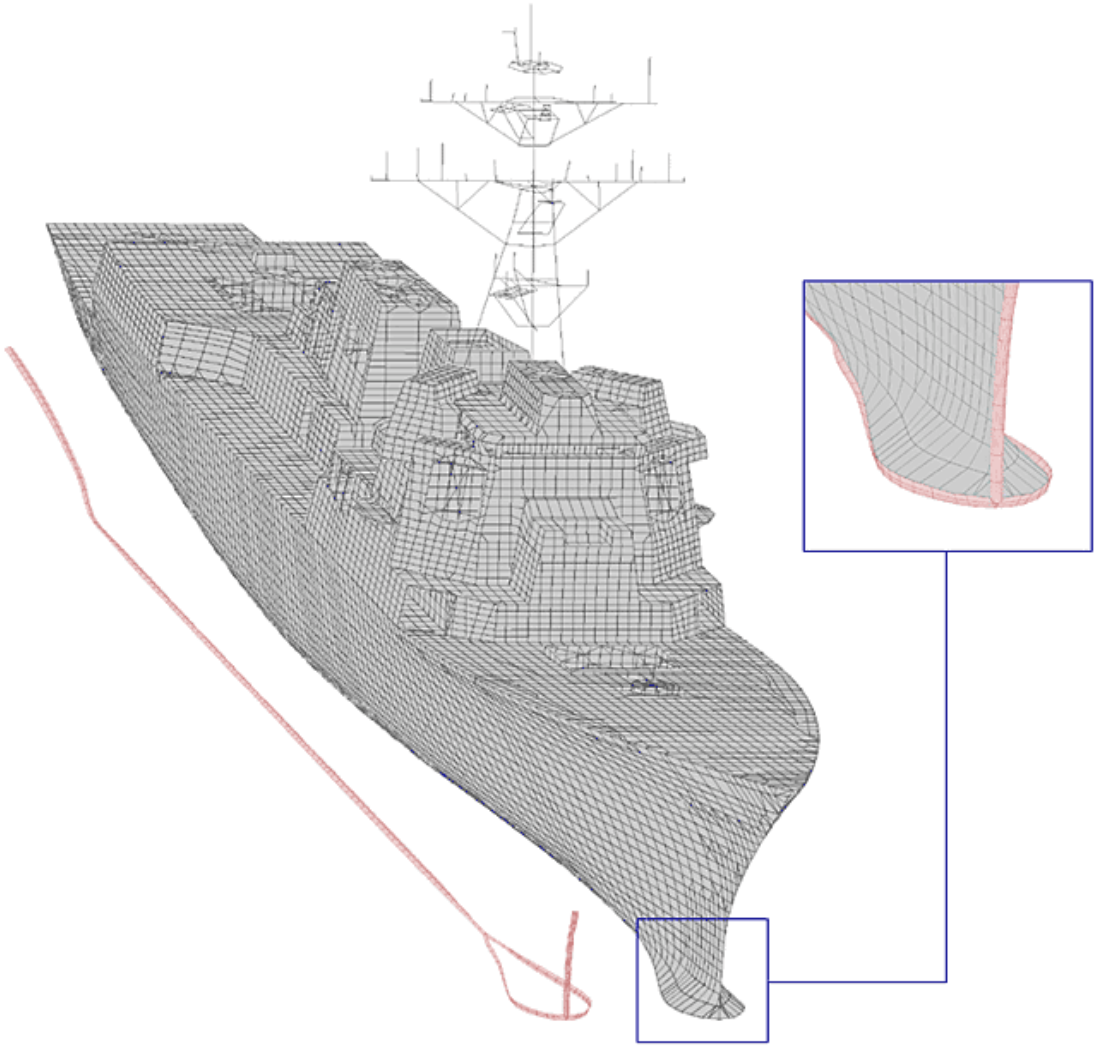

Figure 50. Completed Keel Wedge Detail

With the seam liner completed along the keel, stern, and bow, the parts making up the remaining inner fluid mesh from 174 inches to 258 inches are added. The **blude** and **block** commands are used to insert these required elements. These parts complete the inner fluid mesh liner and the transition of the waterline to the required 258 inches. Commands needed to generate the parts for the starboard side are included below.

```
c  part - stern
blude 2 stern 1 2;1 31;1 2;
      [-6.0e+01-7] -6.0e+01 ;-185 185;218 251;
c part – stern top
```

```
blude 2 sterntop 1 2;1 6 11 16 21;1 2;-72 -65;-200 -108 0  108 200;250
270;
c part - stbd aft top liner
blude 4 stbdaft 1 8;1 2;1 3;-66 95;-231 -224;232 270;
c part - stbd aft wedge
block 1 2;1 2;1 2;44 96;-225 -218;251 258;
c part - stbd aft-mid transition
block 1 2;1 2; 1 2 3; 95 143; -238 -231; 220 240 260;
c part - stbd mid top liner
blude 4 stbdmid 1 6 10;1 2; 1 3 5; 143 287 431;-281 -274;202 228 258;
c part - stbd mid wedge
block 1 2 3 4;1 2;1 2;287 335 383 431;-272 -265;248 258;
c part - stbd midfwd transition
block 1 2;1 2;1 2 3 4;431 479;-362 -355;177 202 228 260;
c part - stbd fwd top liner
blude 4 stbdfwd 1 20 75 130 183;1 2;1 3 5 7;479 815 2376 3937 5595;
-362 -355; 177 202 228 254;
```

The above steps complete the inner fluid mesh liner. Next, wetted **facesets** of the inner fluid mesh liner are selected to form the outer fluid mesh liner. This consists of five facesets; stern, starboard, port, sonar and bow. The following **blude** commands generate the eight inch thick outer fluid mesh liner.

```
c part – outer sonar mesh liner
blude 6 sonar2 1 11 21;1 2 3;1 2;4897 5376 5581;-88 0 88;-18 -10;
c part – outer bow mesh liner
block 1 2;1 3 5;1 2 3 4 5 6 7 8 9 10 11 12 13 14;
5603 5611;-5.7 0 5.7;-15 5 13 27 54 81 107 128 153 177
201 227 253 258;
c part – outer starboard/port mesh liner
blude 4 stbdfc2 1 203;1 2;1 43;-77 5610;-370 -362;-15 258;
c part – outer stern mesh liner
blude 2 sternfc2 1 2;1 11 21 31;1 3 5 7;-77 -69;-212 -77 77 212;219 225
249 262;
```

With the inner and outer fluid mesh liner completed, the transition to the 258 inch waterline is completed. Now it is possible to complete the bulk fluid extrusion. All the steps involved in the generation of the full fluid mesh are illustrated in Figure 51.

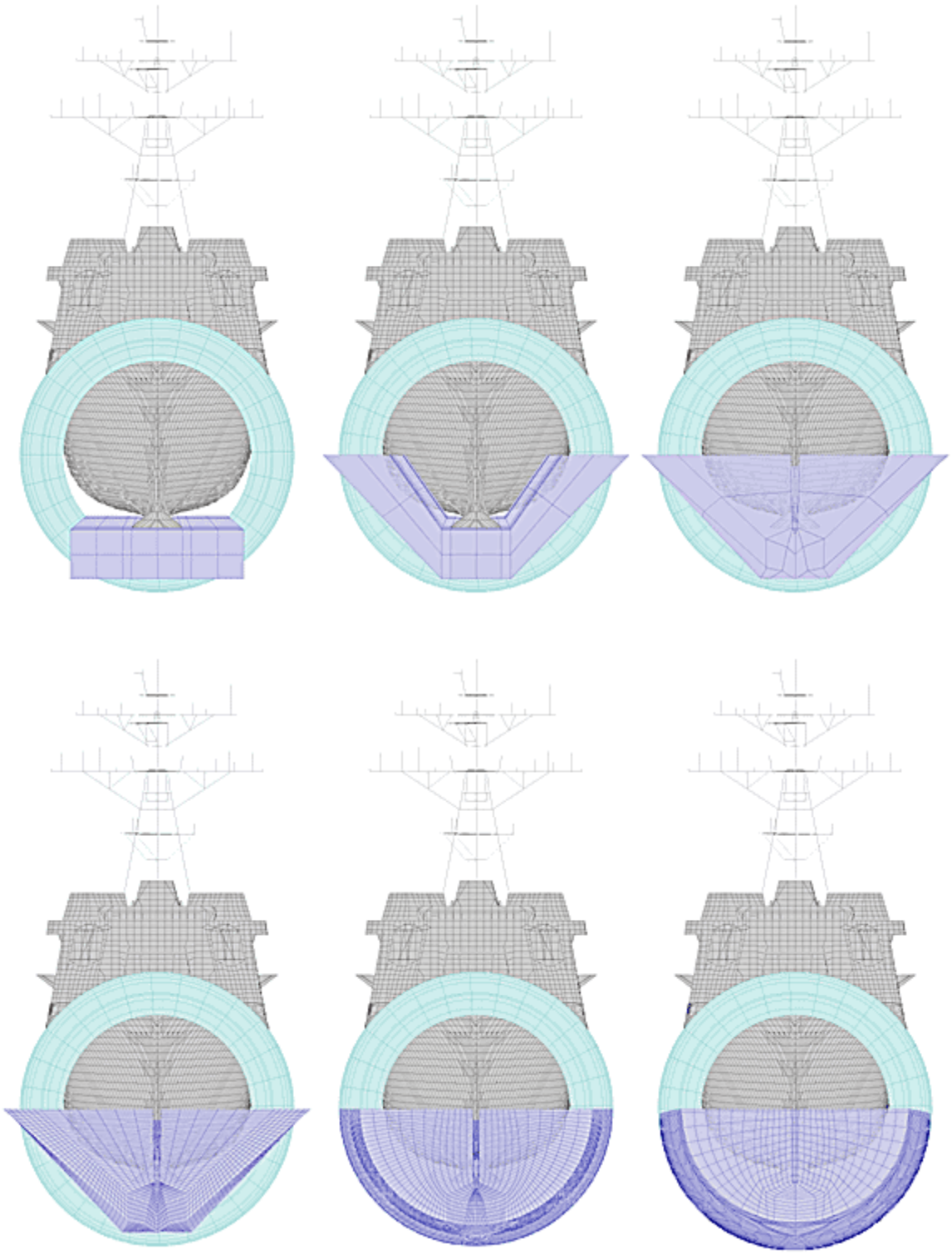

Figure 51. Extrusion Steps Involved in Generating Bulk Fluid Mesh

The **blude** command is used to extrude the fluid from the faceset, which is defined around the outer fluid mesh liner. Next, the fluid mesh is projected onto the outer mesh liner and the surface definition 1 defined below. Nodal placement around the sonar

dome is the most critical aspect to a smooth extrusion around this area. Due to the complex nature of the sonar dome's topology, the underlying hex mesh must be carefully placed. This generates a high-quality mesh once the extrusion is completed. All of the **pb** commands are included because of the complexity of nodal placement around the sonar dome area.

```
curd 39 csp3 00 5.7300000e+03 -400 258
 3.6896423e+03 -5.0757333e+02 258
 2.7076841e+03 -5.2353564e+02 258
 1.6300530e+03 -5.1728485e+02 258
 8.6507593e+02 -4.9359436e+02 258
 -189 -400 258;;;

ld 1 csp2 00 -400 5.7300e+03 -5.0757333e+02 3.6896423e+03
-5.2353564e+02 2.7076841e+03 -5.1728485e+02 1.6300530e+03
-4.9359436e+02 8.6507593e+02 -4.00e+02 -189;;;

sd 1 cr 0 0 258 1 0 0 1

blude 6 hull
1 2 3 4 5 6 7 8 9;
1 3 4 5 6 7 9;
1 2 3;
-189 864 962 1050 4272 4900 5130 5440 5599;
-300 -120 -87 0 87 120 300;
-170 -85 0;
pb 1 7 1 9 7 3 z 258
pb 1 1 1 9 1 3 z 258
pb 1 1 2 9 1 2 y -408
pb 1 7 2 9 7 2 y 408
pb 1 1 1 9 1 1 y -529
pb 1 7 1 9 7 1 y 529
pb 9 1 3 9 1 3 xyz 5.595005e+03 -1.500761e+01 2.579903e+02
pb 9 7 3 9 7 3 xyz 5.595000e+03 1.500193e+01 2.580000e+02
pb 9 4 3 9 4 3 xyz 5.581300e+03 5.100000e-04 -1.499900e+01
pb 9 5 3 9 5 3 xyz 5597.01 9.30512 3.37763
pb 9 3 3 9 3 3 xyz 5597.13 -9.14273 3.72616
pb 9 6 3 9 6 3 xyz 5.595915e+03 9.742917e+00 6.257613e+00
pb 9 2 3 9 2 3 xyz 5.595553e+03 -1.038978e+01 6.127446e+00
pb 9 2 1 9 2 1 xyz 5.730005e+03 -1.560088e+02 -1.103219e+02
pb 9 6 1 9 6 1 xyz 5.730005e+03 1.594628e+02 -1.088397e+02
mb 9 1 1 9 7 1 x 120
pb 8 6 3 8 6 3 xyz 5.450397e+03 9.670407e+01 8.202327e+00
pb 8 5 3 8 5 3 xyz 5.447996e+03 8.732797e+01 -1.500001e+01
pb 8 2 3 8 2 3 xyz 5.450398e+03 -9.668196e+01 8.138701e+00
pb 8 3 3 8 3 3 xyz 5.447996e+03 -8.732797e+01 -1.500001e+01
pb 7 6 3 7 6 3 xyz 5.136343e+03 4.880568e+01 1.066124e+00
pb 7 5 3 7 5 3 xyz 5.136000e+03 3.315440e+01 -1.500001e+01
pb 7 2 3 7 2 3 xyz 5.136343e+03 -4.880568e+01 1.066124e+00
pb 7 3 3 7 3 3 xyz 5.136000e+03 -3.315440e+01 -1.500001e+01
```

```
pb 6 4 3 6 4 3 xyz 4.8977266e+03 -2.6471224e-01 -1.5000000e+01
pb 6 5 3 6 5 3 xyz 4.8976187e+03 3.9398472e+00 -1.3536760e+01
pb 6 6 3 6 6 3 xyz 4.8975176e+03 8.1757593e+00 -1.2061778e+01
pb 6 3 3 6 3 3 xyz 4.8976011e+03 -4.0054498e+00 -1.3624668e+01
pb 6 2 3 6 2 3 xyz 4.8975366e+03 -8.1263466e+00 -1.2105322e+01
pb 5 4 3 5 4 3 xyz 4.273454e+03 0.000000e+00 -1.500000e+01
pb 5 3 3 5 3 3 xyz 4.2734189e+03 -6.2688303e+00 -1.4156364e+01
pb 5 2 3 5 2 3 xyz 4.273408e+03 -1.240751e+01 -1.323699e+01
pb 5 6 3 5 6 3 xyz 4.273338e+03 1.240318e+01 -1.323210e+01
pb 5 5 3 5 5 3 xyz 4.2734160e+03 6.3945718e+00 -1.4141220e+01
pb 4 6 3 4 6 3 xyz 1.054310e+03 1.243838e+01 -5.696558e+00
pb 4 2 3 4 2 3 xyz 1.054305e+03 -1.250031e+01 -5.546331e+00
pb 4 5 3 4 5 3 xyz 1.0542629e+03 7.2172804e+00 -1.0043599e+01
pb 4 3 3 4 3 3 xyz 1.0542683e+03 -7.2584434e+00 -9.9672928e+00
pb 4 4 3 4 4 3 xyz 1.053646e+03 0.000000e+00 -1.500000e+01
pb 3 6 3 3 6 3 xyz 9.571483e+02 1.222872e+01 3.812949e+00
pb 3 2 3 3 2 3 xyz 9.575593e+02 -1.236469e+01 5.200229e+00
pb 3 5 3 3 5 3 xyz 9.5766785e+02 5.9354124e+00 4.7393906e-01
pb 3 3 3 3 3 3 xyz 9.6200000e+02 -8.7000000e+01 0.0000000e+00
pb 3 3 3 3 3 3 xyz 9.5775385e+02 -5.2975903e+00 7.4877626e-01
pb 2 6 3 2 6 3 xyz 8.601647e+02 1.226210e+01 4.734522e+01
pb 2 2 3 2 2 3 xyz 8.604533e+02 -1.268168e+01 4.801646e+01
pb 2 5 3 2 5 3 xyz 8.6057495e+02 7.4088326e+00 4.4255207e+01
pb 2 3 3 2 3 3 xyz 8.6066663e+02 -7.7640843e+00 4.4602432e+01
pb 2 4 3 2 4 3 xyz 8.615573e+02 -2.864847e-01 4.131967e+01
pb 1 1 3 1 1 3 xyz -7.700000e+01 -2.122000e+02 2.580000e+02
pb 1 7 3 1 7 3 xyz -7.700000e+01 2.122000e+02 2.580000e+02
pb 1 4 3 1 4 3 xyz -6.928600e+01 0.000000e+00 2.107500e+02
pb 1 3 3 1 3 3 xyz -6.930050e+01 -2.811738e+01 2.108130e+02
pb 1 5 3 1 5 3 xyz -6.930050e+01 2.811738e+01 2.108130e+02
pb 1 6 3 1 6 3 xyz -6.972451e+01 8.387547e+01 2.124850e+02
pb 1 2 3 1 2 3 xyz -6.972451e+01 -8.387547e+01 2.124850e+02
pb 9 3 2 9 3 2 xyz 5.5970000e+03 -2.7481813e+01 -6.0065796e+01
pb 9 5 2 9 5 2 xyz 5.5970000e+03 2.7481783e+01 -6.0065804e+01
pb 9 5 1 9 5 1 xyz 5.7300000e+03 7.9594002e+01 -1.3400101e+02
pb 9 5 1 9 5 1 xyz 5.7300000e+03 4.3620052e+01 -1.3961447e+02
pb 9 3 1 9 3 1 xyz 5.7300000e+03 -7.9594002e+01 -1.3400101e+02
pb 9 3 1 9 3 1 xyz 5.7300000e+03 -4.3620045e+01 -1.3961450e+02
pb 9 6 1 9 6 1 xyz 5.7300000e+03 9.7406075e+01 -1.2995883e+02
pb 9 2 1 9 2 1 xyz 5.7300000e+03 -9.7406075e+01 -1.2995883e+02
pb 3 4 3 3 4 3 xyz 9.583840e+02 0.000000e+00 -3.673548e+00
pb 2 4 3 2 4 3 xyz 8.586234e+02 -1.132471e-01 4.117999e+01
pb 9 2 2 9 2 2 xyz 5596.41 -100.923 -32.1407
pb 9 6 2 9 6 2 xyz 5596.41 100.923 -32.1407
bb 9 1 1 9 7 2 99;
bb 1 1 1 1 7 2 98;
merge
```

The placement of the vertices forming the bulk of the fluid mesh present the most challenging aspect of the fluid mesh generation. Remaining mesh generation requires filling in the bow and stern areas with conical shaped parts. These parts are bluded to the **facesets,** which were formed using the **pick sets** command during construction of the bow and the stern plugs. The **bb** command is used to define the slave side of the block

boundary interfaces and is defined in the fluid mesh generation above. Use of the **bb** command allows the mesh that is extruded from the fluid mesh to be projected down onto the conical bow area (Figure 52). The **bptol** command is then used to merge the parts formed from the bow and stern plugs to the fluid mesh.

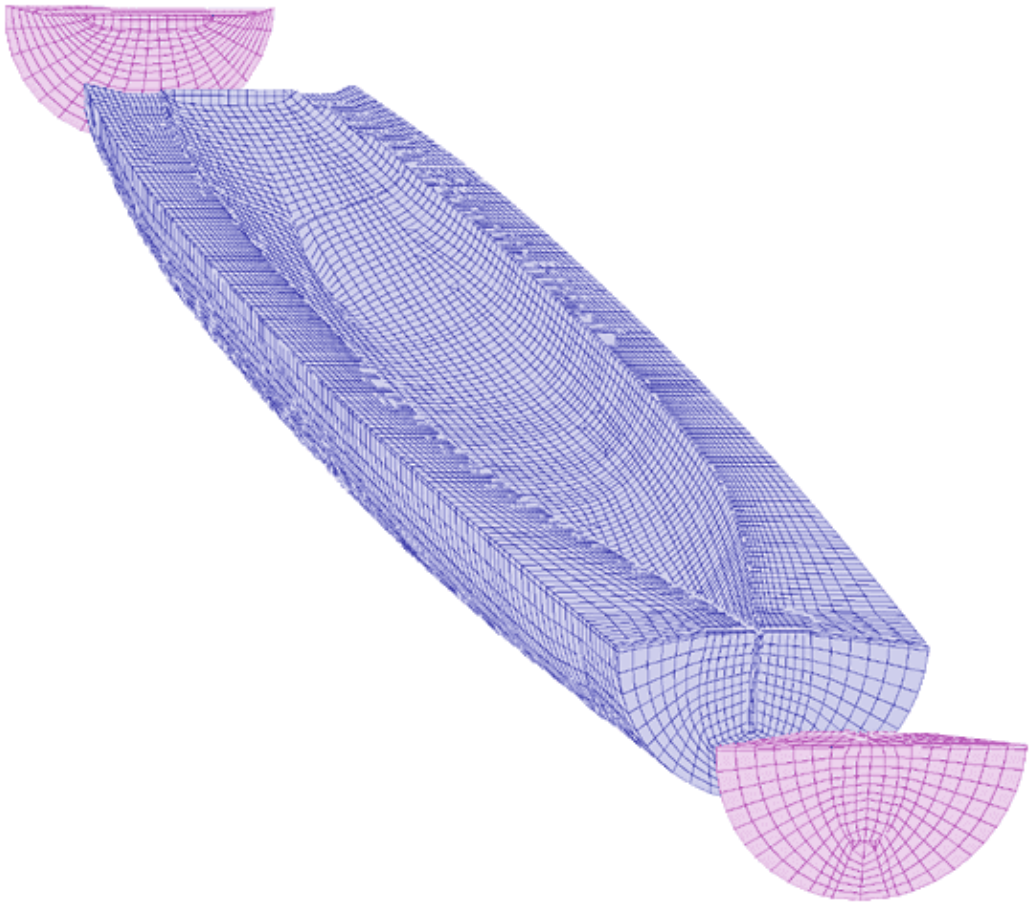

Figure 52. Bow and Stern Plug Construction Filling 1/2 Fluid Mesh

```
fset stern = lb6
c part – stern plug
blude 1 stern 1 2;1 2;1 2;-77 -189;-212 212;210 258;
fset lowerstern = lb6
c part – lower stern plug
blude 2 lowerstern 1 11; 1 50 101; 1 50;-189 -77;-307 0 307;-142 258;
bb 1 1 1 2 3 1 98;
fset bow = lb2
c part – bow plug
blude 1 bow2 1 7;1 50 101;1 50;5597 5730;-400 0 400;-142 -15;
bb 1 1 1 2 3 1 99;
merge
```

```
c ensure normals are outward facing on the daa1 boundary
orpt - 2952 0 5
c faceset forming the daa1 boundary for the 1/2 fluid mesh
fset daa1 = lb6
```

The above commands complete the work done to construct the one-half fluid mesh. To achieve the desired full fluid mesh size, the commands are repeated, adding on the additional volume to the one-half fluid mesh (Figure 53). Commands for the bulk fluid mesh and the bow and stern plugs for the full fluid mesh are contained below. The **orpt** command is used prior to the faceset selection that defines the DAA1 boundary for the model. Using the **orpt** command ensures that the normal vectors are facing outward on the boundary. This is a requirement for the LS-DYNA/USA code.

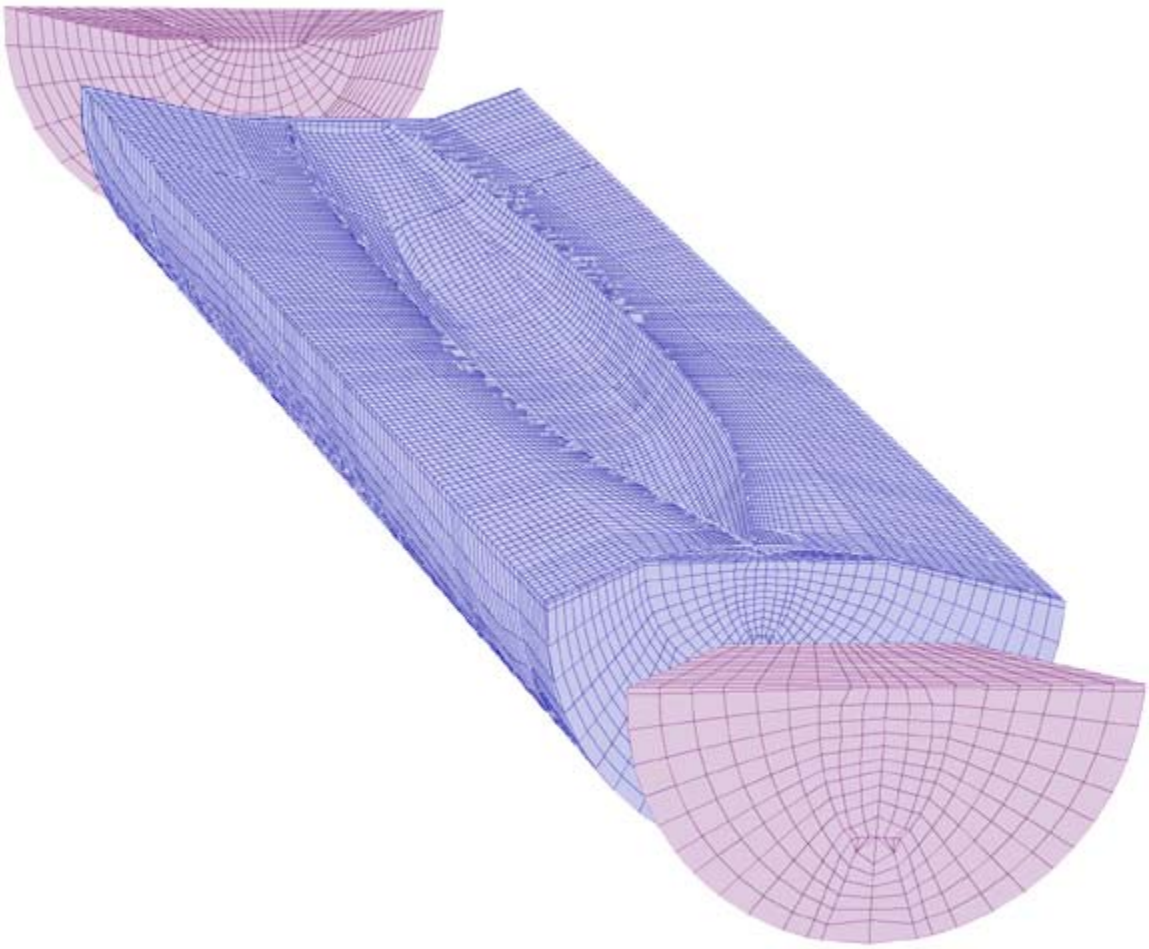

Figure 53. Bow and Stern Plug Completing the Full Fluid Mesh

```
c surface forming the outer dimension of the full fluid mesh
sd 20 cy 0 0 258 1 0 0 840
c part – bulk fluid mesh forming the full mesh
blude 5 daa1 1 2;1 2 3;1 2;-665 6202;-840 0 840;-340 -142;
bb 1 1 1 1 3 2 18;
bb 2 1 1 2 3 2 19;
merge

c faceset forming the full mesh stern plug
fset stern2 = lb6
c part – stern2 full fluid mesh plug
blude 1 strn2 1 2;1 2 3;1 2;-189 -665;-840 0 840;-342 -142;
bb 1 1 1 2 3 1 18;
merge
c faceset forming the full mesh bow plug
fset bow = lb6
c part – full mesh bow plug
blude 1 bow 1 2;1 2 3;1 2;5730 6202;-840 0 840;-342 -142;
bb 1 1 1 2 3 1 19;
orpt – 2952 0 5
c faceset forming the daa1 boundary for the full fluid mesh
fset daa1 = lb6
```

This completes the commands required to generate the full fluid mesh. The work contained in this appendix is sufficient enough to generate a fluid mesh similar to the ones used in this thesis. Selection of curve definitions and facesets will be slightly different, but good vertice placement around the critical areas mentioned above should generate a mesh of high quality. Figure 54 shows the completed coupled ship/fluid mesh model.

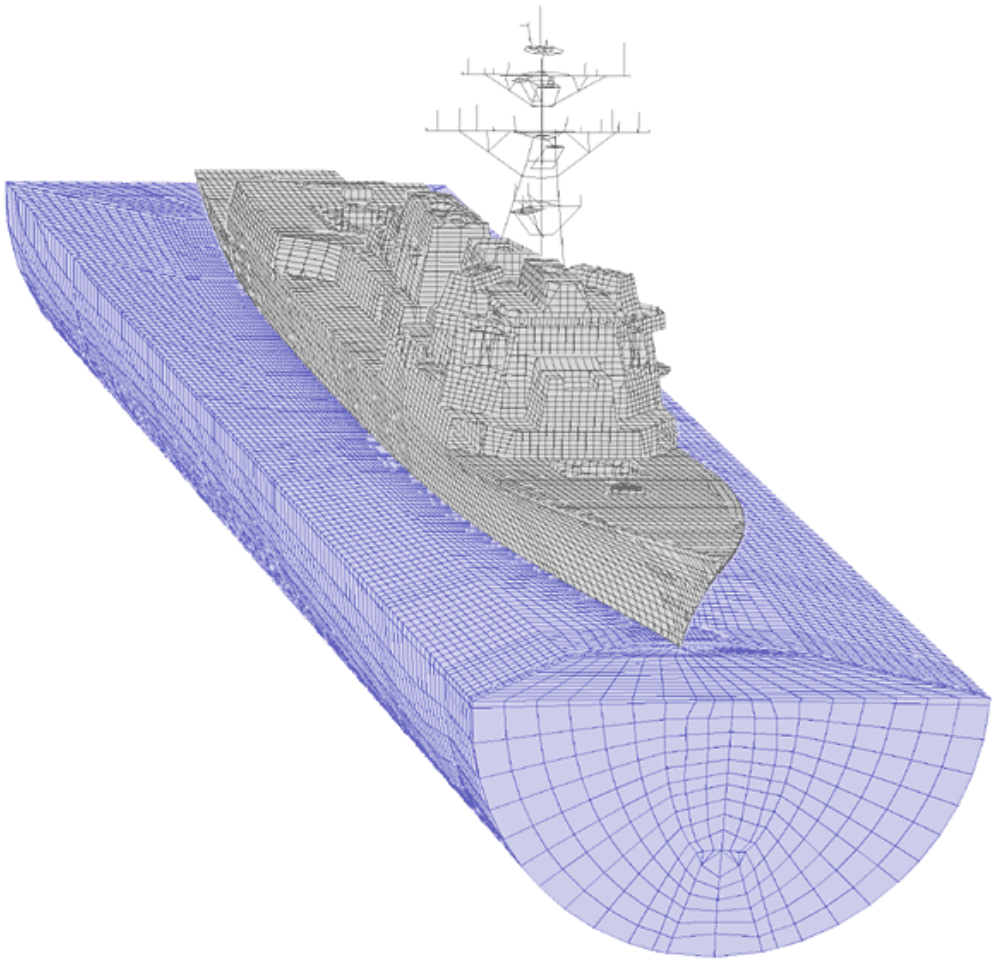

Figure 54. Complete Coupled Ship/Fluid Mesh Model

APPENDIX D: USA/LS-DYNA INPUT DECKS

This appendix provides examples of the LS-DYNA and USA code keyword file and input deck used for each of the four models presented. References 8 and 9 provide explanations of the variables used for each model. The USA input decks for all four models are identical with the exception of NSTRC, NGENF, SX, SY, SZ. These USA variables define the number of node points in the coupled structure/fluid model, the total number of DAA face elements in contact with the fluid volume elements, and the xyz cartesian coordinates of the closest point on the DAA boundary to the charge for each of the fluid meshes. Additionally, the following variables have been left blank due to confidentiality of the actual shock trial charge geometry: DEPTH, XC, YC, ZC, SX, SY, SZ, WEIGHT, SLANT, CHGDEP, XV, YV, and ZV.

LS-DYNA KEYWORD FILE:

```
*TITLE
 SHOT3: 200MS COUPLED SHIP/FLUID-SHOT3 FULL MESH
*CONTROL_TERMINATION
0.2,0,0,0,0
*CONTROL_TIMESTEP
XXXX,0.9,0,0.0,0.0,1,0
*CONTROL_PARALLEL
1,0,1
*DEFINE_CURVE
1
0.,XXXX
0.2,XXXX
*DEFINE_CURVE
2
0.0,0.0
0.2,0.0
*DATABASE_HISTORY_NODE
120217,142489,211371,210993,212058,211904,212196,210430
210808,210894,414953,221188,220589,221102,222060,222436
221601,414367,416419,416269,222240,230461,231696,242399
312302,320746,330759,330764,330769,340167,340992,350220
350052
*DATABASE_NODOUT
*DATABASE_BINARY_D3PLOT
*DATABASE_BINARY_D3THDT
```

```
*DATABASE_EXTENT_BINARY
0,0,3,1,1,1,1,1
0,0,0,0,0,0
*BOUNDARY_USA_SURFACE
2,1,0
*INITIAL_DETONATION
-1,XXXX,XXXX,XXXX.,0.0
XXXX,0.00XXXX,XXXX,XXXX,XXXX,2947
$ Fluid Nodes
*NODE
-THE NODE SECTION CONTAINS NODAL COORDINATES OF FLUID MESH
GENERATED BY TRUEGRID.
*MAT_ACOUSTIC
 *PART
   999999
   999999    999999       90
*SECTION_SOLID
   999999       8
*ELEMENT_SOLID
-THE ELEMENT SOLID SECTION CONTAINS ELEMENT CONNECTIVITY
GENERATED BY TRUEGRID.
*SET_SEGMENT
-THE SET SEGMENT SECTION CONTAINS DAA BOUNDARY ELEMENTS
GENERATED BY TRUEGRID.

-REMAINING KEYWORD FILE CONTAINS NASTRAN TO LS-DYNA SHIP
CONVERSION.  THESE WILL NOT BE LISTED DUE TO THE LENGTH OF THE
REMAINING FILE.
```

USA FLUMAS INPUT DECK

```
DDG81 FULL MESH SHOT 3 COUPLED ANALYSIS: FLUMAS
flunam geonam strnam daanam          $ FLUNAM GEONAM GRDNAM DAANAM
F F F T                              $ PRTGMT PRTTRN PRTAMF CALCAM
T F F F                              $ EIGMAF TWODIM HAFMOD QUAMOD
F F T F                              $ PCHCDS NASTAM STOMAS STOINV
F F F T                              $ FRWTFL FRWTGE FRWTGR FRESUR
F T F F                              $ RENUMB STOGMT ROTGEO ROTQUA
F F F F                              $ PRTCOE STRMAS SPHERE ROTSYM
F F F F                              $ OCTMOD CAVFLU FRWTFV INTCAV
F F                                  $ BOTREF MASREF
0 XXXXX 0 5090                       $ NSTRC  NSTRF  NGEN   NGENF
0 0 0                                $ NBRA   NCYL   NCAV
0.9345E-4 XXXXX                      $ RHO    CEE
2                                    $ NVEC
XXX.  0.  0. 1.                      $ DEPTH CXFS CYFS CZFS
14.7 386.4                           $ PATM GRAVAC
0                                    $ NSRADI
0                                    $ NSORDR
```

USA AUGMAT INPUT DECK

```
DDG81 FULL MESH SHOT3 COUPLED ANALYSIS: AUGMAT
strnam flunam geonam prenam          $ STRNAM FLUNAM GEONAM PRENAM
F F F F                              $ FRWTGE FRWTST FRWTFL LUMPFM
F F F T                              $ FLUSKY DAAFRM SYMCON DOFTAB
F F F F                              $ PRTGMT PRTTRN PRTSTF PRTAUG
F F F F                              $ MODTRN STRLCL INTWAT CFADYN
11                                   $ NTYPDA
XXXXX XXXX 3 3                       $ NSTR   NSFR   NFRE   NFTR1
1                                    $ NSETLC
0 1 5090 1                           $ NDICOS JSTART JSTOP  JINC
```

USA TIMIT INPUT DECK

```
DDG81 FULL MESH SHOT3 COUPLED ANALYSIS: TIMINT
prenam posnam                        $ PRENAM POSNAM
resnam                               $ RESNAM WRTNAM
F T F F                              $ REFSEC FLUMEM XXXXXX XXXXXX
F F F                                $ INCTSR CENINT BUOYAN
1                                    $ NTINT
0.0 XXXX                             $ STRTIM DELTIM
T F F F                              $ EXPWAV SPLINE VARLIN PACKET
F T F F                              $ HYPERB EXPLOS DOUBDC VELINP
F F F F                              $ BUBPUL SHKBUB XXXXXX XXXXXX
1                                    $ NCHARG
0.                                   $ HYDPRE
```

```
XXXX XXXX XXXX          $ XC     YC     ZC
XXXX XXXX XXXX          $ SX     SY     SZ
201                     $ JPHIST
1. 0.                   $ PNORM  DETIM
XXXX                    $ DTHIST
1                       $ CHGTYP
XXXX XXX XXX            $ WEIGHT SLANT  CHGDEP
99999 99999             $ NSAVER NRESET
0 0 0 0                 $ LOCBEG LOCRES LOCWRT NSTART
F F F F                 $ FORWRT STBDA2 ASCWRT XXXXXX
XXXX XXXX XXXX          $ XV     YV     ZV
F                       $ DISPLA
```

APPENDIX E. USA CODE DISPARITY

The input values for the initialization of the initial pressure caused by the explosive disturbance are of particular concern in setting up the LS-DYNA and USA modules. LS-DYNA code requires the use of the *INITIAL_DETONATION command that flags the code that determines the acoustic mesh boundary and applies the pressure time history to the boundary. This command line requires the following input [Ref. 7]:

Table 18 LS-DYNA *INITIAL_DETONATION Command Inputs

PID (Part ID Number)	-1 for an acoustic boundary with the USA code
X,Y,Z:	The Cartesian coordinate xyz point of charge detonation.
PEAK:	Peak pressure at the node which is one element away from the ship hull and is along the path with the shortest distance from charge location to the ship hull.
DECAY	Decay constant associated with the peak value.
XS,YX,ZS	The Cartesian coordinate xyz point on the DAA boundary point that is closest to the charge.
NID (Node ID Number)	Node number which is one element away from the ship hull.

The timit module requires the following input for the initialization of the pressure profile for the USA code [Ref. 8]:

Table 19 USA TIMIT Initialization Command Inputs

XC, YC, ZC	The Cartesian coordinate xyz point of charge detonation
SX,SY,SZ	The Cartesian coordinate xyz point on the DAA boundary that is closest to the charge
SLANT	Slant standoff is the distance between the charge and the closest point on the structure.
XV,YV,ZV	The Cartesian coordinate xyz of the point on element away from the ship hull (along the shortest distance path from the charge location to the ship hull)

The inconsistency between the two codes is due to the slant definition in the USA timit module manual. This specifies that the slant is the “distance between the charge and the closest point on the structure”. During the study of the incident and shock wave

pressure profiles, discrepancy arose between the four fluid meshes investigated. This lead to discussions with Dr. John DeRuntz, author of the USA code, into possible disparities between the pressure profiles for the various fluid meshes. The USA timit manual is correct if the analysis is conducted without the use a fluid element volume, such as the simulation of a submarine underwater explosion. However, it was concluded that the manual was incorrect in the definition of SLANT for a coupled fluid/structure surface ship model. The slant should be the distance between the charge and the closest point on the DAA boundary, not the distance from the charge to the closest point on the hull. By making this correction in the timit module and running the ship shock simulation again, disparities between the two pressure profiles for the fluid meshes were removed.

LIST OF REFERENCES

1. OPNAV Instruction 9072.2, "Shock Hardening of Surface Ships", 12 January 1987
2. Title 10, Section 2366, United States Code (10 USC 2366)
3. Gansler, Dr. Jacques S., USD (A&T), *Defense News*, April 1988
4. Shin, Y.S. and Park, S.Y., "Ship Shock Trial Simulation of USS John Paul Jones (DDG 53) Using LS-DYNA/USA: Three Dimensional Analysis", 70th Shock and Vibration Symposium Proceedings, Vol. I, November 1999.
5. Malone, P.E., "Surface Ship Shock Modeling and Simulation: Extended Investigation", Master's Thesis, Naval Postgraduate School, Monterey, CA, 2000.
6. XYZ Scientific Applications, Inc., *TrueGrid User Manual Version 2.4*, Livermore, CA, 2002.
7. Livermore Software Technology Corporation, *LS-DYNA Keyword User's Manual*, Version 960, LSTC, Livermore, CA, March 2001.
8. DeRuntz, Jr., J.A., *The Underwater Shock Analysis (USA) Manual*, Unique Software Applications, Colorado Springs, CO, May 1996.
9. Cole, R.H., *Underwater Explosions*, pp. 1-15, Princeton University Press, 1948.
10. Shin, Y.S., "Naval Ship Shock and Design Analysis", Course Notes for Underwater Shock Analysis, Naval Postgraduate School, Monterey, CA, 1996.
11. DeRuntz, Jr., J.A. "The Underwater Shock Analysis Code and Its Applications", 60th Shock and Vibration Symposium, Vol. I, pp. 89-107, November 1989.
12. DeRuntz, Jr. J.A. and Rankin, C. C., "Applications of the USA-STAGS-CFA Code to Nonlinear Fluid-Structure Interaction Problems in Underwater Shock of Submerged Structures," Proceedings of the 60th Shock and Vibration Symposium, 1989.
13. MacNeal-Schwendler Corporation, "MSC/NASTRAN Quick Reference Guide," Version 69, Los Angeles, CA, 1996.
14. Gibbs and Cox, Inc., "DDG-81 Flight IIA Shock Simulation", Presentation at the Naval Postgraduate School, August 2002.
15. Riedel, CDR J., "USS Winston S. Churchill (DDG-81) Shock Trial Overview", Presentation at the Naval Postgraduate School, February 2002.
16. DeRuntz, Jr., J.A., *The Underwater Shock Analysis (USA) Manual*, Unique Software Applications, Colorado Springs, CO, May 1996.

17. Shin, Y.S., “LS-DYNA Training Guide: Nonlinear Dynamic Analysis of Structures in 3-D Code Coupled with Underwater Shock Analysis Code for Ship Shock Modeling and Simulation”, Naval Postgraduate School, July 2002.
18. Santiago, L.D., “Fluid-Interaction and Cavitation Effects on a Surface Ship Model Due to an Underwater Explosion”, Master’s Thesis, Naval Postgraduate School, September1996.
19. Sevin, E., “Doubly Asymptotic Analysis of Shock-Wave-Excited Submarines”, Defense Nuclear Agency, October 1978.
20. Geer, T.L., “An objective Error Measure for the Comparison of Calculated and Measured Transient Response Histories”, The Shock and Vibration Bulletin, SAVIAC, NRL, Washington, DC, June 1984.
21. Geers, T.L., “Validation of Computer Codes”, Course Notes 1999.
22. Russel, D.D., “Error Measures for Comparing Transient Data: Part II: Error Measure Case Study”, 68th Shock and Vibration Symposium Proceedings, Vol. I, November 1997.
23. Shin, Y.S., “Damping Modeling Strategy for Naval Ship Systems”, Report NPS-ME-03-001, Naval Postgraduate School, January 2003.
24. Russell, D.D., “DDG53 Shock Trial Simulation Acceptance Criteria”, 69th Shock and Vibration Symposium, October 1998.

INITIAL DISTRIBUTION LIST

1. Defense Technical Information Center
   Ft. Belvoir, VA

2. Dudley Knox Library
   Naval Postgraduate School
   Monterey, CA

3. Mechanical Engineering Department Chairman, Code ME
   Naval Postgraduate School
   Monterey, CA

4. Naval/Mechanical Engineering Curriculum Code 34
   Naval Postgraduate School
   Monterey, CA

5. Professor Young S. Shin, Code ME/Sg
   Department of Mechanical Engineering
   Naval Postgraduate School
   Monterey, CA

6. Michael J. Harrington
   Gibbs and Cox, Inc.
   Arlington, VA

7. Michael C. Winnette
   Carderock Division
   Naval Surface Warfare Center
   West Bethesda, MD

8. Gust Constant
   Naval Sea Systems Command
   Arlington, VA

9. CAPT David H. Lewis
   Program Manager (PMS 400D)
   Aegis Shipbuilding
   Washington, DC

10. CDR Jeff Riedel
    DDG-51 Class Post Delivery Manager (PMS 400PSA)
    Naval Sea Systems Command
    Washington, DC